



**UNIVERSIDADE FEDERAL DO PARÁ
INSTITUTO DE GEOSCIÊNCIAS
PROGRAMA DE PÓS-GRADUAÇÃO EM GEOLOGIA E GEOQUÍMICA**

TESE DE DOUTORADO Nº 164

**ORIGEM E EVOLUÇÃO DO COMPLEXO GRANITOIDE
NEOARQUEANO DE VILA JUSSARA: IMPLICAÇÕES PARA
A EVOLUÇÃO CRUSTAL DA PROVÍNCIA CARAJÁS**

Tese apresentada por:

FERNANDO FERNANDES DA SILVA

Orientador: Prof. Dr. Davis Carvalho de Oliveira (UFPA)

**BELÉM
2022**

Dados Internacionais de Catalogação na Publicação (CIP) de acordo com ISBD
Sistema de Bibliotecas da Universidade Federal do Pará
Gerada automaticamente pelo módulo Ficat, mediante os dados fornecidos pelo(a) autor(a)

S5860 Silva, Fernando Fernandes da.
Origem e evolução do complexo granitoide neoarqueano de vila
Jussara: implicações para a evolução crustal da província Carajás /
Fernando Fernandes da Silva. — 2022.
x, 100 f. : il. color.

Orientador(a): Prof. Dr. Davis Carvalho de Oliveira
Tese (Doutorado) - Universidade Federal do Pará, Instituto de
Geociências, Programa de Pós-Graduação em Geologia e
Geoquímica, Belém, 2022.

1. Granitoide. 2. Neoarqueano. 3. Sintectônico . 4.
Colocação. 5. Isótopos . I. Título.

CDD 552



**Universidade Federal do Pará
Instituto de Geociências
Programa de Pós-Graduação em Geologia e Geoquímica**

**ORIGEM E EVOLUÇÃO DO COMPLEXO GRANITOIDE
NEOARQUEANO DE VILA JUSSARA: IMPLICAÇÕES PARA
A EVOLUÇÃO CRUSTAL DA PROVÍNCIA CARAJÁS**

TESE APRESENTADA POR:

FERNANDO FERNANDES DA SILVA

Como requisito parcial à obtenção de Grau de Doutor em Ciências na Área de GEOQUÍMICA E PETROLOGIA, linha de pesquisa EVOLUÇÃO CRUSTAL E METALOGÊNESE.

Data de Aprovação: 15 / 07 / 2022

Banca Examinadora:

Daví Carvalho de Oliveira
Prof. Dr. Daví Carvalho de Oliveira
Orientador – UFPA

Valdecir de Assis Janasi
Prof. Dr. Valdecir de Assis Janasi
Membro – USP

Claudio Nery Lamarão
Prof. Dr. Claudio Nery Lamarão
Membro – UFPA

Bhrenno Marangoanha
Prof. Dr. Bhrenno Marangoanha
Membro – UFPA

Moacir José Bueno Macambira
Prof. Dr. Moacir José Bueno Macambira
Membro – UFPA

A minha família e amigos

AGRADECIMENTOS

A elaboração deste trabalho não teria sido possível sem a colaboração, estímulo e empenho de diversas pessoas e instituições:

Agradeço inicialmente à Universidade Federal do Pará (UFPA), juntamente com o Programa de Pós-Graduação em Geologia e Geoquímica (PPGG), pela infraestrutura e suporte financeiro necessários à realização deste trabalho.

Ao orientador prof. Dr. Davis Carvalho de Oliveira, pela oportunidade, apoio e incentivo durante esses anos.

Ao Professor Roberto Dall'Agnol pelo incentivo, oportunidades, conhecimento compartilhado e disposição para guiar o trabalho para o melhor caminho possível.

A meus Pais e minha irmã que sempre me apoiaram e incentivaram em todas as etapas da minha vida.

A memória da minha falecida esposa que foi parte integrante desse trabalho e a considero como uma coautora.

Aos colegas Ingrid Viana e Luan Alexandre os quais compartilharam temas de doutorado e mestrado na mesma área desta tese, o meu muito obrigado pelas inúmeras discussões, momentos de desespero compartilhado, risada e momentos de descontração.

Ao Conselho Nacional de Desenvolvimento Científico e Tecnológico (CNPq) pela concessão da bolsa de estudo (Processo 140077/2018-9) e taxa de bancada. O presente trabalho foi realizado com apoio da Coordenação de Aperfeiçoamento de Pessoal de Nível Superior - Brasil (CAPES) - Código de Financiamento 001.

Ao Fundo de Amparo à Pesquisa do Estado do Pará (FAPESPA; Processo 133/2008-0), e aos projetos de pesquisa Vale/FAPESPA (ICAAF n. 053/2011) e INCT/GEOCIAM (CNPq/FAPESPA/CAPES/PETROBRAS; Processo 573733/2008-2), pelo apoio financeiro durante a execução desta pesquisa.

Ao Grupo de Pesquisa Petrologia de Granitoides (GPPG) do Instituto de Geociências (IG-UFPA), em especial aos integrantes da sala 3, pelas conversas, companhia e auxílio durante esses anos.

Ao professor Marco Antonio Galarza, do Laboratório de Geologia Isotópica (Pará-Iso) da UFPA, pelo suporte na aquisição dos dados de U-Pb LA-MC-ICP-MS e Sm-Nd, além da ajuda no tratamento dos dados de Lu-Hf.

Ao Laboratório de Geocronologia de Alta Resolução da Universidade de São Paulo (GeoLab/USP), em especial ao corpo técnico Dr. Kei Sato e Dr. Artur Takashi Onoe pelo

grande auxílio prestado durante as etapas de aquisição de dados U-Pb SHRIMP. Ao professor Cristiano Lana, do Laboratório de Geologia Isotópica da Universidade Federal de Ouro Preto (UFOP), pelo apoio na obtenção das análises de Lu-Hf em zircão.

Ao professor Cláudio Nery Lamarão e à Gisele T. Marques, pelo suporte na aquisição das imagens BSE e CL de alta resolução dos cristais de zircão, no Laboratório de Microanálises do IG-UFPA.

Aos professores do PPGG, pelo conhecimento transmitido. Aos funcionários da secretaria do programa de pós-graduação, pelo auxílio nas questões administrativas e pela atenção dispensada. Aos demais funcionários do IG, pela dedicação e atenção.

A minha companheira de vida Karol Cunha a qual que me ajudou, me deu forças e incentivou para a conclusão das etapas finais do trabalho, obrigado por tudo!

Gostaria de expressar toda a minha gratidão e apreço a todos aqueles que, direta ou indiretamente, contribuíram para que esta tarefa se tornasse realidade. A todos quero manifestar os meus sinceros agradecimentos.

“A tarefa não é tanto ver aquilo que ninguém viu, mas pensar o que ninguém ainda pensou sobre aquilo que todo mundo vê” *Arthur Schopenhauer*

RESUMO

Novas informações sobre a geologia, aliadas à obtenção de dados geoquímicos e isotópicos (U-Pb, Hf e Nd) da Suíte Vila Jussara, são apresentadas com objetivo de discutir um modelo petrogenético para os granitoides neoarqueanos da Província Carajás. Esta suíte surge como uma série de plút ons com formas sigmoidais, coalescentes e alongados na direção E-W, os quais seguem a tendência regional. As áreas centrais dos plút ons são levemente deformadas, enquanto que as porções marginais apresentam aspecto milonítico e são delimitadas por zonas de cisalhamento sinistral pertencentes ao sistema transcorrente da Cinturão de Cisalhamento Itacaiúnas. Esses granitoides apresentam um amplo espectro composicional, com quatro litotipos individualizados: (i) biotita-hornblenda monzogranito seriado, que é subdividido em tipos oxidados e reduzidos; (ii) biotita-hornblenda tonalito; (iii) biotita monzogranito; e (iv) granitoide porfirítico (hornblenda biotita monzogranito/granodiorito). Os dados geocronológicos U-Pb e Pb-Pb em zircão forneceram idade de cristalização de 2.74 Ga para a variedades graníticas e granitoides porfiríticos, e para a variedade biotita-hornblenda tonalito, idade de 2.76 Ga. Os dados isotópicos de Nd e Hf, sugerem que os magmas da suíte Vila Jussara não são juvenis [ϵ_{Nd} (-3,5 a 1,5) e ϵ_{Hf} (-1,2 a 3,5)] e foram derivados de rochas de idade mesoarqueana ($T_{\text{DM}} > 3.0$ Ga). O modelo petrogenético adotado para gerar os magmas primários desta suíte admite como rocha geradora os granulitos mesoarqueanos da área Ouro Verde do subdomínio Canaã dos Carajás. Relações de campo, dados geoquímicos e isotópicos sugerem que os granitoides que compõem a Suíte Vila Jussara não são formados a partir de um único magma parental, mas por múltiplas injeções de magmas gerando extensa hibridização. Seus magmas foram colocados ao longo de estruturas pré-existentes sob regime tectônico transtensional dominado por cisalhamento puro em um contexto sintectônico pós-colisional.

Palavras-chave: Granitoides. Geoarqueano. Sintectônico. Colocação. Isótopos. Carajás.

ABSTRACT

New information on the geology, combined with the acquisition of geochemical and isotopic data (U-Pb, Hf and Nd) from the Vila Jussara Suite, are presented in order to discuss a petrogenetic model for the Neoarchean granitoids of the Carajás Province. This suite appears as a series of coalescing plutons with sigmoidal and elongated shapes, in the E-W direction, which follow the regional trend. The central areas of the plutons are slightly deformed, while the marginal portions have a mylonitic appearance and are delimited by sinistral shear zones belonging to the transcurrent system of the Itacaiúnas Shear Belt. These granitoids present a broad compositional spectrum, with four individualized lithotypes: (i) biotite-hornblende serial monzogranite, which is subdivided into oxidized and reduced types; (ii) biotite-hornblende tonalite; (iii) biotite monzogranite; and (iv) porphyritic granite (hornblende biotite monzogranite/granodiorite). The geochronological data U-Pb and Pb-Pb in zircon provided an age of crystallization of 2.74 Ga for the granitic and porphyritic granite varieties, and for the biotite-hornblende tonalite variety, an age of 2.76 Ga. The isotopic data of Nd and Hf suggest that the magmas of the Vila Jussara suite are not juveniles [ϵ Nd (-3.5 to 1.5) and ϵ Hf (-1.2 to 3.5)] and were derived from rocks of Mesoarchean age ($TDM > 3.0$ Ga). The petrogenetic model adopted to generate the primary magmas of this suite admits as source rock the Mesoarchean granulites from the Ouro Verde area of the Canaã dos Carajás subdomain. Field relationships, geochemical and isotopic data suggest that the granitoids that make up the Vila Jussara Suite are not formed from a single parental magma, but by multiple magma injections generating extensive hybridization. Its magmas were placed along pre-existing structures under a transtensional tectonic regime dominated by pure shear in a post-collisional syntectonic context.

Keywords: Granitoids. Neoarchean. Syntectonic. Emplacement. Isotopes. Carajás.

SUMÁRIO

DEDICATÓRIA	iv
AGRADECIMENTOS	v
EPÍGRAFE	vii
RESUMO	viii
ABSTRACT	ix
1 INTRODUÇÃO.....	1
1.1 APRESENTAÇÃO	1
1.2 LOCALIZAÇÃO E ACESSO	3
1.3 CONTEXTO GEOLÓGICO REGIONAL.....	4
1.3.1 Domínio Rio Maria	6
1.3.2 Domínio Sapucaia	9
1.3.3 Domínio Canaã dos Carajás e Bacia Carajás.....	10
1.4 APRESENTAÇÃO DO PROBLEMA	15
1.5 OBJETIVOS.....	16
1.6 MATERIAIS E MÉTODOS	17
1.6.1 Pesquisa bibliográfica	17
1.6.2 Mapeamento geológico e estrutural.....	17
1.6.3 Análise petrográfica e microestrutural	18
1.6.4 Geoquímica	18
1.6.5 Geocronologia.....	19
1.6.6 Análise isotópica Lu-Hf	20
1.6.7 Análise isotópica Sm-Nd	21
2 LITHOLOGICAL AND STRUCTURAL CONTROLS ON THE EMPLACEMENT OF A NEOARCHEAN PLUTONIC COMPLEX IN THE CARAJÁS PROVINCE, SOUTHEASTERN AMAZONIAN CRATON (BRAZIL).....	23
3 GEOCHEMISTRY, SHRIMP U-PB ZIRCON GEOCHRONOLOGY, AND HF-ND ISOTOPE COMPOSITION ON THE NEOARCHEAN PLUTONIC COMPLEX OF THE VILA JUSSARA FROM CARAJÁS PROVINCE, AMAZONIAN CRATON: PETROGENESIS AND TECTONIC IMPLICATIONS	39
4 CONCLUSÕES E CONSIDERAÇÕES FINAIS.....	88
REFERÊNCIAS	89

1 INTRODUÇÃO

1.1 APRESENTAÇÃO

Os diferentes processos de formação da crosta continental primitiva ainda são objeto de extensa discussão e as quais estão muito distantes de um consenso (De Wit 1998, Moyen *et al.* 2006, Hamilton, 2011, Bédard *et al.* 2013). Quase todos os núcleos Arqueanos nos diferentes crátons apresentam suas rochas com aspectos de campo variáveis, que passam de gnaisses homogêneos a migmatitos altamente heterogêneos como produto direto da sobreposição metamórfica pós-magmática (Martin 1994). O grande processo de retrabalhamento crustal por sucessivos eventos tectono-termal que esses terrenos sofrem acabam por dificultar o processo de reconstrução geodinâmica. A melhor tentativa de reconstruir uma história crustal e os diferentes eventos que podem ter ocorrido é através dos granitoides, especialmente aqueles plútôns sintectônicos. Desde a geração de magma na área fonte até a completa cristalização, os plútôns sintectônicos podem registrar eventos geológicos de curta duração relacionados à fusão e à deformação da crosta continental (Paterson & Tobisch 1992, Karlstrom *et al.* 1993, Bodorkos *et al.* 2000, Petford *et al.* 2000, Rosemberg 2004, Florisbal *et al.* 2012).

Na província de Carajás foram descritos vários plútôns graníticos deformados neoarqueanos com características geoquímicas que variam de magnesianas à ferrosas e afins dos granitos tipo-A (Dall'Agnol *et al.* 2017). Sua origem tem sido associada à fusão parcial de rochas maficas a intermediárias da crosta inferior, e são classificados como granitoides do tipo A 'deformados', subalcalinos, metaluminosos a fracamente peraluminosos (Sardinha *et al.* 2006, Barros *et al.* 2009, Feio *et al.* 2012, Marangoanha *et al.* 2019). O entendimento da estrutura interna desses granitoides, bem como sua relação com a estruturação regional e deformação no estado sólido é fundamental para restringir as relações espaço-tempo-temperatura-deformação durante a cristalização dos plútôns. Neste aspecto, as zonas de cisalhamento representam os principais canais para o transporte de magma, fornecendo um importante mecanismo de posicionamento para muitos plútôns sintectônicos relacionados aos regimes de deformação transpressiva na Província Carajás.

No Subdomínio Sapucaia (porção centro-norte da Província Carajás; Figura 2) ocorre um cenário geológico-estrutural composto de grupos distintos de granitos ferrosos cristalizados sob diferentes estados de oxidação e espacialmente associados a tonalitos magnesianos. Este aspecto indica uma evolução magmática mais complexa envolvendo líquidos gerados sob diferentes fugacidades de oxigênio (fO_2) e processos de mistura. A área

investigada neste estudo está situada ao redor da área de Vila Jussara, que representa uma seção relativamente bem preservada da crosta meso e neoarqueana. Esta tese apresenta os resultados de uma abordagem integrada aplicada a um complexo granitoide neoarqueano formado por vários plútuns coalescentes ao longo do cinturão de cisalhamento de Itacaiúnas, e tem como objetivo discutir as evidências de sucessivas injeções de líquidos e determinar a(s) fonte(s) destes magmas, assim como discutir o papel desempenhado pela tectônica transcorrente durante a colocação dos mesmos. Para isso, foi feito um estudo detalhado integrando petrografia, observação estrutural, dados geoquímicos e isotópicos Sm-Nd e U-Pb/Lu-Hf em zircão. Além disso, testes de modelagem geoquímica para determinar a composição do *melt* e dos resíduos permitirá identificar as fontes específicas e quantificar o papel de cada magma nos processos envolvidos na origem destes granitoides. Isto subsidiará a proposta de um modelo de formação para os granitoides neoarqueanos da Província Carajás e, consequentemente, dos principais processos que levaram à configuração atual do Subdomínio Sapucaia, o que significará um avanço na compreensão dos aspectos evolutivos da Província Carajás.

A presente tese está ligada ao tema de pesquisa desenvolvido pelo Grupo de Pesquisa Petrologia de Granitoides (GPPG) e está vinculada à linha de pesquisa Evolução Crustal e Metagênese que está inserida na área de concentração Geoquímica do Programa de Pós-Graduação em Geologia e Geoquímica (PPGG) da Universidade Federal do Pará (UFPA). Seus resultados estão vinculados às metas e objetivos propostos pelo projeto Origem e história tectônica dos granitoides arqueanos do Domínio Carajás, SE do Craton Amazônico, financiado pelo Conselho Nacional de Desenvolvimento Científico (CNPq; Processos: 435552/2018-0 e 311647/2019-7).

A estrutura organizacional deste documento inclui, inicialmente, um capítulo de caráter introdutório (Capítulo 1), que aborda os pontos relacionados à apresentação e localização da área de estudo ao contexto geológico regional da Província Carajás, com ênfase aos estudos das associações litológicas do Domínio Sapucaia. Compreende também a apresentação do problema, os objetivos a serem alcançados e metodologia aplicada. Os resultados alcançados neste trabalho serão apresentados e discutidos na forma de dois artigos científicos (capítulos 2, 3), que já foram publicados e/ou submetidos a periódicos internacionais, e abordados de forma integrada no capítulo final (Capítulo 4). Os artigos serão apresentados na seguinte ordem:

CAPÍTULO 2 – Artigo 1: Lithological and structural controls on the emplacement of a Neoarchean plutonic complex in the Carajás province, southeastern Amazonian craton (Brazil). Publicado na revista Journal of South America Earth Science.

Este trabalho reúne dados sobre geologia, petrografia, análise meso e microestrutural referentes aos granitoides neoarqueanos de Vila Jussara. Esse estudo permitiu caracterizar as variedades granitoides existentes e suas relações. Com base na definição das zonas de maior e menor concentração de deformação nos corpos, através das feições microestruturais, foi mostrado que os magmas geradores das rochas de Vila Jussara foram colocados em regimes deformacionais ligados à reativação das maiores zonas de cisalhamento da Província Carajás.

CAPÍTULO 3 – Artigo 2: Geochemistry, SHRIMP U-Pb Zircon geochronology, and Hf-Nd isotope composition on the Neoarchean Vila Jussara granitoid complex from Carajás Province, Amazonian Craton: petrogenesis and tectonic implications.

Foi submetido para publicação à revista A (*Qualis CAPES*). Se propõe a discutir os processos petrogenéticos envolvidos na geração dos granitoides neoarqueanos de Vila Jussara, com base em dados de campo, geocronológicos e isotópicos, além de um estudo envolvendo comportamento e elementos traços e maiores durante processos de magma. Isso permitiu discutir o papel de uma fonte granulítica (máfica e félscica) na geração de magmas de assinatura tipo A, e que possibilitou montar um modelo geodinâmico para explicar a origem dos granitoides neoarqueanos da porção centro-norte da Província Carajás.

1.2 LOCALIZAÇÃO E ACESSO

A área de estudo (Figura 1) localiza-se a sul do município de Canaã dos Carajás, e a leste de Água Azul do Norte, no sudeste do estado do Pará, e está inserida na Folha SB-22-Z-A-V (Rio Parauapebas). O acesso à área de trabalho é feito a partir de Marabá, pela BR 155, até Eldorado dos Carajás. A partir desse município, têm-se duas opções: a primeira é seguindo a mesma rodovia até Xinguara e, em seguida, a PA 279. Após entra-se à direita em uma estrada não pavimentada, seguindo acesso até o limite sul da área. A segunda opção é seguindo a PA 275 até Parauapebas, em seguida a PA 160 até Canaã dos Carajás e, por fim, a estrada de acesso não pavimentadas até vila Jussara, que fornece acesso aos limites norte da área de trabalho.

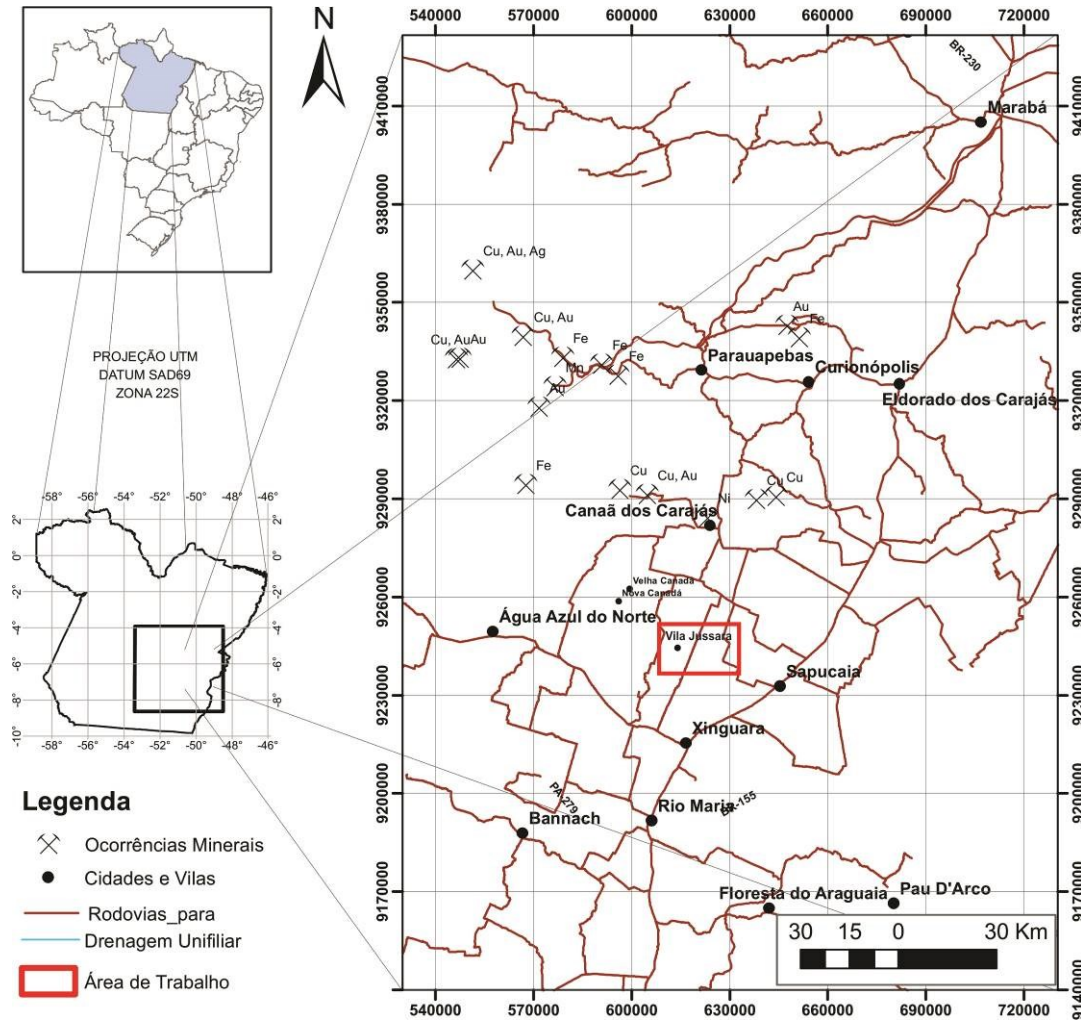


Figura 1 - Mapa de localização e principais acessos da área de estudo.

1.3 CONTEXTO GEOLÓGICO REGIONAL

A Província Carajás está situada na porção sudeste do Cráton Amazônico (Almeida *et al.* 1981) e faz parte do contexto geológico da Província Carajás (Santos 2003; Figura 2a) ou Amazônia Central (Tassinari & Macambira 1999, 2004; Figura 2b). A mesma é limitada a leste pelo Cinturão Araguaia, de idade neoproterozoica; a norte, pela Província Maroni-Itacaiúnas (segundo a proposta de Tassinari & Macambira 2004); a sul e a oeste é parcialmente coberta pelas sequências sedimentares fanerozoicas da Bacia Parecis e pelas rochas vulcânicas do Grupo Iriri. Após algumas tentativas de subdivisão da província em domínios tectônicos, Souza *et al.* (1996) propuseram que esta fosse dividida em dois blocos: Terreno Granito-Greenstone de Rio Maria (TGGRM) e Bloco Carajás. Mais recentemente, Vasquez *et al.* (2008), em revisão à geologia do Estado do Pará e seguindo a proposta de Santos (2003), propuseram a designação de domínios Rio Maria e Carajás para estes blocos. O primeiro, de idade mesoarqueana (3,0 - 2,87 Ga), comprehende as rochas mais antigas e de

características ígneas bem preservadas (Macambira & Lafon 1995, Althoff *et al.* 2000, Souza *et al.* 2001, Oliveira *et al.* 2011, Almeida *et al.* 2011, 2013). Já o segundo, seria formado por um embasamento mesoarqueano (3,0 - 2,85 Ga) intensamente retrabalhado e afetado por eventos tectonotermalis de idade neoarqueana (2,76 a 2,73 Ga) e representado por uma vasta sequência vulcanossedimentar e intrusões granitoides sintectônicas (Dall'Agnol *et al.* 2006, Feio *et al.* 2012, 2013).

A partir deste quadro, trabalhos realizados por pesquisadores do Grupo de Pesquisa Petrologia de Granitoides (GPPG-UFPa) mostraram que a área considerada como embasamento da Bacia Carajás, que se estenderia desde a borda sul da mesma até o limite com o TGGRM, não corresponderia a uma crosta arqueana tectonicamente homogênea, o que levou à adoção das denominações Subdomínio Canaã dos Carajás e Subdomínio Sapucaia para as porções norte e sul deste segmento da província, respectivamente (Dall'Agnol *et al.* 2013). Este último seria formado por granitoides tipo TTG, sanukitóides e leucogranitos diversos, análogos àqueles identificados no Domínio Rio Maria, sendo porém, afetados por eventos neoarqueanos. A seguir, serão apresentadas as principais unidades que formam a Província Carajás, de acordo com a mais recente divisão tectono-estratigráfica apresentada por Dall'Agnol *et al.* (2013).

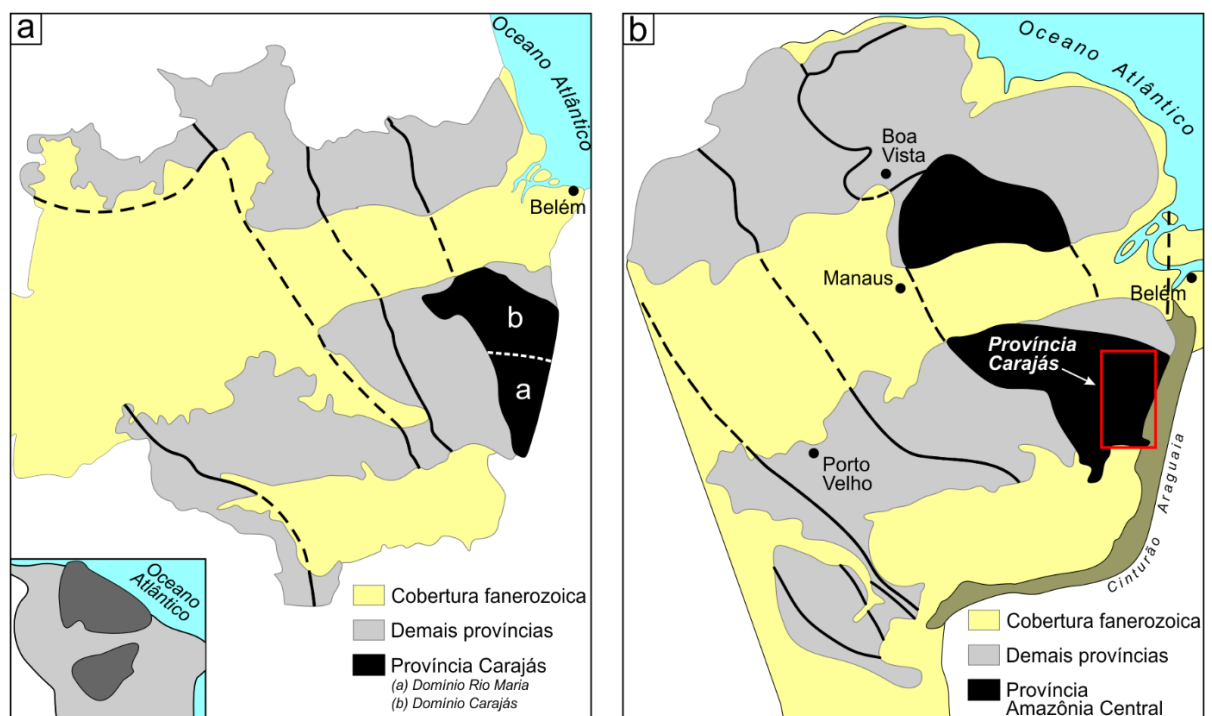


Figura 2 - Mapa de localização do Cráton Amazônico no continente sul-americano, evidenciando as províncias geocronológicas segundo (a) Santos (2003) e (b) Tassinari & Macambira (2004), com destaque para a Província Carajás.

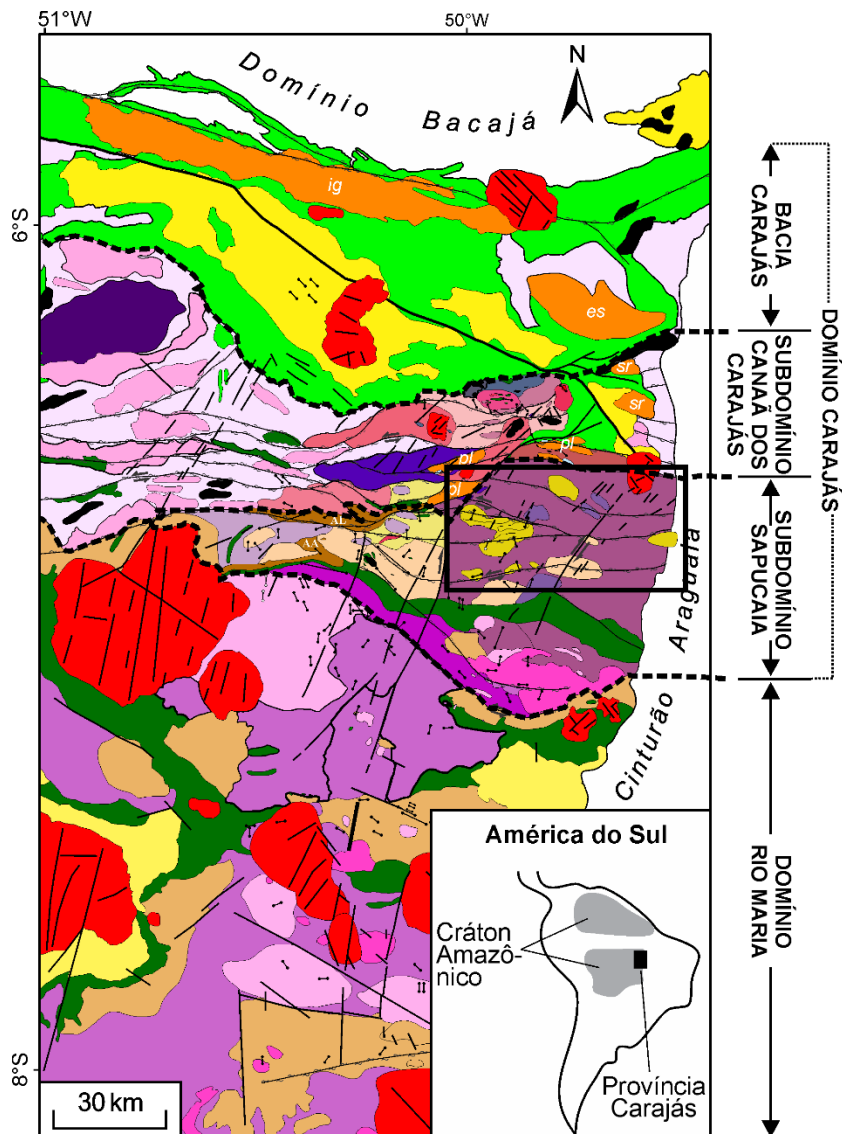
1.3.1 Domínio Rio Maria

O Domínio mesoarqueano de Rio Maria (Dall’Agnol *et al.* 2006) é caracterizado pelas associações *greenstone belts* do Supergrupo Andorinhas, com idade estimada de 3,0 a 2,9 Ga (Avelar 1996, Lafon *et al.* 2000, Macambira & Lancelot 1991, Pimentel & Machado 1994, Rolando & Macambira 2003, Souza *et al.* 2001), e Grupo Tucumã (Araújo & Maia 1991), além de diversos granitoides, similares àqueles caracterizados nos clássicos terrenos arqueanos, que são divididos em: (i) série TTG antiga (2,96–2,93 Ga), representada pelo Tonalito Arco Verde, Trondhjemito Mogno e Tonalito Mariazinha (Almeida *et al.* 2011, Macambira & Lafon 1995, Rolando & Macambira 2003). São batólitos de biotita tonalitos/trondhjemitos foliados (NW–SE a E–W), com exceção do Tonalito Mariazinha, que exibe orientação NE–SW e variações para N–S; (ii) granitoides de alto-Mg (sanukitoides), como o Granodiorito Rio Maria, de 2,87 Ga, e rochas associadas (Medeiros & Dall’Agnol 1988, Oliveira *et al.* 2009). Relacionadas a esta unidade, ocorrem ainda o Quartzo-Diorito Parazônia (Guimarães 2009) e o Granito Rancho de Deus (Dias 2009); (iii) Suíte Guarantã, de 2,87 a 2,86 Ga (Althoff *et al.* 2000), formada pelos leucogranodioritos-granitos de alto Ba-Sr dos plútons Guarantã, Trairão e Azulona (Almeida *et al.* 2011, Dias 2009). São rochas geoquimicamente similares aos TTG arqueanos (em termos de ETR), e distintos dos granitos de alto-K, e sua origem é interpretada a partir da mistura de magmas de composição trondhjemítica (TTG) e leucogranítica rico em Ba e Sr, derivadas de magmas sanukitoides (Almeida *et al.* 2011); (iv) Leucogranitos potássicos de afinidade cálcio-alcalina, de 2,87 Ga, caracterizados pelo granito Mata Surrão e corpos similares (Lafon *et al.* 1994). Os sedimentos do Grupo Rio Fresco (DOCEGEO 1988), recobrem parte do embasamento arqueano de Rio Maria. Posteriormente, este terreno foi intrudido por granitos tipo-A (1,88 Ga) e diques associados (Dall’Agnol *et al.* 2005, Dall’Agnol & Oliveira 2007).

Tabela 1. Síntese geocronológica do Domínio Rio Maria

DOMÍNIO RIO MARIA			
Unidades Estratigráficas	Tipo de Rocha	Idade em Zircão	Método
Granito Mata Surrão	Granito	2872±10 (1) 2875±11 (2) 2881±2 (2)	Evaporação de Pb
Suite Guarantã			
Granodiorito Trairão	Granodiorito	2869±12(3)	U-Pb LA-MC-ICPMS
	Granodiorito	2868±5 Ma (4)	Evaporação de Pb
Granito Guarantã	Granito	2870±5 Ma (5) 2864±8 Ma (3) 2870±16 Ma (3)	Evaporação de Pb Evaporação de Pb U-Pb LA-MC-ICPMS
Suite Rio Maria			
Granodiorito Rio Maria	Granodiorito	2874±9 Ma (6) 2872±5 Ma (7) 2877±6 Ma (2)	U-Pb LA-MC-ICPMS U-Pb LA-MC-ICPMS Evaporação de Pb
Rochas associadas	Quartzo-diorito Diorito	2878±4 Ma (8) 2880±4 Ma (2)	Evaporação de Pb
Quartzo Diorito Parazônia	Quartzo-diorito	2876±2 (9)	Evaporação de Pb
Granito Rancho de Deus	Granito	2898±27Ma (3)	U-Pb LA-MC-ICPMS
TTG's Antigos			
Tonalito Mariazinha	TTG	2925±3Ma (10) 2962±8Ma (10)	Evaporação de Pb Evaporação de Pb
Trondhjemito Mogno	Trondhjemito	2961±16Ma (10) 2972±9Ma (10) 2959±5Ma (10) 2932±3 (10) 2932±3Ma (10)	U-Pb LA-MC-ICPMS U-Pb LA-MC-ICPMS Evaporação de Pb
Tonalito Arco Verde	Tonalito	2941±5Ma (10) 2948±4Ma (10) 2961±14Ma (10) 2973±11Ma (10)	Evaporação de Pb
Greenstone Belts			
Complexo Serra Azul	-	2970±7 Ma (7)	U-Pb LA-MC-ICPMS
Grupo Tucumã	Vulcânica Félsica	2868±8 Ma (11)	Pb-Pb
Grupo Serra do Inajá	Fm. Quixadá	2988±4 Ma (2)	U-Pb LA-MC-ICPMS
Grupo Lagoa Seca	Metagrauvacas Metavulcânica	2904±29 Ma (12) 2979±5 Ma (12)	U-Pb LA-MC-ICPMS
Grupo Gradaús	Dacito	3002±3 Ma (13)	U-Pb LA-MC-ICPMS

(1) Lafon *et al.* 1994, (2) Rolando & Macambira (2003), (3) Almeida *et al.* 2013, (4) Almeida *et al.* 2008, (5) Althoff *et al.* (2000), (6) Macambira & Lancelot (1991), (7) Pimentel & Machado (1994), (8) Dall'Agnol *et al.* (1999), (9) Guimarães (2009), (10) Almeida *et al.* (2011), (11) Avelar *et al.* 1999, (12) Macambira & Lancelot 1996, (13) Tassinari *et al.* 2005.



Legenda

- ↗ Diques ↘ Falhas ↙ Zona de cisalhamento
- Área de estudo
- Granitos anorogênicos: 1,88 Ga

DOMÍNIO CANAÃ DOS CARAJÁS E BACIA CARAJÁS

- Cobertura sedimentar (formações Águas Claras e Gorotire)
- Suite Plaquê: 2,73 Ga
- Diopsidio-Norito Pium: 2,74 Ga
- Intrusões máficas-ultramáficas (Complexo Luanga e Suite Cateté): 2,76 Ga
- Granitos subalcalinos: Complexo granítico Estrela (es), Suite Planalto (pl) e granitos Serra do Rabo (sr) e Igarapé Gelado (ig): 2,76 - 2,73 Ga
- Suíte Pedra Branca: 2,76 Ga
- Supergrupo Itacaiúnas: 2,77 - 2,73 Ga
- Granito Bom Jesus: 2,83 Ga
- Granito Cruzadão: 2,84 Ga
- Granito Boa Sorte: 2,85 Ga
- Granito Serra Dourada: 2,86 - 2,83 Ga
- Complexo tonalítico Campina Verde: 2,87 - 2,83 Ga
- Trondjemito Rio Verde: 2,96 - 2,93 Ga
- Granito Canaã dos Carajás: 2,96 - 2,93 Ga
- Complexo Xingu: 2,97 - 2,85 Ga
- Tonalito Bacaba: 3,0 Ga
- Ortogranulito Chicrim-Cateté: 3,0 Ga

DOMÍNIO SAPUCAIA

- Leucogranito Velha Canadá: 2,74 Ga
- Suite Vila Jussara: 2,74 Ga
- Leucogranito potássico (Granito Xinguara): 2,86 Ga
- Leucogranodiorito/granito de alto Ba-Sr (leucogranodioritos Nova Canadá e Pantanal): 2,87 Ga
- TTG mais jovens (trondjemitos Água Fria e Colorado): 2,87 - 2,86 Ga
- Sanukitoide (granodioritos Água Azul e Água Limpa): 2,88 Ga
- Tonalito São Carlos: 2,93 Ga
- TTG mais antigo (Tonalito Caracol): 2,93 Ga
- Greenstone belt (Grupo Sapucaia)

DOMÍNIO RIO MARIA

- Cobertura metassedimentar (Grupo Rio Fresco)
- Leucogranito potássico (Granito Mata Surrão): 2,87 Ga
- Suite granítica/leucogranodiorítica de alto Ba-Sr (Suite Graranã): 2,87 - 2,86 Ga
- Suite sanukitoide Rio Maria: 2,87 Ga
- TTG (tonalitos Arco Verde e Mariazinha, e trondjemito Mogno): 2,98 - 2,92 Ga
- Greenstone belts (Supergrupo Andorinhas): 2,97 - 2,90 Ga

Figura 3 - Mapa geológico da Província Carajás (modificado de Gabriel *et al.* 2014), mostrando a mais recente compartmentação tectônica segundo Dall'Agnol *et al.* (2013; linhas tracejadas).

1.3.2 Subdomínio Sapucaia

O conhecimento sobre a geologia do Subdomínio Sapucaia é recente e os estudos realizados na região de Água Azul do Norte levaram ao atual quadro geológico: (i) *greenstone belts* do Grupo Sapucaia, caracterizadas por rochas metamáficas, metaultramáficas e metassedimentares (Costa *et al.* 1994, DOCEGEO 1988); (ii) Tonalito Caracol, de 2,93 Ga (Almeida *et al.* 2011, Leite *et al.* 2004), que ocorre como uma estreita faixa NW–SE a norte do Domínio Rio Maria; (iii) Tonalito São Carlos, de idade 2,93 Ga, que é constituído de anfibólio-biotita tonalitos, distintos daqueles da série TTG, e sanukitoides arqueanos (Silva *et al.* 2014); (iv) granodioritos Água Azul e Água Limpa, de afinidade sanukitoide, com idade Pb-Pb de 2,88 Ga (Gabriel *et al.* 2010, Sousa *et al.* 2010); (v) trondjemitos Água Fria, de 2,86 Ga (Leite 2001, Leite *et al.* 2004) e Colorado, de ~2,87 Ga (Silva *et al.* 2014); (vi) Granito Xinguara, de afinidade cálcio-alcalina e alto-K, que apresenta idade Pb-Pb em zircão de 2,86 Ga (Leite *et al.* 2004), e ocorre intrusivo no Complexo Tonalítico Caracol e Granodiorito Rio Maria e, segundo Leite (2001), tem origem relacionada à fusão parcial de rochas tipo TTG. Esta unidade foi recentemente desvinculada do Domínio Rio Maria (Dall'Agnol *et al.* 2013) em função de seu padrão deformacional muito similar às rochas do Domínio Sapucaia; (vii) leucogranodioritos-granitos de alto Ba-Sr, similares à Suíte Guarantã, foram recentemente descritos no Domínio Sapucaia. Eles estão representados pelos corpos do Leucogranodiorito Nova Canadá (Leite-Santos & Oliveira 2014) e Leucogranodiorito Pantanal (Teixeira *et al.* 2013); (viii) granitos neoarqueanos, representados pelo leucogranito de alto-K Velha Canadá (2,74 Ga; Leite-Santos *et al.* 2016, Santos *et al.* 2010) e granitos subalcalinos agrupados na Suíte Vila Jussara (2,75–2,73 Ga; Dall'Agnol *et al.* 2017; Silva *et al.* 2020).

Tabela 2. Síntese geocronológica do Domínio Sapucaia

Unidades Estratigráficas	Tipo de Rocha	Idade em Zircão	Método
Granito Xinguara	Leucomonzogranito	2865±1 Ma (1)	Pb-Pb
Trondjemito Água Fria	Trondjemito	2843±10 (2)	U-Pb ICP
Trondjemito Colorado	Trondjemito	2864±21 (1)	Pb-Pb
		2872±2 (3)	Pb-Pb
Sanukidoite Água Azul	Granodiorito	2884±2 Ma (4)	Pb-Pb
		2879±1 Ma (5)	
Granodiorito Água Limpa	Granodiorito	2879±1 (5)	Pb-Pb TIMS
Tonalito Caracol	Tonalito	2936±3 (1)	Pb-Pb
Leucogranito Velha Canadá	Granodiorito	2948±5 (1)	
		2733±1 (6)	Pb-Pb TIMS
		2747±2 (6)	Pb-Pb TIMS
Suíte Vila Jussara	Bit-Anf Monzogranito	2754±2 Ma (7)	Pb-Pb TIMS
	Biotita Granodiorito	2749±3 Ma (7)	Pb-Pb TIMS
	Bit Anf Tolanito	2752±5 Ma (7)	Pb-Pb TIMS

(1) Leite *et al.* (2004); (2) Almeida *et al.* (2011); (1) Leite *et al.* (2004); (3) Silva A.C *et al.* (2010); (4) Sousa *et al.* (2010); (5) Gabriel *et al.* (2010); (6) Santos P.J.L. *et al.* (2010); (7) Silva *et al.* 2020

1.3.3 Subomínio Canaã dos Carajás e Bacia Carajás

O Complexo Xingu foi o nome utilizado inicialmente para denominar uma associação litológica heterogênea constituída por gnaisses, migmatitos, granitoides variados, rochas supracrustais tipo *greenstone belt*, e complexos básicos a ultrabásicos (Araújo & Maia 1991, Cordeiro & Saueressig 1980, DOCEGEO 1988, Ianhez *et al.* 1980, Medeiros Filho & Meireles 1985, Silva *et al.* 1974), com idade 2972±16 Ma em granodiorito na região de Tucumã (Avelar *et al.* 1999), e 2859±4 Ma em metagranitoides na região de Curionópolis (Machado *et al.* 1991), idade esta interpretada como de metamorfismo.

O avanço do conhecimento sobre a geologia deste complexo permitiu o reconhecimento de que, na verdade, a unidade carecia de dados para individualização, o que levou ao abandono do termo ‘Complexo Xingu’ no Domínio Bacajá (Macambira *et al.* 2001, Vasquez *et al.* 2008) e no Domínio Rio Maria (Dall’Agnol *et al.* 2006, Leite 2001, Vasquez *et al.* 2008), ficando restrito apenas aos domínio Sapucaia e Canaã dos Carajás, os quais trabalhos recém desenvolvidos mostraram que o Complexo Xingu, nesta região, também está passível de individualização em novas unidades (Dall’Agnol *et al.* 2017, Feio *et al.* 2013, Gabriel & Oliveira 2014, Leite-Santos & Oliveira 2016, Moreto *et al.* 2011, 2015, Oliveira *et al.* 2018, Rodrigues *et al.* 2014). Dados geocronológicos recentes indicam idades de 2950 ± 25 Ma e 2857±6,7 Ma atribuídas à cristalização dos protólitos e metamorfismo, respectivamente, de gnaisses do Complexo Xingu na área do Depósito de Cu do Salobo (Melo

et al. 2014), além daquelas definidas por Delinardo *et al.* (2014, 2015) em ortopiroxênio-diopsídio gnaisses, que atribui essas rochas à unidade Ortogranulito Chicrim-Cateté, que apontam para idades de cristalização do protólito obtidas em zircão (U-Pb SHRIMP e LA-MC-ICP-MS) entre 3,06 e 2,93 Ga, posteriormente metamorfizados entre 2,89 e 2,83 Ga, sob fácies granulito em condições de ultra alta temperatura. O Granulito Ouro Verde possui idade de cristalização entre 3,06-2,93 Ga, e de metamorfismo entre 2,89-2,84 (Pidgeon *et al.* 2000, Machado *et al.* 1991, Maragoanha *et al.* 2019b). Os granulitos félscicos do Granulito Ouro Verde têm composição tonalítica/trondhjemítica e caráter sódico (Marangoanha *et al.* 2019b). Juntas estas unidades representam o embasamento metamórfico do Domínio Carajás (Hirata *et al.* 1982, Pidgeon *et al.* 2000, Machado *et al.* 1991 Marangoanha *et al.* 2019b).

As unidades granitoides são representadas pelo Tonalito Bacaba de 3,0 Ga (Moreto *et al.* 2011), caracterizado por tonalitos de granulação fina, faneríticos, com hornblenda e biotita como principais minerais máficos, hidrotermalmente alterados. O Granito Sequeirinho apresenta coloração cinza claro, textura equigranular e porfirítica, de granulação fina a média, com idade de 3,0 Ga (Moreto *et al.* 2015). O Granito Canaã dos Carajás, de idade 2959 ± 6 Ma (Feio *et al.* 2013) é caracterizado por leucogranitos fortemente deformados, de assinatura cálcio-alcalina e afinidade sódica, que foram afetados por zonas de cisalhamento E-W e NE-SW. O Trondhjemito Rio Verde, datado em 2929 ± 3 Ma e 2868 ± 4 Ma (Feio *et al.* 2012), é composto por rochas foliadas e com bandamento composicional, e são geoquimicamente similares aos típicos TTG arqueanos. O Complexo Tonalítico Campina Verde, datado em 2872 ± 1 Ma e 2850 ± 7 Ma (Feio *et al.* 2013) é representado por duas associações litológicas distintas: biotita tonalitos a granodioritos, com dioritos e monzogranitos subordinados; e biotita-hornblenda tonalitos, com granodioritos e monzogranitos subordinados. Geoquimicamente, estas rochas são distintas dos típicos TTG arqueanos, e definem uma série cálcio-alcalina expandida (Feio *et al.* 2013). O Granito Cruzadão (Feio *et al.* 2013), composto por leucogranitos deformados, segundo o *trend* NW-SE e E-W, têm assinatura geoquímica transicional entre as séries cálcio-alcalina e alcalina, e admite-se 2845 ± 15 Ma como idade mínima de cristalização. O granito Boa Sorte (Rodrigues *et al.* 2014) é representado por biotita monzogranitos de assinatura cálcio-alcalina, fortemente fracionado, e idade de cristalização em torno de 2,85 Ga. O granito Bom Jesus é formado por monzo- e sienogranitos foliados e bandados, com orientação NE-SW e E-W. São rochas cálcio-alcalinas com idade mínima de cristalização em 2833 ± 6 Ma (Feio *et al.* 2013). O Granito Serra Dourada (Feio *et al.* 2013, Moreto *et al.* 2011) é caracterizado por leucomonzogranitos com granulação média a grossa, deformado, com foliação vertical E-W, e de assinatura cálcio-alcalina, datado em 2,86

Ga (Moreto *et al.* 2011) e 2,83 Ga (Feio *et al.* 2013).

O Supergrupo Itacaiúnas é formado por rochas metavulcanossedimentares que ocupam parte da Bacia Carajás, e representado pelos grupos Igarapé Salobo, Grão-Pará, Igarapé Bahia, Igarapé Pojuca e Buritirama (DOCEGEO 1988). Machado *et al.* (1991) admitem idades em torno de 2,76 Ga para as rochas desata unidade. O magmatismo máfico-ultramáfico neoarqueano é formado por pequenos corpos intrusivos no embasamento mesoarqueano da porção norte da Província Carajás. Seus principais representantes são: (i) Suíte Cateté (Macambira & Vale 1997), composta por gabros, noritos, piroxenitos, serpentinitos e peridotitos, alongados e alinhados preferencialmente segundo as direções E–W e N–S; (ii) Complexo Intrusivo Luanga, representado por rochas ultrabásicas e básicas acamadas, que ocorrem próximo à Serra Pelada (Jorge João *et al.* 1982, Medeiros Filho & Meireles 1985); (iii) Gabro Santa Inês (DOCEGEO 1988, Meireles *et al.* 1984, Pinheiro 1997), que expõe-se como um corpo constituído por gabros porfíriticos, leucogabros, microgabros e anortositos, de fraca foliação, e alongado segundo NE–SW, no extremo oeste do Domínio Carajás.

A Suíte Pedra Branca (Feio *et al.* 2013) é composta por granitoides sódicos de assinatura toleítica, e ocorrem associados aos granitos da Suíte Planalto, na região de Canaã dos Carajás, que apresentam idade U–Pb 2,76 Ga (TIMS; Sardinha *et al.* 2004) e 2,75 Ga (Feio *et al.* 2013). O Diopsídio-Norito Pium é localizado na porção central do domínio, e é representado por um grande corpo de direção E–W. Segundo Ricci & Carvalho (2006) e Vasquez *et al.* (2008), essa unidade é composta por noritos, gabronoritos, hornblenda gabronoritos e hornblenda gabros, com idade de cristalização de 2746 ± 1 Ma (Santos *et al.* 2013).

O embasamento mesoarqueano e as rochas supracrustais da Bacia Carajás são cortados por granitoides subalcalinos sin-tectônicos do Neoarqueano, representados pelo Complexo Granítico Estrela, de 2,76 Ga (Barros *et al.* 2001, 2009) e pelos granitos Serra do Rabo (2,74 Ga; Barros *et al.* 2009, Sardinha 2002), Igarapé Gelado (2,73 Ga; Barbosa 2004, Barros *et al.* 2009), Sossego e Curral (2,74; Moreto *et al.* 2015). Os granitos da Suíte Planalto (Dall'Agnol *et al.* 2013, Feio *et al.* 2012, Gomes 2003, Hühn *et al.* 1999, Oliveira *et al.* 2010) são formados por sieno- a monzogranitos, com proporções variadas de biotita e hornblenda, apresentam características geoquímicas similares aos de granitos tipo-A, e idades que variam entre 2,74 e 2,71 Ga.

A Suíte Plaquê é caracterizada por uma série de muscovita-biotita leucogranitos peraluminosos, estratoides e alongados segundo o *trend* E–W (Araújo *et al.* 1988, Jorge João & Araújo 1992), datados em 2,73 Ga (Avelar *et al.* 1999). Acredita-se que sua ocorrência

tenha sido superestimada, já que, ao longo dos anos, diversos trabalhos de caracterização destes granitoides apontam para anfibólio-biotita granitos afins daqueles que constituem a Suíte Planalto, o que colocou em xeque o real significado da Suíte Plaquê (Feio *et al.* 2012, Gomes 2003, Oliveira *et al.* 2010).

Sobrepostas ao Supergrupo Itacaiúnas, ocorrem as rochas sedimentares da Formação Águas Claras, que são divididas estratigraficamente, com base nas diferenças litológicas e ambientes de formação (Nogueira *et al.* 1995): (i) membro inferior, formado por pelitos, siltitos e arenitos, possivelmente depositados em plataforma marinha; e (ii) membro superior, caracterizado por arenitos litorâneos (parte inferior), e fluviais (parte superior). Embora sua idade seja bastante controversa, alguns autores ainda consideram essa unidade como arqueana, sendo posicionada no topo do Grupo Grão-Pará (Pinheiro & Holdsworth 2000).

Os granitos anorogênicos da Suíte Serra dos Carajás são similares àqueles afins já descritos na província, particularmente no Domínio Rio Maria, mas apresentam peculiaridades geoquímicas que sugerem fontes e história de cristalização distintos dos demais (Dall'Agnol *et al.* 1994). São representados pelos granitos Central, Carajás, Cigano, Pojuca, Rio Branco e Gogó da Onça (Dall'Agnol *et al.* 2006, Santos *et al.* 2013, Teixeira *et al.* 2017).

Tabela 3. Síntese geocronológica das principais unidades do Domínio Canaã dos Carajás e Bacia Carajás.

Unidades Estratigráficas	Tipo de Rocha	Idade em Zircão	Método
Enderbito Café	Tonalito	2743 ±13 (1)	U-Pb SHRIMP
	Trondjemito	2730 ±7 (1)	U-Pb LAICPMS
Norito Pium	Quartzo gabbro	2735 ±5 (2)	U-Pb LA-ICP-MS
	Granito	2744 ±1 (3)	Pb-Pb TIMS
Granito velho salobo	Granito	2547 ± 5 (4)	U-Pb SHRIMP
	Leucogranito	2747 ±2 (5)	Pb-Pb TIMS
Leucogranito Velha Canada	Granito	2706 ±5 (6)	U-Pb LA-ICP-MS
	Granito	2710 ±10 (2)	U-Pb LA-ICP-MS
Suíte Planalto	Granito	2729 ±29 (7)	Pb-Pb TIMS
	Granito	2730 ±5 (7)	U-Pb SHRIMP
Suíte Plaquê		2731 ±26 (8)	Pb-Pb TIMS
	Granito	2731.9 ±0.8 (9)	Pb-Pb TIMS
Igarapé Gelado		2734 ±4 (10)	Pb-Pb TIMS
	Granito	2743 ±2 (11)	U-Pb TIMS
Granito Serra do Rabo	Leucomonzogranito	2744 ±5 (12)	U-Pb SHRIMP
	Granito	2747 ±1 (12)	Pb-Pb TIMS
Suite Vila União	Granito	2763 ±7 (13)	Pb-Pb TIMS
	anfibolito	2732 ±3 (14)	U-Pb LA-ICP-MS
Complexo Estrela	metavulcânica	2745 ±1 (15)	U-Pb LA-ICP-MS
	basalto	2745 ±5 (16)	U-Pb SHRIMP
Supergrupo Itacaiúnas (Greenstones)	metavulcânica	2748 ±34 (17)	U-Pb SHRIMP
	basalto	2749 ±6,5 (16)	U-Pb SHRIMP
Granulito Ouro Verde	Granulito máfico	2844 ±7,8 Ma (1)*	U-Pb SHRIMP
	Granulito felsico	2853 ±19 Ma (11)*	U-Pb SHRIMP
	Granulito felsico	2865 ±11 Ma (1)*	U-Pb SHRIMP
	Granulito máfico	2870 ±4,9 Ma (1)*	U-Pb SHRIMP
	Leucosoma	2873 ±53 Ma (18)*	U-Pb LA-ICP-MS
	Granulito máfico	2890 ±7 Ma (18)*	U-Pb LA-ICP-MS
	Granulito felsico	2935 ±8 Ma (18)	U-Pb LA-ICP-MS
	Granulito felsico	2946 ±19 Ma (1)	U-Pb SHRIMP
Granulito Ouro Verde	Granulito felsico	2950 ±8,4 Ma (1)	U-Pb SHRIMP
	Granulito felsico	3055 ±9 Ma (1)	U-Pb SHRIMP
Granulito Ouro Verde	Granulito felsico	3066 ±7 Ma (1)	U-Pb SHRIMP
Granito Canaã dos Carajás	Leucomonzogranito	2928 ±1 Ma (19)	Pb-Pb
		2959 ±6 Ma (2)	U-Pb LA-MC-ICPMS
Complexo Tonalítico Bacaba		2993 ±7 Ma (20)	
	Tonalito	2997 ±5 Ma (20)	U-Pb LA-MC-ICPMS
Complexo tonalítico Campina Verde		3005 ±8 Ma (20)	
	Granodiorito	2820 ±22 Ma (2)	U-Pb LA-MC-ICPMS
Trondjemito Rio Verde	Granodiorito	2869 ±4 Ma (2)	U-Pb LA-MC-ICPMS
	Bt trondjemito	2929 ±3 Ma (2)	Pb-Pb
Complexo tonalítico Campina Verde	Bt trondjemito	2923 ±15 Ma (2)	Pb-Pb
	Tonalito	2849 ±18 (2)	U-Pb LA-ICP-MS
		2850 ±7 (2)	U-Pb LA-ICP-MS

*são consideradas como idade de metamorfismo. (1) Marangoanha *et al.* (2019a); (2) Feio *et al.* (2013); (3) Santos *et al.* (2013); (4) Melo *et al.* (2016); (5) Leite-Santos (2016); (6) Feio *et al.* (2012); (7) Avelar *et al.* (1999); (8) Barbosa (2004); (9) Galarza *et al.* (2017); (10) Sardinha (2002); (11) Sardinha *et al.* (2006); (12) Marangoanha *et al.* (2019b); (13) Barros *et al.* (2004); (14) Machado *et al.* (1991); (15) Galarza *et al.* (2008); (16) Martins *et al.* (2017); (17) Tallarico *et al.* (2005); (18) Delinardo Silva (2021); (19) Sardinha *et al.* 2004; (20) Moreto *et al.* (2010)

1.4 APRESENTAÇÃO DO PROBLEMA

A porção norte da Província Carajás é caracterizada pela dominância de granitos *stricto sensu* (associações mesoarqueanas e granitos neoarqueanos da Suíte Planalto) e associações charnoquíticas (Diopsídio-Norito Pium, Trondjemita Pedra Branca e Enderbito Café), sendo que as relações de campo entre as associações neoarqueanas ainda são pouco conclusivas (Feio *et al.* 2012, Galarza *et al.* 2017, Moreto *et al.* 2011, 2015, Oliveira *et al.* 2018, Santos *et al.* 2013, Marangoanha *et al.* 2020). Neste contexto, os granitoides reduzidos do tipo A da Suíte Vila Jussara apresentam, em linhas gerais, características semelhantes às da Suíte Planalto estudadas por Feio *et al.* (2012). Por sua vez, Dall’Agnol *et al.* (2017) mostram que a afinidade geoquímica é menor no caso das variedades de granitoides tipo A oxidados e magnesianos. Além disso, há evidências de que processos magmáticos envolvendo mistura de líquidos gerados em diferentes condições de fO_2 (ferrosos reduzidos e oxidados e magnesianos), e provavelmente com fontes distintas, possam ter ocorrido de forma mais expressiva nos plútôns de Vila Jussara do que se estimava inicialmente. Dentre as principais evidências que sugerem a formação destes plútôns a partir da coalescência de diferentes pulsos de magma, destacam-se: contatos irregulares e difusos entre diferentes variedades litológicas; enclaves parcialmente reabsorvidos de tonalito em granitos e granodioritos; ocorrência frequente de fenocristais de K-feldspato em enclaves maficos; e presença de textura rapakivi. Apesar das similaridades existentes entre as rochas que formam as suítes Planalto e Vila Jussara, os processos e diferentes tipos de granitoides identificados permitem supor que esta última possui origem e evolução mais complexa do que aquela atribuída aos demais granitos neoarqueanos que ocorrem nesta porção da província. Isto torna ainda mais relevante o aprofundamento dos estudos que procuram compreender a contribuição dos processos que envolvem mistura de magmas de diferentes composições (múltiplas injeções) na formação da Suíte Vila Jussara.

A utilização de dados isotópicos possibilitará estimar possíveis fontes para estes magmas, bem como confrontar as hipóteses assumidas com modelos adotados na literatura que discutem a origem de granitos análogos na região de Carajás e em outros cráticos. Para isso, se faz necessária a realização de mapeamento geológico detalhado nas áreas de ocorrência das rochas da Suíte Vila Jussara, o refinamento de idades de cristalização U-Pb em zircão em alguns corpos desta suíte, assim como a obtenção de dados isotópicos de Sm-Nd, Lu-Hf, para que se possam discutir as prováveis fontes dos magmas e estimar o período de sua separação das rochas fonte. A obtenção e interpretação destes dados permitirá um avanço

significativo para a compreensão dos processos que levaram à formação e estabilização da crosta arqueana dessa região e poderá auxiliar no melhor entendimento da nova proposta de compartimentação tectônica do Domínio Carajás.

Com base no exposto acima, listam-se as principais questões a serem respondidas para que se possa propor um modelo petrológico para origem e evolução dos granitos neoarqueanos da área de Vila Jussara:

- (1) Quais as características petrográficas e assinaturas geoquímicas dos magmas que deram origem aos granitos da Suíte Vila Jussara? Os vários corpos de granitos neoarqueanos subalcalinos podem ser enquadrados em uma única suíte? Esses granitos podem ser correlacionados aos demais granitos neoarqueanos já estudados na Bacia Carajás (granitos Estrela, Serra do Rabo e Igarapé Gelado) e na área de Canaã dos Carajás (suíte Planalto e Vila União)?
- (2) Devido à grande variação composicional dessas rochas (granitoides ferrosos reduzidos e oxidados e cálcico-alcalinos magnesianos), quais processos petrológicos foram determinantes na gênese e evolução dos magmas da Suíte Vila Jussara? Qual o papel de processos de mingling e mixing entre magmas versus cristalização fracionada? Os magmas geradores da suíte seriam produto de fusão do embasamento mesoarqueano com possível mistura de magmas derivados de fontes distintas ou os processos seriam mais complexos e envolveriam participação de líquidos mantélicos? Qual o papel dos líquidos cálcico-alcalinos ou magnesianos na origem e evolução da suíte?
- (3) As rochas aflorantes na área de pesquisa, assim como aquelas das demais regiões dos domínios Canaã dos Carajás e Sapucaia, encontram-se em geral moderadamente a intensamente recristalizadas. Tal aspecto é resultado da atuação de processos no estágio *subsolidus* ligados à colocação de seus magmas ou representam efeitos de metamorfismo regional superimposto? Quais suas implicações para a evolução do Domínio Canaã dos Carajás;
- (4) Em que cenário geológico-tectônico se deu a formação e evolução das rochas da área de Vila Jussara? Qual o seu papel dentro do contexto evolutivo da Província Carajás?

1.5 OBJETIVOS

Tendo em vista os problemas assinalados e discutidos no item anterior, esse trabalho visa contribuir para a definição dos processos envolvidos na formação e evolução dos magmas das Suíte Vila Jussara, a partir da caracterização isotópica de suas principais

variedades e refinamento de suas idades de cristalização, bem como da definição de suas rochas fonte. Pretende-se dessa forma, contribuir para o avanço do conhecimento sobre a evolução tectônica e magmática da Província Carajás e esclarecer o real significado dessa suíte no contexto do Sudomínio Sapucaia. Para tanto deverão ser atingidos os seguintes objetivos específicos:

- (1) Mapear a distribuição das principais variedades granitoides da Suíte Vila Jussara, e caracterizar as relações entre elas;
- (2) Esclarecer a história deformacional deste segmento do Domínio Sapucaia, enfatizando os processos de colocação e deformação dos granitoides nele mapeados;
- (3) Reavaliar os contrastes e afinidades existentes entre a Suíte Vila Jussara e os demais granitos neoarqueanos de áreas adjacentes;
- (4) Definir os processos petrológicos envolvidos na evolução dos corpos da Suíte Vila Jussara (cristalização fracionada ± assimilação ou mistura de magmas, ou associação entre eles) e a maneira como se dá a possível interação entre diferentes líquidos;
- (5) Refinar os dados geocronológicos e definir com mais rigor as idades de cristalização\colocação dos corpos;
- (6) Definir as assinaturas isotópicas de seus magmas e identificar a(s) sua(s) fonte(s), além de propor um modelo tectono-magmático que discuta a origem dos mesmos.

1.6 MATERIAIS E MÉTODOS

1.6.1 Pesquisa bibliográfica

Foi realizado levantamento bibliográfico referente à geologia da Província Carajás, principalmente relacionado à granitogênese neoarqueana da província e às rochas mesoarqueanas do Domínio Canaã dos Carajás, além de temas específicos relacionados à evolução crustal, petrogênese, geologia estrutural, microtexturas e microestruturas, metamorfismo, geoquímica, geocronologia, geoquímica isotópica dos sistemas Sm-Nd e Lu-Hf, e granitoides arqueanos.

1.6.2 Mapeamento geológico e estrutural

Foi realizada uma etapa de campo para o adensamento de amostragem das litologias (para estudos petrográfico, microestrutural, geoquímico, geocronológico e isotópico) e de suas feições estruturais. Além desses, foram utilizados bancos de dados do Grupo de Pesquisa

Petrologia de Granitoides, da Universidade Federal do Pará (GPPG/UFPA) adquiridos em etapas de campo realizadas entre os anos de 2010 e 2014. Nessas etapas de campo, foram realizados trabalhos de cartografia geológica, com mapeamento na escala 1:220.000 da área, através de perfis transversais à estruturação regional dominante, dando ênfase aos levantamentos de dados estruturais em afloramentos específicos, relações de contato, feições deformacionais atribuídas à atuação de zonas de cisalhamento e outras feições estruturais relevantes. Utilizou-se para isso, imagens de radar SRTM (*Shuttle Radar Topography Mission*), com resolução de 15 metros (banda C), imagens de satélite (Landsat TM e *Google Earth*) e imagens com dados aerogeofísicos (magnetometria e aerogamaespectrometria) levantados pelo Serviço Geológico do Brasil (CPRM) devidamente processados em ambiente SIG. Foram utilizados bússola e, para localização das amostragens, GPS (*Global Position System*) com precisão de aproximadamente 3 metros, com os pontos locados em base georreferenciada.

1.6.3 Análise petrográfica e microestrutural

A partir da análise macroscópica preliminar das amostras coletadas em campo, representativas das diferentes unidades estudadas, foram feitas posterior seleção e confecção de 90 lâminas delgadas ou polidas para o estudo em microscópio petrográfico em luz transmitida, visando: identificação dos minerais (Deer *et al.* 1992, Kerr 1959) e descrição sistemática; estudo das texturas magmáticas, metamórficas, deformacionais e de alteração (Hibbard 1995, Passchier & Trouw 2005, Yardley *et al.* 1990); estimativa da ordem de cristalização dos minerais (Dall'Agnol 1982, Hibbard 1995); obtenção de composições modais (Chayes 1956, Hutchison 1974) com contador automático de pontos Stageledge, da marca Endeeper (entre 1.500 e 2.000 pontos por amostra); e classificação das rochas conforme estabelecido pela IUGS (Le Maître *et al.* 2002).

1.6.4 Geoquímica

Após prévia seleção petrográfica, um total de 61 amostras representativas dos diferentes litotipos foram escolhidas para realização de análises litogeoquímica. As amostras selecionadas para as análises foram trituradas, pulverizadas, homogeneizadas e quarteadas na Oficina de Preparação de Amostras (OPA) do Instituto de Geociências (IG) da Universidade Federal do Pará (UFPA). Tais análises foram realizadas nos laboratórios comerciais Acme Analytical Laboratories Ltd. (Canadá) e ALS Geochemistry Laboratories (Brasil), sendo os

elementos maiores e menores (SiO_2 , TiO_2 , Al_2O_3 , Fe_2O_3^* , MnO , MgO , CaO , Na_2O e P_2O_5) analisados por ICP-AES (*Inductively Coupled Plasma – Atomic Emission Spectrometry*), enquanto que os elementos traço (Ba, Rb, Sr, Zr, Nb, Y, Hf, Ta e Th), incluindo os elementos terras raras (La, Ce, Pr, Nd, Sm, Eu, Gd, Tb, Dy, Ho, Er, Tm, Yb e Lu), foram analisados por ICP-MS (*Inductively Coupled Plasma - Mass Spectrometry*). Os dados obtidos permitiram realizar a caracterização geoquímica, com base nos procedimentos indicados em Ragland (1989) e Rollinson (1993), e diagramas elaborados com auxílio do programa GCDkit (Janoušek *et al.* 2003).

Tais dados geoquímicos obtidos, associados aos dados de química mineral disponíveis na literatura, também foram utilizados em modelagem geoquímica com o objetivo de definir os processos que controlaram a evolução magmática dos granitoides e dos protólitos dos granulitos estudados (fusão parcial, cristalização fracionada, mistura de magmas, assimilação etc.). Para isso, utilizou-se o programa GENESIS 4.0 desenvolvido por Teixeira (2005) para modelagem de elementos maiores, além de planilhas no programa EXCEL (Microsoft) desenvolvidas pelo autor da tese para modelagem de elementos traço.

1.6.5 Geocronologia

Ao total, foram feitas 4 análises geocronológicas por meio dos métodos U-Pb em zircão (*in situ*) obtidas pelos sistemas SHRIMP IIe (*Sensitive High Resolution Ion Microprobe*), no Laboratório de Geologia de Alta Resolução da Universidade de São Paulo (GeoLab/USP).

Em torno de 10 a 20 kg de cada amostra representativa foram trituradas, moídas e peneiradas nas frações 125–175 ou 75–125 μm , realizadas na Oficina de Preparação de Amostras (OPA) e no Laboratório de Preparação Mineral (LPM), ambos na UFPA. Os cristais de zircão foram separados por meio de líquido pesado (bromofórmio) e separador magnético isodinâmico do tipo *Frantz*. Entre 60 e 80 cristais de zircão de cada amostra foram selecionados com o auxílio de lupa binocular e, em seguida, montados em um disco de epóxi em conjunto com os padrões analíticos, polidos até a metade de sua espessura a fim de expor o interior dos cristais, e revestida com uma película de carbono. Antes das datações com o método U-Pb, foram examinadas estruturas internas, sobrecrescimentos, fraturas, inclusões e defeitos físicos dos cristais, utilizando imagens de elétrons retroespalhados (BSE – *Backscattered Electron Images*) e catodoluminescência (CL – *Cathodoluminescence*), obtidas pela microssonda eletrônica modelo JEOL JXA-8230, do Laboratório de Microanálises da

UFPA, operando sob condições de voltagem de aceleração de 15 kV e corrente do feixe de 20 μA , com distância de trabalho de 11 mm.

As análises realizadas pelo sistema SHRIMP IIe seguem os procedimentos analíticos segundo Stern (1998), Williams (1998) e Sato *et al.* (2008, 2014), e os padrões utilizados são SL 13 para a composição referência do U (238 ppm; Sato *et al.* 2014), e o zircão TEMORA-2 ($416,78 \pm 0,33$ Ma; Black *et al.* 2003) para razões isotópicas padrão. O *spot* apresenta tamanho de 30 μm . Os dados foram reduzidos utilizando o *software* SQUID 1.03 (Ludwig 2001) e as idades calculadas usando Isoplot 4.15 (Ludwig 2008). Os erros da razão isotópica são 1σ .

1.6.6 Análise isotópica Lu-Hf

Das amostras com idades obtidas por U-Pb, 4 foram selecionadas para aquisição de dados pelo método isotópico Lu-Hf (3 Anfibolio-biotita Monzogranitos oxidado e reduzido e 1 granitoide híbridos), cuja análise pontual foi feita preferencialmente no mesmo sítio ou no mesmo domínio de idade concordante do zircão. As análises isotópicas de Hf foram realizadas no Laboratório de Geologia Isotópica da Universidade Federal de Ouro Preto (UFOP), utilizando-se um ICP-MS multicoletor da Thermo-Scientific Neptune Plus acoplado a um laser Photon-Machines 193 ArF Excimer. Os dados foram coletados no modo estático durante 60 segundos de ablação com um furo de diâmetro de 50 μm . Introduziu-se nitrogênio ($\sim 0,080$ l/min) ao gás carregador da amostra (argônio) por meio de um sistema de nebulização Aridus. A intensidade típica do sinal foi cerca de 10 V para o ^{180}Hf . Os isótopos ^{172}Yb , ^{173}Yb e ^{175}Lu foram monitorados simultaneamente durante cada etapa das análises para permitir a correção de interferências isobáricas dos isótopos Lu e Yb na massa 176. Os isótopos ^{176}Yb e ^{176}Lu foram calculados utilizando-se as razões $^{176}\text{Yb}/^{173}\text{Yb}$ de 0,796218 (Chu *et al.* 2002) e $^{176}\text{Lu}/^{175}\text{Lu}$ de 0,02658 (valor *in-house* da JWG – Johann Wolfgang Goethe-Universität Frankfurt am Main). A correção para o fracionamento de massa instrumental utilizou uma lei exponencial e um valor $^{179}\text{Hf}/^{177}\text{Hf}$ de 0,7325 (Patchett & Tatsumoto 1980) para a correção das razões isotópicas de Hf. O viés (bias) de massa dos isótopos de Yb geralmente difere levemente daqueles dos de Hf com um fator típico do $\beta\text{Hf}/\beta\text{Yb}$ entre 1,04 e 1,06 quando se usam o valor de 1,35274 definido por Chu *et al.* (2002). Esse fator foi determinado para cada sessão analítica por meio da média da razão $\beta\text{Hf}/\beta\text{Yb}$ de múltiplas análises da solução JMC 475 dopada com variáveis quantidades de Yb, e todas as análises por ablação a laser do zircão (normalmente $n > 50$) com uma intensidade de sinal $^{173}\text{Yb} > 60$ mV. O comportamento do viés (bias) de massa do Lu foi assumido seguir aquele do Yb. As razões isotópicas de Yb e Lu

foram corrigidas usando o β Hf das etapas de integração individual de cada análise ($n = 60$) dividida pela média do fator da sessão analítica completa. Os resultados foram calibrados com o uso dos zircões padrão Temora (415 Ma; Hf = 0,282680), Mud Tank (730 Ma; Hf = 0,282501) e 91500 (1065 Ma; Hf = 0,282307). Para o cálculo de ϵ Hf, foi usado os valores de condrito de Bouvier *et al.* (2008); $^{176}\text{Lu}/^{177}\text{Hf} = 0,0336$ e $^{176}\text{Hf}/^{177}\text{Hf} = 0,282785$) e constante de decaimento de $1,865 \times 10^{-11}$ ano $^{-1}$ (Scherer *et al.* 2001). A média do manto empobrecido é definida por Andersen *et al.* (2009) com razões $^{176}\text{Lu}/^{177}\text{Hf}$ e $^{176}\text{Hf}/^{177}\text{Hf}$ de 0,0388 e 0,283250, respectivamente, e média da crosta continental de 0,015, definida por Griffin *et al.* (2002).

1.6.7 Análise isotópica Sm-Nd

Análises isotópicas de Sm-Nd foram realizadas em 17 amostras representativas dos granitoides neoarqueanos híbridos de Vila União, utilizando o espectrômetro de massa Finnigan MAT 262 do Laboratório de Geologia Isotópica (Pará-Iso) da UFPA. Os dados de idade modelo obtidos foram utilizados como parâmetro indicativo de fontes de magma, mistura de componentes e evolução crustal. Esse método foi descrito inicialmente por Lugmair (1974) e Lugmair *et al.* (1975), tendo as primeiras aplicações para rochas ígneas determinadas por DePaolo & Wasserburg (1976) e Hamilton *et al.* (1977). Os procedimentos analíticos adotados por este laboratório para a determinação de idade modelo em rocha total estão descritos em Avelar (2002) e Moura (1992).

A preparação prévia das amostras consiste, primeiramente, na Trituração, feita pelos trituradores de mandíbula primário e secundário, realizada na OPA/UFPA, seguida de pulverização, feita com o gral de ágata, no Laboratório de Sedimentologia (UFPA), e quarteamento de ~500g/amostra. A técnica analítica de abertura e separação do sistema isotópico de Sm-Nd é iniciada utilizando uma solução traçadora mista de $^{150}\text{Nd}/^{149}\text{Sm}$ em 100 mg de material, conforme a metodologia descrita por Oliveira *et al.* (2008) e, em seguida, digeridos HF:HNO₃ em frasco de Teflon dentro de recipiente PARR a 150°C por uma semana. Após a evaporação, a solução é novamente atacada com os mesmos ácidos e colocada para secar e, em seguida, diluída com HCl (6N). Após a evaporação, o resíduo é solubilizado em HCl (2N). Após a última evaporação, os lantanídeos foram separados dos outros elementos por troca cromatográfica usando a resina *BioRad Dowex 50WX-8*, HCl (2N) e HNO₃ (3N). A extração de Sm e Nd dos demais lantanídeos foi executada por troca cromatográfica aniónica usando resina *Dowex AG1-X4* com a mistura de HNO₃ (7N) e metanol. As frações concentradas de Sm e Nd coletadas são então evaporadas. Em seguida, 1 ml de HNO₃ ** (2%)

é adicionado em cada fração separada de Sm e Nd, sendo as amostras levadas ao espectrômetro ICP-MS para leitura de suas razões isotópicas em média de dez (Nd) a seis (Sm) blocos cada amostra. As razões isotópicas são normalizadas para $^{146}\text{Nd}/^{144}\text{Nd} = 0,7219$ (o fracionamento de massa foi corrigido no modo exponencial) e a constante de desintegração usada é de $6,54 \times 10^{-12}$ ano $^{-1}$. Os padrões de Nd “La Jolla” e a solução de calibração Neptune forneceram valores de $^{143}\text{Nd}/^{144}\text{Nd}$ de 0,511834 (± 5) e 0,511732 (± 9) (2σ , média de 50 leituras), respectivamente. Os valores de TDM foram calculados usando o modelo de DePaolo (1981) por meio da macro Isoplot 4.15 (Ludwig 2008) que funciona no programa EXCEL (Microsoft).

**2 LITHOLOGICAL AND STRUCTURAL CONTROLS ON THE EMPLACEMENT
OF A NEOARCHEAN PLUTONIC COMPLEX IN THE CARAJÁS PROVINCE,
SOUTHEASTERN AMAZONIAN CRATON (BRAZIL)**

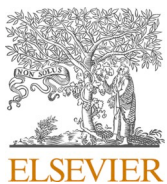
Fernando Fernandes da Silva

Davis Carvalho de Oliveira

Roberto Dall'Agnol

Luciano Ribeiro da Silva

Ingrid Viana da Cunha



Lithological and structural controls on the emplacement of a Neoarchean plutonic complex in the Carajás province, southeastern Amazonian craton (Brazil)



Fernando Fernandes da Silva ^{a,b,*}, Davis Carvalho de Oliveira ^{a,b}, Roberto Dall'Agnol ^{a,b,c}, Luciano Ribeiro da Silva ^{a,b}, Ingrid Viana da Cunha ^{a,b}

^a Grupo de Pesquisa Petrologia de Granitoides (GPPG), Instituto de Geociências (IG), Rua Augusto Corrêa, 01, CEP-66075-900, Belém, PA, Brazil

^b Programa de Pós-Graduação em Geologia e Geoquímica Universidade Federal do Pará (UFPA), IG-UFPA, Belém, PA, Brazil

^c Instituto Tecnológico Vale, Belém, PA, Brazil

ARTICLE INFO

Keywords:

Granitoid
Shear zone
Archean
Carajás
Amazonian craton

ABSTRACT

New geological and geochronological (Pb-Pb evaporation) data from the Vila Jussara suite, a representative of the Neoarchean granitoids of the Carajás province, southeastern Amazonian craton (Brazil), are discussed. The Vila Jussara suite crops out as a series of coalescing plutons elongated in the E-W direction. These plutons generally have sigmoidal shapes, and steep dips (75–85°) that follow the regional trend. The centermost areas of plutons are generally slightly deformed, while the marginal portions display mylonitic aspect and are delimited by sinistral shear zones belonging to the transcurrent system of the Itacaiúnas shear belt. These granitoids cover a large compositional spectrum, with four main lithotypes: (i) Seriated biotite-hornblende monzogranite; (ii) biotite-hornblende tonalite; (iii) porphyritic biotite monzogranite-granodiorite; and (iv) porphyritic hornblende-biotite monzogranite-granodiorite. The microstructural analysis of the studied rocks reveals: (i) microfractures in feldspar phenocrysts, filled with a quartz-feldspar matrix; (ii) preferred orientation of euhedral feldspar crystals in an igneous matrix; and (iii) evidence of moderate-to high-temperature of solid-state deformation (>500 °C). These microstructures and field observations point to a continuum of deformation, from the (sub) magmatic state down to sub-solidus conditions. Dating of three types of granitoids out of four gives ages of 2754 ± 2.2 Ma, 2752 ± 5.7 Ma and 2745 ± 3 Ma. The different granitoid varieties of the Vila Jussara suite were thus emplaced simultaneously. It is proposed that emplacement of the granitoids was controlled by shear zones reactivated during oblique collision and that plutons were constructed by multiple injections of magmas, generating extensive hybridization.

1. Introduction

Granitoids are excellent tectonic markers, as well as tracers for crustal growth, reworking and deformation. From magma generation in the source to complete crystallization, syntectonic plutons may record short-lived geological events related to crustal melting and deformation of the continental crust (Paterson and Tobisch, 1992; Karlstrom et al., 1993; Bodorkos et al., 2000; Petford et al., 2000; Rosenberg, 2004; Florisbal et al., 2012). The common geometrical and temporal relationship between synkinematic granitic plutons and crustal-scale shear zones is indicative of a very close link between them, whereby either

shear zones control ascent and emplacement of granite magmas (Brown and Solar, 1998), or magma emplacement triggers nucleation of shear zones (Neves et al., 1996). Weinberg et al. (2004) postulate that shear zones associated with magmatism evolve into an upward pathway characterized by a network of magma sheets linked to inflating chambers within shear zones. In the Archean tectonic context in particular, shear zones represent major channels for magma transport, providing an important emplacement mechanism for many syntectonic plutons related to transpressive deformation regimes (Hutton et al., 1990; D'lemos et al., 1992; Hutton and Reavy, 1992; Hutton, 1988; Vigneresse et al., 1996). In this case, the understanding of the internal fabric of the

* Corresponding author. Grupo de Pesquisa Petrologia de Granitoides (GPPG), Instituto de Geociências (IG), Rua Augusto Corrêa, 01, CEP-66075-900, Belém, PA, Brazil.

E-mail address: ffernandes@ufpa.br (F.F. Silva).

granitoids, as well as their relationship with the regional structure and the framework of the magmatic flow and solid-state deformation is critical in order to constrain space/time/temperature/deformation relationships during pluton crystallization (e.g. Paterson et al., 1989 for review).

The dominant granitoids in Archean terranes are the tonalite-trondjemite-granodiorite (TTG) association and diversified magnesian leucogranites (Almeida et al., 2011). However, although they are comparatively rare in Archean terranes, magnesian charnockitic granitoids and ferroan or A-type granites have also been described in these terranes worldwide (Bandyopadhyay et al., 2001; Larin et al., 2006; Misra et al., 2002; Moore et al., 1993; Rajesh et al., 2009; Smithies and Champion, 1999; Zhou et al., 2015; Zozulya et al., 2005). In the Carajás province of the Amazonian craton, various Neoarchean deformed granite plutons with A-type geochemical characteristics have been described (Estrela Complex and Igarapé Gelado Granite, Barros et al., 2009; Serra do Rabo granite, Sardinha et al., 2006; Planalto suite, Cunha et al., 2016; Feio et al., 2012; Vila União granites, Marangoanha et al., 2019). The Neoarchean granitoids of the Vila Jussara suite that will be studied here also occur in the Carajás province and have strong analogies with these A-type granites. However, they are distinguished by the presence of reduced ferroan varieties, together with oxidized ferroan and magnesian granitoids (Dall'Agnol et al., 2017). This aspect indicates a more complex magmatic evolution for the Vila Jussara complex, involving liquids generated under different fO_2 and also probably mixing processes.

This paper presents the results of an integrated approach applied to a granitic complex formed of several plutons emplaced along the Itacaiúnas shear belt in the northern Carajás province, southern Amazonian craton. We present meso- and microstructural observations from different parts of the Vila Jussara plutons, supported by recently acquired mineralogical, petrographic and Pb-Pb geochronological data, in order to constrain the relationships between magmatism, shearing and multistage deformation. Moreover, the microstructural evolution is

extensively discussed in order to demonstrate the different deformation mechanisms that could have prevailed during the shearing of these rocks as progressive syndeformational crystallization took place. The main objective of the present paper is to discuss the evidence of successive multiple injections of liquids and the role played by transcurrent tectonics during the emplacement and construction of syntectonic plutons, in order to understand the structure and stabilization of the Archean crust.

2. Regional geology

2.1. The Carajás province

The Amazonian craton (Almeida et al., 1981), located in the north of the South America continent (Fig. 1a), is composed of different geochronological provinces, among which we find the Archean Carajás province (Fig. 1b). Santos (2003) considered the Carajás province as an independent geochronological province, while Tassinari and Macambira (2004) regarded it as part of the Central Amazon province, which is subdivided into two blocks (Carajás and Xingu-Iricoumé). The Carajás province was initially subdivided by Souza et al. (1996) in two blocks, subsequently redefined by Santos (2003) and Vasquez et al. (2008) as two main tectonic domains: the Rio Maria domain (3.0–2.86 Ga) and the Carajás domain (3.0–2.73 Ga). Later on, Dall'Agnol et al. (2013), using a wide set of geological data, showed that the Carajás domain is not tectonically homogeneous and subdivided it into the Canaã dos Carajás domain in the north and the Sapucaia domain in the south (Fig. 1c).

The Rio Maria domain is composed of supracrustal sequences (3.0–2.9 Ga) and four granitoid suites, with ages between 2.98 and 2.86 Ga (Althoff et al., 2000; Oliveira et al., 2009; Almeida et al., 2011, 2013; Ronaib and Oliveira, 2013). The granitoid suites include: (i) TTG associations represented by the Arco Verde, Caracol and Mariazinha tonalites and the Mogno trondjemite, formed during two main magmatic events at 2.96 Ga and 2.93 Ga; (ii) the Rio Maria sanukitoid suite with an

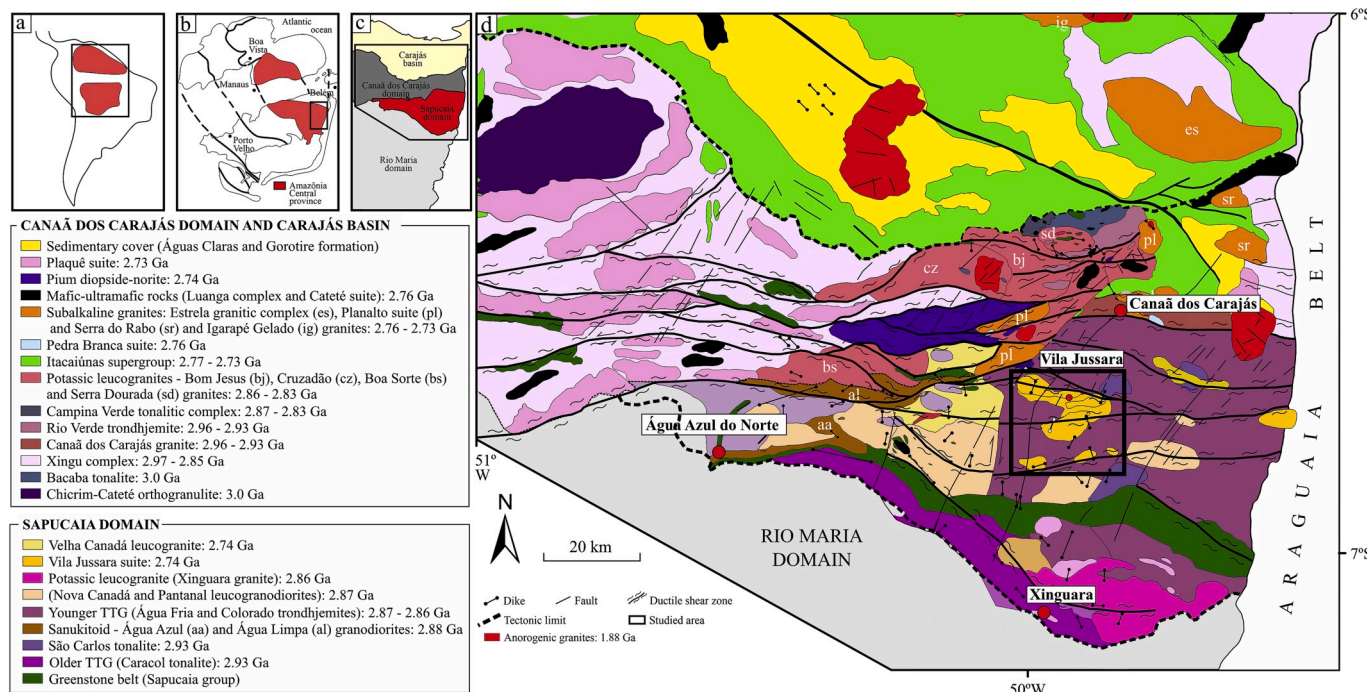


Fig. 1. Regional geology and tectonic context of the Vila Jussara area: a) South American platform with the Amazonian craton highlighted; b) map of the Amazonian Craton showing the Amazonian Central province (Tassinari and Macambira, 2004); c) Tectonic compartmentalization of the Carajás Province proposed by Dall'Agnol et al. (2013); d) Detailed geological map of the Carajás Province (the study area is highlighted), modified from Vasquez et al. (2008), Oliveira et al. (2010), Feio et al. (2013).

age of 2.87 Ga and consisting of granodiorites with associated mafic to intermediate rocks found as enclaves or, locally, layered rocks; (iii) the 2.87 Ga Guarantã suite formed of high Ba-Sr calc-alkaline leucogranodiorite; and (iv) 2.87–2.86 Ga potassic leucogranites of calc-alkaline affinity, represented by the Mata Surrão granite and small stocks. The rocks of the Rio Maria domain are weakly deformed, showing WNW-ESE magmatic and tectonic planar fabrics, and intruded by 1.88 Ga (Paleoproterozoic) anorogenic granites (Barbosa et al., 1995; Paiva Jr. et al., 2011; Teixeira et al., 2019).

The Sapucaia domain is largely dominated by Mesoarchean TTG associations petrologically similar but younger than those of the Rio Maria domain. The Mesoarchean rocks of this domain were intensely deformed and intruded by granite plutons during the Neoarchean. The domain consists of TTG associations (Colorado and Água Fria trondjemites) and amphibole-bearing tonalites (São Carlos tonalite) (Santos et al., 2013; Silva et al., 2014); furthermore, it also contains sanukitoid associations (Água Azul and Água Limpa granodiorites; Gabriel and Oliveira, 2014), high Ba-Sr calc-alkaline leucogranodiorite to leucogranites (Pantanal and Nova Canadá granodiorites; Teixeira et al., 2013; Leite-Santos and Oliveira, 2014, 2015), and Neoarchean granitoids showing geochemical affinity with A-type granites, as represented by the Vila Jussara suite (Dall'Agnol et al., 2017) (Fig. 1d).

The Canaã dos Carajás domain is dominantly composed of 2.87–2.85 Ga high-K calc-alkaline granites (Boa Sorte, Bom Jesus, Cruzadão and Serra Dourada granites; Feio et al., 2013; Rodrigues et al., 2014) that were intruded at ~2.74 Ga by enderbite-charnockite (Pium diopside-norite; R. S. Santos et al., 2013) and granites (Planalto suite; Feio et al., 2012). We also find rare occurrences of TTG (the Rio Verde trondjemite at ~2.93 Ga), amphibole-bearing tonalites (the 3.0 Ga Bacaba tonalite; Moreto et al., 2011; and the 2.87–2.85 Ga Campina Verde tonalitic complex), sodic leucogranites of calc-alkaline affinity (the 2.93 Ga Canaã dos Carajás granite; Feio et al., 2013). These Archean units are intruded by 1.88 Ga anorogenic plutons (Teixeira et al., 2018).

The structural pattern in the Sapucaia domain (SD) and Canaã dos Carajás domain (CCD) is marked by moderate-to-strong heterogeneous deformation compared to the less deformed Rio Maria domain. Both domains are composed of E-W oriented plutonic bodies, which show E-W magmatic and tectonic foliations and subvertical dips.

2.2. The Itacaiúnas compressive oblique belt

The Itacaiúnas belt, as defined by Araújo and Maia (1991) is a tectonic belt that covers the areas corresponding to the recently delineated Canaã dos Carajás and Sapucaia domains. It is characterized kinematically by an oblique compressive regime. The structural features related to this belt affect all Mesoarchean and Neoarchean stratigraphic units. Geometrical and kinematic criteria allow characterizing two distinct structural domains along the belt, dominated, respectively, by imbricated thrust faults and transcurrent faults. The study area belongs to the imbricate domain (Araújo and Maia, 1991). This domain is linked to essentially compressive kinematics and is marked by imbricated systems of oblique thrusts, which extend from the southern border of the Serra dos Carajás (Carajás basin) to the limit with the Rio Maria domain (Fig. 1d). The Itacaiúnas belt presents a general E-W orientation that stands out through rocks of several lithological units; such distribution defines, on a regional scale, an inclined composite mega banding, on average 60° SSW. This regional-scale geometric arrangement is also verified internally in the different lithological units. These units, lenticular in shape, display different degrees of deformation, evidencing the heterogeneous nature of the deformation. There are also lenticular areas free of deformation (Araújo and Maia, 1991; Costa et al., 1995; Holdsworth and Pinheiro, 2000).

Depending on the intensity of the deformation and the nature of the deformed lithotypes, the lenticularization process generates planar features that may be classified as transposition foliation, schistosity or compositional banding. These structures are grouped under the

denomination of “mylonitic foliation”. The mylonitic domain contains a lineation dominantly oriented NW-SE and plunging toward the SW. Associated with the shear zones, oblique thrusts were developed, and they show systematically S and SL tectonites. The analysis of kinematic criteria such as shear bands, phenocryst rotation and S-C relationships, indicates zones of concentration of sinistral deformation, where the mass transport was mainly from SW to NE (Araújo et al., 1988; Araújo and Maia, 1991).

3. Geological and petrological framework of the Vila Jussara suite

3.1. General geological aspects of the Vila Jussara suite

The Vila Jussara suite is made of several granitoid plutons located south of Canaã dos Carajás town, in the Sapucaia domain of the Carajás province (Fig. 1d). The Sapucaia domain is characterized by the occurrence of extensive Neoarchean plutonic magmatism in a Mesoarchean crust formed dominantly of TGG, greenstone belts, sanukitoids and leucogranites (Gabriel and Oliveira, 2014; Santos et al., 2013; Teixeira et al., 2013; Silva et al., 2014; Leite-Santos and Oliveira, 2014). The plutons of the Vila Jussara suite, together with those occurring in the north of the province, the Planalto suite (Canaã dos Carajás domain), and the Estrela granite complex, Serra do Rabo and Igarapé Gelado granite plutons, are part of a sequence of dominantly granitic intrusions emplaced in the Carajás province during a major Neoarchean (2.75–2.73 Ga) magmatic plutonic event.

In its type-area, the Vila Jussara suite is defined by three main coalescent, elongated and amalgamated granite plutons, which constitute a set of ridges with variable elevations between 280 and 400 m. These plutons have a roughly sigmoidal shape and a near E-W trend in map view, with steeply-dipping margins (Fig. 6a and b). They are concordant with the regional trend and are associated with poorly exposed shear zones, up to 60 km long. The main shear zones are observed along the borders of the plutons, where striped rocks with gneissic structure are exposed (Fig. 2a), as well as partly recrystallized mylonitic rocks, showing a stretching lineation somewhat obliterated through the recovery process. This lineation is defined by quartz ribbons and elongated feldspar porphyroblasts and it is parallel to the alignment of biotite and amphibole. It plunges to SE at low to moderate angles (Fig. 6d).

The plutons show many different enclaves, including MMEs, which confirm the intrusive nature of the granitoids (Fig. 2b and c). In the strongly deformed zones at pluton margins, a number of overprinting dike-like (Fig. 2a) to lensoidal structures can be seen, most of which are nearly-parallel to the main gneissic fabric. Such an orientation suggests that shearing was coeval with the emplacement of several generations of felsic intrusions, which in turn could provide a direct age estimate for the main period of movement along the shear zones. Due to geometric and kinematic partitioning of the deformation, the central portions of the granite bodies contain domains of low strain, contrasting with the highly strained edges affected by the large-scale shear zones.

In the low-strain central domains, two fabrics can be observed: (i) a diffuse subvertical composite banding with millimetric to centimetric spacing likely of primary origin, i.e. (sub) magmatic and (ii) a lineation-bearing foliation with a WNW-ESE main direction and NNE or SSW, up to 75° dips. In these low-strain domains, partially preserved TTG xenoliths may be found (Fig. 2b). The high-strain border domains, along the regional-scale shear zones, display a widely distributed protomylonitic foliation with a main direction of WNW-ESE and subvertical SC-type structures, where centimetric to decimetric ductile-brittle shear bands are commonly observed. As already described, the overall structure of these high-strain zones is that of a banded gneiss, which is prime evidence of emplacement of the plutons along the shear zones. The structural framework identified in both the low- and high-strain domains is concordant with the long axes of the granites and the tectonic foliation in the country rocks. However, the intensity and orientation of



Fig. 2. Field relationships in the Vila Jussara granitoids a) Sheared, strongly deformed border zone of a pluton showing concordant strips of tonalite (gray) and granite (rose); b) Large TTG xenolith; c) Ellipsoidal enclave (MME) surrounded by a mafic rim of biotite and amphibole (heterogeneous nucleation).

both the primary (sub)magmatic and the tectonic fabrics vary locally.

3.2. Petrographic classification

The granitoids of the Vila Jussara suite cover a large compositional spectrum, ranging from tonalite and granodiorite to *sensu stricto* granite. Four groups were distinguished on the basis of dominant modal composition, textural features and field occurrence: seriated biotite-hornblende monzogranite to subordinate syenogranite (BHM), biotite-hornblende tonalite (BHT), and porphyritic granitoids varying from monzogranite to granodiorite, which comprise biotite-bearing (BG) and hornblende-biotite-bearing (HBG) rocks. These two varieties of porphyritic granitoids will be often treated below as a single group, because they are intimately associated in the field, which does not necessarily imply they are comagmatic. All granitoids are dominantly leucocratic rocks, presenting colors ranging from reddish gray to whitish gray due to variations in the plagioclase/microcline ratio, with dark spots corresponding to aggregates mafic mineral. These rocks have phaneritic textures, varying from medium-grained (1–5 mm) to coarse-grained (>5–12 mm) and equigranular to porphyritic (potassium feldspar megacrysts). Textural aspects of each petrographic variety are illustrated in Fig. 3. Regarding the mafic content, the M' values vary

between 11% and 27.4% (average of 17.26%) for BHM; from 8.61% to 22.5% (average 13.03%) for BG and from 16.70% to 31.50% (average 20.20%) for HBG; finally, the tonalite (BHT) is slightly more enriched in mafic minerals with M' from 16.80% to 37.80% (average 27.08%). Hornblende and biotite are the main mafic minerals in most granitoids, except for the BM in which amphibole is an accessory phase. The primary accessory minerals are titanite 1 (primary), opaque minerals, apatite, zircon, allanite, and epidote 1 (primary), while the secondary minerals consist of sericite, chlorite, epidote 2 (secondary), scapolite, titanite 2 (secondary), and albite.

Representative modal compositions of each granitoid variety are shown in Table 1, and the overall results of the modal analysis are plotted in a QAP diagram (Fig. 4).

3.3. Field relationships and spatial distribution of the granitoid varieties

The central portions of the plutons (low-strain domains) are dominantly composed of BHM (Fig. 6a and b). The marginal portions of the plutons (high-strain domains) expose mainly porphyritic granitoid (BG and HBG) and tonalite (BHT) (Fig. 6a and b) showing complex interactions, such as BHT forming mega enclaves, ellipsoidal in shape, and with interdigitated contacts with porphyritic granitoids (Fig. 5a and b).

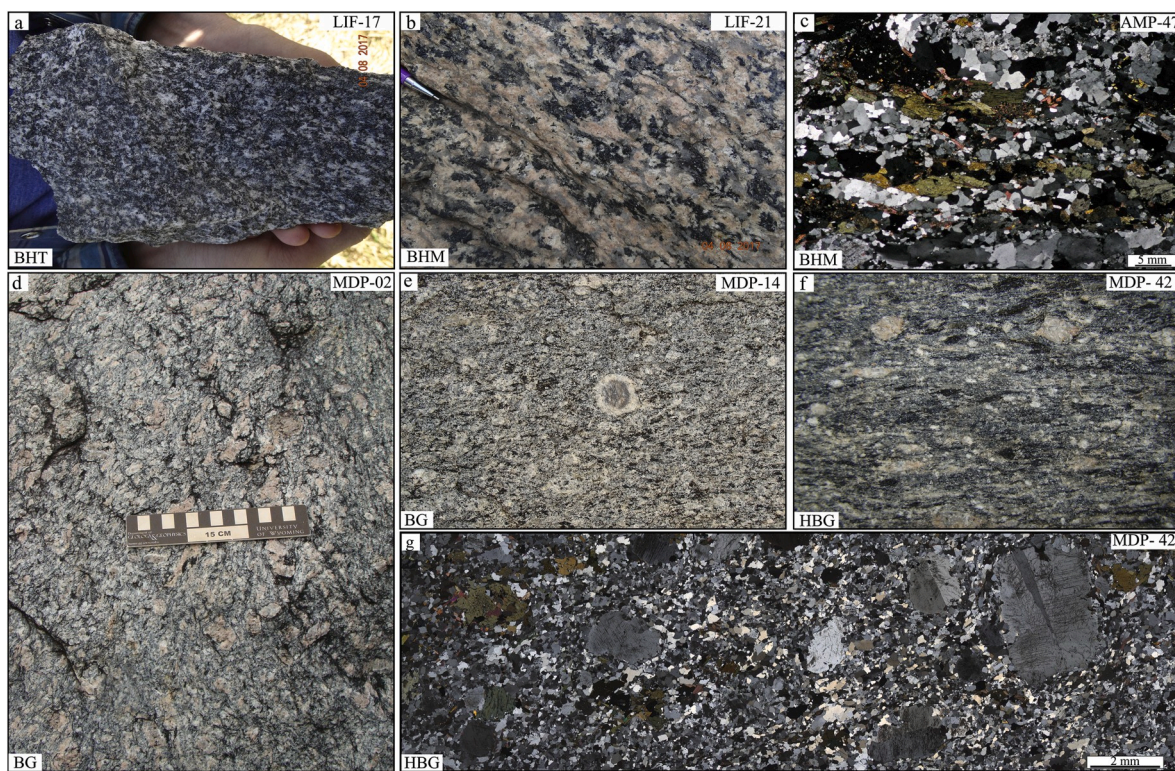


Fig. 3. Textural aspects of the Vila Jussara granitoids. a) Foliated biotite-hornblende tonalite (BHT); b) Seriated biotite-hornblende monzogranite (BHM); c) BHM sample with a dominantly magmatic microstructure; d) Typical texture of a porphyritic granitoid (BG; monzogranite type); e) BG facies (monzogranite variety) showing rapakivi texture; f) Macroscopic aspect of a HBG facies (granodiorite type), with strong deformation marked by stretched feldspar grains; g) Microscopic aspect of the porphyritic texture of a HBG sample. Fig. 3c, g are transmitted-light optical microscope images taken with polarized light and crossed polars.

Table 1

Modal compositions of representative samples of the different granitoid varieties from the Vila Jussara suite.

Unit	Vila Jussara																	
Lithotype	BHM				HBG				BG				BHT					
Sample	LIF 24	AMP 27	MYF 77	AMP 88A	MDP 12B	MDP 42C	ADE 01D	MDP 42B	MDP 14C2	LIF 30	MDP 55	MDP 02A	LIF 13C	AMP 77	AFD 6	MDP 02E	MYF 40	MDP 02C
Mineral (%)																		
Quartz	36	28.6	26.4	33.1	33.4	32.4	29.8	33.2	31.4	36.9	31.3	35.2	28.6	24	36	20.9	26.6	30.8
Plagioclase	28.5	14.8	32.5	23.4	30.5	27.5	41.2	26.8	29.6	34.6	33.6	17.4	31	27.7	48.2	38.4	54.3	30
K-Feldspar	26.2	36.9	26.2	27.4	16.6	21.7	12.5	13.2	15.1	17.9	16.5	29.8	31.7	35.8	0.7	2	1.3	6.8
Amphibole	0.9	9.1	9.8	11	5.2	7.1	5.4	7.1	8.8	0.2	0.7	0.4	0.4	0.2	9.5	26.3	8.7	13.4
Biotite	8	–	8.9	4.1	11	5.8	9	5.8	13.4	8.4	13.8	13.1	6.5	9	5.3	7	7.3	14.2
Σ Accessories*	1.7	0.6	2.4	1	3	5.2	2.4	4.9	1.8	1.8	3.6	3.8	1.6	0.6	0.7	4.35	1	3.8
Mafic (M')	9.1	19.1	21.1	16	19.3	18.2	16.8	26	24	10.4	18.3	17.3	8.6	9.8	15.5	37.8	16.8	31.6

Accessory minerals comprise: Titanite, Epidote, Zircon, Allanite, Apatite, and Opaques.

Furthermore, a mingling/mixing relationship occurs all along the plutons between BHM magma and that of granodioritic composition (HBG), as evidenced by the presence of feldspar xenocrysts or even partially digested granite fragments in the latter (Fig. 5c and d).

Swarms of mafic microgranular enclaves (MME type) occur all along the plutons, although being especially more preserved in the central portions. These enclaves vary in composition from quartz diorite to tonalite or locally hornblende-biotite granodiorite. Megacrysts of plagioclase and occasionally quartz occur in the dark matrix. These enclaves are commonly ellipsoidal (Fig. 2c), the length of their long axis varying from a few centimeters up to 3 m. Such elongated shapes reflect the stretching of partially crystallized magmas. At the enclave-granite interface, the granite host is locally enriched in biotite and amphibole (heterogeneous nucleation along the enclave margin; Machlin, 2007; Philpotts and Ague, 2009) (Fig. 2c). On the other hand, small enclaves show strong evidence of mixing (hybridization) with the host granite,

such as, e.g., gradational contacts. In a more advanced stage of hybridization, the disaggregation of these enclaves produces rocks with schlieren textures and clots of fine-grained mafic material that are heterogeneously distributed in the host granite.

4. Microstructures

The rocks from the central portions of the plutons exhibit euhedral to subhedral equigranular texture (Fig. 7a, b, c) with relatively well-preserved igneous characteristics as evidenced by preservation of feldspar crystals (Pl_1 and Kfs_1) with magmatic shape and oscillatory zoning in euhedral plagioclase grains, in addition to euhedral to subhedral mafic minerals (Bt_1 , Hbl_1 , and primary accessory minerals). However, we observe microstructures that originated by both cataclastic and intracrystalline plasticity mechanisms, such as the preferred orientation of euhedral to subhedral feldspar crystals, mafic minerals and elongated

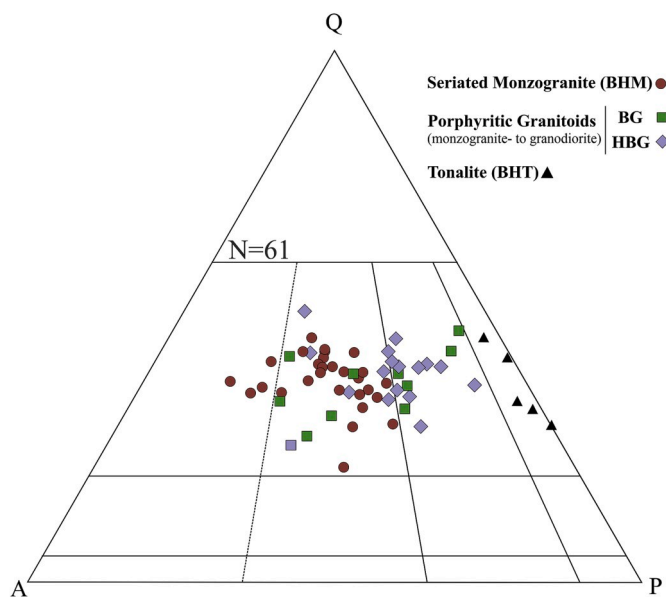


Fig. 4. Q-A-P plot (Le Maitre, 2002) and petrographic classification of the Vila Jussara granitoids. The modal compositions of the 61 samples (N) used in the Q-A-P diagram were determined on thin sections using the Endeeper Hardlodge software. 2000 points were counted per section on a mesh of 0.4 mm. The granitoids were named following the recommendations of the International Union of Geological Sciences (IUGS) Subcommission on the Systematics of Igneous Rocks (Le Maitre, 2002).

aggregates of recrystallized quartz, which may indicate continuity between (sub) magmatic and solid-state flow. Microcline macrocrysts with intragranular microfractures filled with quartz that show petrographic continuity with quartz grains in the rock matrix indicate deformation in the presence of melt (submagmatic deformation; Fig. 7d), as described by Passchier & Trouw, (2005). Undulatory extinction, deformation bands in grains of Pl_1 , Mc_1 and Qtz_1 , deformation twins in Pl_1 , Mc_1 and Hbl_1 , as well as elongated aggregates of Qtz_2 grains with sutured or straight grain boundaries, are, respectively additional clues of ductile straining and evidence of dynamic recrystallization through grain boundary migration (GBM) and subgrain rotation (SGR). Straight grain boundaries and polygonal granoblastic microstructure inside Qtz_2 aggregates indicate that these recrystallized quartz grains were subjected to post-deformational static recrystallization via grain boundary area reduction (GBAR; Passchier and Trouw, 2005).

Rocks from the high-strain border domains (BG, HBG and BHT) are characterized mainly by the development of mylonitic foliation and by rounded to sigmoidal feldspar porphyroclasts (Pl_1 and Mc_1), surrounded by hornblende, biotite and recrystallized quartz aggregates (Qtz_2) with grains showing sutured to straight contacts (Fig. 7e and f), indicating GBM and SGR, followed by GBAR. Such a deformational behavior is similar to that observed in quartz from the low-strain domains. The Pl_1 and Mc_1 porphyroclasts generally occur as relict nuclei defining a core-mantle microstructure. These porphyroclasts have smooth and undulatory extinction, deformation twins, intragranular microfractures and irregular to sutured or, less frequently, straight grain boundaries. Their mantle is made of small new feldspar grains (Pl_2 and Mc_2) resulting from dynamic recrystallization via SGR and migration of low-temperature grain boundaries (bulging - BLG, Fig. 7g). Straight grains boundaries

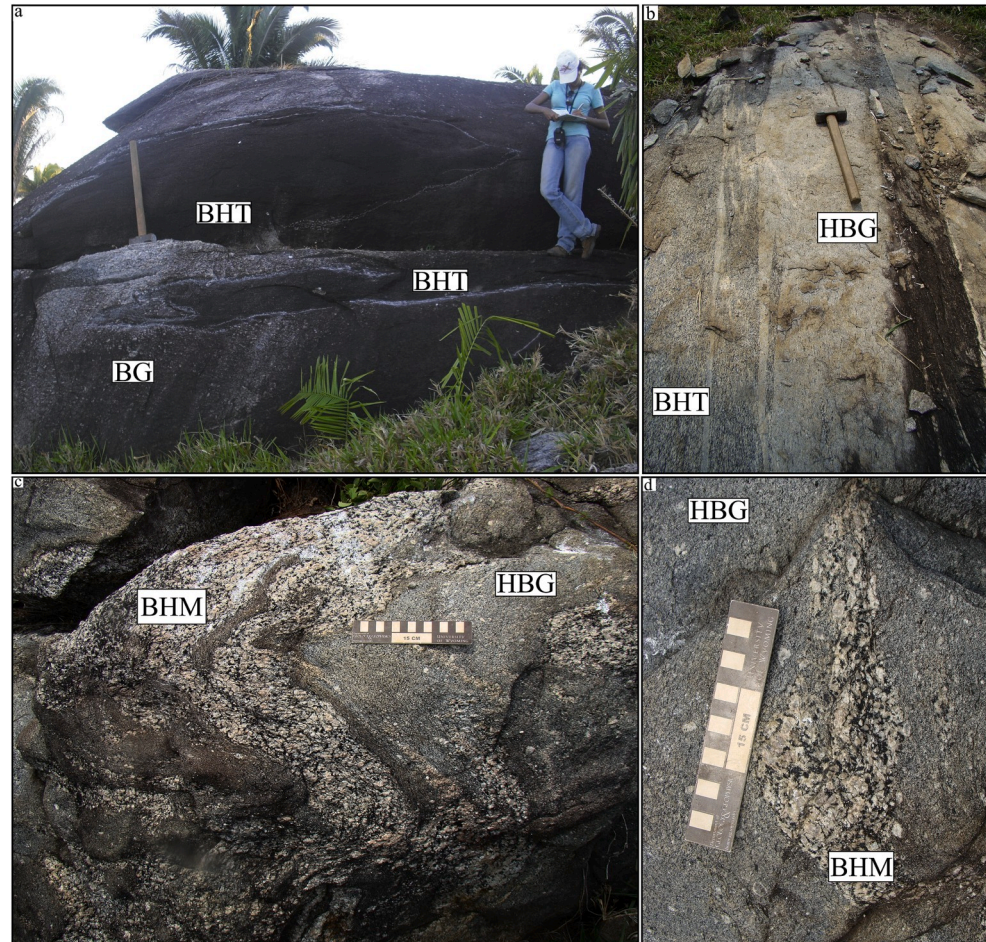


Fig. 5. Contact relationships between the granitoid lithotypes of the Vila Jussara suite. a) Mega enclave of tonalite (BHT) in porphyritic biotite granitoid (BG); b) Interdigitated contact between tonalite (BHT) and porphyritic biotite-hornblende granitoid (HBG) at the sheared margin of a pluton; c) Relationship as in Fig. 5 b, but between seriated biotite-hornblende monzogranite (BHM) and (HBG); d) BHM enclave within HBG facies, partially digested and containing feldspar xenocrysts coming from the host.

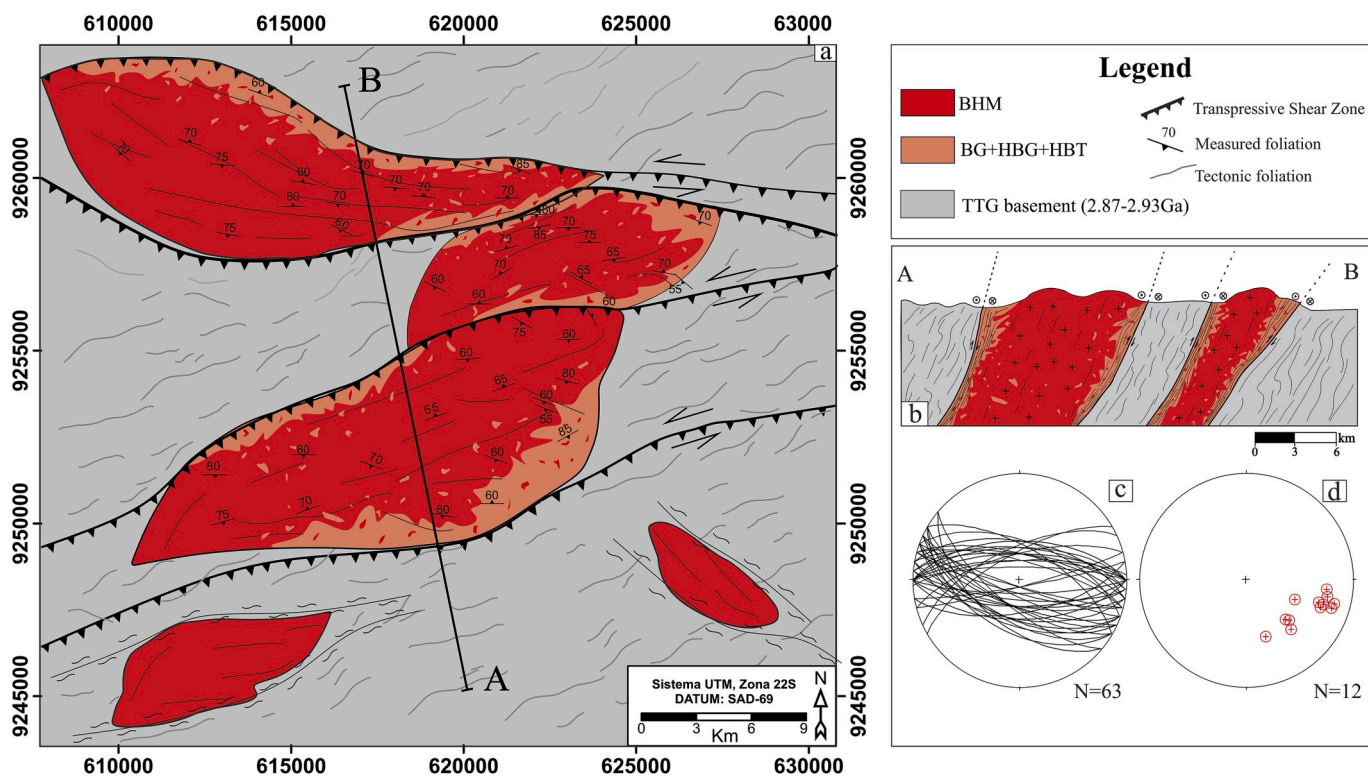


Fig. 6. Structure and petrology of the Vila Jussara granitoids in their type-area: a) Geological map showing the spatial distribution of the lithofacies (the BHM variety is concentrated in the core of plutons, while the porphyritic rocks and the tonalite varieties (BHT) are found mostly in the border zones where they are interdigitated with the BHM facies); b) N-S section across the plutons (see location in Fig. 6 a); Lower hemisphere, equal-area projection of c) foliation and d) mineral lineation.

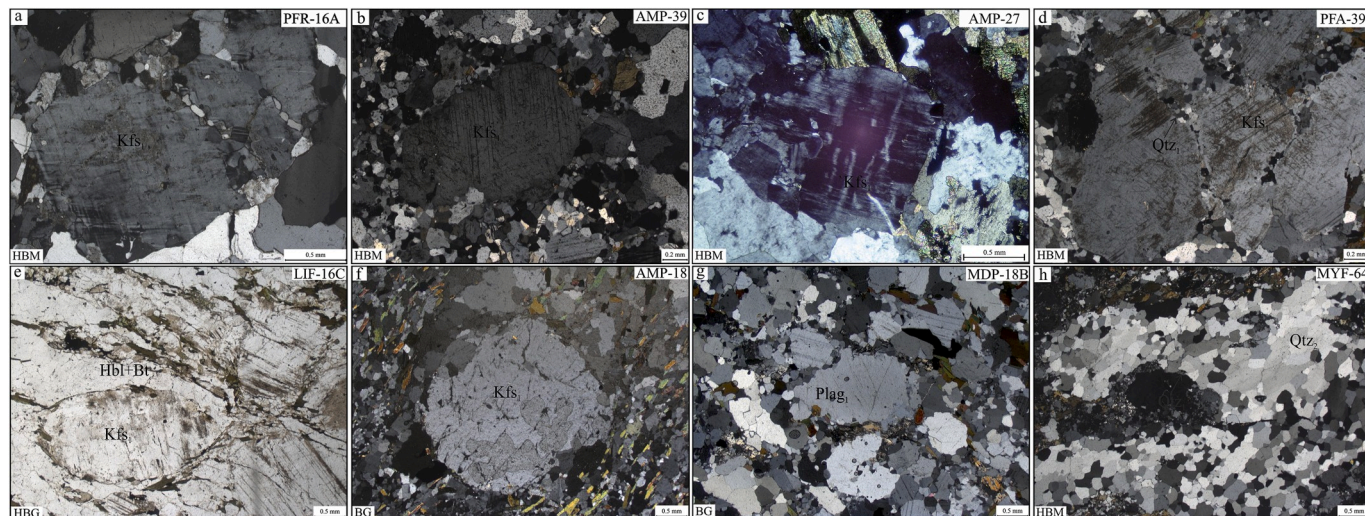


Fig. 7. Microphotographs in crossed polars showing microstructures of the Vila Jussara granitoids (the first four illustrated samples are from low-strain domains and the last four samples are from high-strain areas at the pluton margins, except the last one which comes from a zone of strain localization in the core of a granitoid). a), b), c), d) Centimetric macrocrysts of microcline in a fine-grained matrix composed of biotite \pm hornblende and quartz. Although the igneous texture is well preserved, occurrence of aggregates of quartz grains with straight or serrated boundaries in the matrix are evidence of dynamic recrystallization through subgrain rotation (SGR) and grain boundary migration (GBM), followed by static recrystallization through grain boundary area reduction (GBAR). In a), d), the microcline macrocryst is cut by microfractures filled with matrix minerals, in which quartz is in petrographic continuity with quartz grains of the surrounding matrix, suggesting deformation in the presence of melt (Passchier and Trouw, 2005). e) and f) σ -type rounded microcline porphyroclasts surrounded by biotite, hornblende and elongated aggregates of quartz grains with serrated or straight boundaries and polygonal granoblastic microstructure, indicating dynamic recrystallization at high temperatures (>500 °C) via SGR and GBM, followed by static recrystallization through GBAR. g) Porphyroclasts of plagioclase and microcline showing core-mantle microstructures. The mantle is very fine-grained and contains domains of coarser new grains with serrated or straight boundaries, indicating dynamic recrustallization via SGR and migration of low grain boundary temperature (bulging - BLG); h) Elongated aggregates of quartz micrograins resulting from dynamic recrystallization via GMB and SGR.

and polygonal granoblastic microstructures in the Pl_2 and Mc_2 mantle, as well as in the Qtz_2 aggregates (Fig. 7h), point again to GBAR, hence to post-deformational static recrystallization under relatively high-temperature conditions. Primary biotite crystals (Bt_1) may occur. However, due to the high deformation intensity, biotite is more commonly observed as aggregates of small recrystallized grains (Bt_2), with irregular to straight grain boundaries. The hornblende grains are euhedral to subhedral and exhibit dominantly brittle deformational behavior, as indicated by the common occurrence of intragranular microfractures, although locally they may show undulatory extinction and, less rarely, a subgrain pattern.

5. Pb-Pb evaporation geochronology

Isotopic analyses by the Pb evaporation method in zircon monocrystals were carried out at the Isotopic Laboratory (Pará-Iso) of the Instituto de Geociências of the Universidade Federal do Pará, according to the methodology developed by Kober (1987). The analyses were obtained on a FINNIGAN MAT 262 thermal ionization mass spectrometer. The results are presented with a deviation of 2σ and corrected for mass fractionation and common Pb or contamination, using the double-stage Pb evolution model proposed by Stacey and Kramers (1975), using the ratio $^{204}\text{Pb}/^{206}\text{Pb}$ adopted by Macambira et al. (1994). Zircon crystals from three samples were analyzed, AMP 27 (BHM), MD-01 (BG) and MYF 40 (BHT). The results are shown in Table 2 and Fig. 8.

The zircon grains are colorless and transparent to dark brown or pink, euhedral to subhedral, and long to slightly elongated with lengths varying from 150 to 300 μm and length/width ratios that range from 2 to 3. Twenty-seven zircon crystals were analyzed for sample AMP 27, among which only 19 gave a sufficient amount of Pb. Analyses of only 5 out of these 19 crystals AMP27/2, AMP27/3, AMP27/7, AMP27/23 and AMP27/27, were used for age calculation, providing a mean age of $2754 \pm 2.2 \text{ Ma}$, which is considered as the minimum age of crystallization. Sample MD-01 had twenty-three zircon crystals. Only four crystals, MD-01/3, MD-01/4, MD-01/13, and MD-01/16, showed satisfactory Pb for calculating an age which was found to be $2749 \pm 3 \text{ Ma}$ on average. For sample MYF 40, a total of 9 zircon crystals was analyzed. Only four zircon crystals out of nine had enough Pb to calculate age, namely, MYF40/1, MYF40/3, MYF40/4, and MYF40/7, providing an average age of $2752 \pm 5.7 \text{ Ma}$.

6. Discussion

6.1. Microtectonic considerations

Estimation of deformation temperature is a fundamental requirement for evaluating deformation rates, magma transport and emplacement mechanisms, as well as the relationships between granitoid genesis and deformation (Hacker et al., 1990; Dunlap et al., 1997; Behr and Platt, 2011). There are several geothermometers based on petrology that aim to estimate the crystallization or metamorphism temperatures (Essene, 1989; Hodges, 1991; Powell and Holland, 2008). However, there are comparatively few analytical techniques available to estimate deformation temperatures (Law, 2014; Passchier and Trouw, 2005). For quartz-feldspathic tectonites such as the most deformed studied granitoids, two main types of deformation geothermometers can be used: (i) The observation of recrystallization microstructures in quartz and feldspars, which allows, mainly using differences in the granulation of new crystals, to identify the mechanisms of dynamic recrystallization, BLG, SGR and GBM that operate at low, moderate and high temperature of deformation respectively. Due to different rheological behaviors, quartz and feldspars show distinct recrystallization microstructures for the same temperature, which allows a safe qualitative evaluation of the temperature range prevailing during their crystal-plastic deformation (Passchier and Trouw, 2005). (ii) A geothermometer based on the opening angle of quartz c-axis frames (Kruhl, 1998), which allows, at least potentially, a quantitative estimate of the deformation temperature. To date, the latter method has not been used in the studied rocks.

Deformation in quartz is controlled by temperature, deformation rate, differential stress and the presence of water in the crystalline lattice or along the crystal boundaries (Luan and Paterson, 1992; Gleason and Tullis, 1995; Kohlstedt et al., 1995; Post et al., 1996). The recrystallized quartz crystals of the studied granitoids show dynamic recrystallization microstructures defined by new crystals, with sutured contacts and relatively coarse granulation, which indicate GBM \pm SGR mechanisms under conditions of low deformation rate and differential stress at temperature higher than 500 °C in the presence of water (regime 3 of Hirth and Tullis, 1992). The deformational behavior of feldspars is strongly temperature-dependent and similar for both plagioclase and alkali-feldspars (Tullis, 1983; Tullis and Yund, 1985, 1987). In the studied granitoids, the very fine granulation in the feldspar mantles suggest dynamic recrystallization via BLG \pm SGR. According to experimental studies, BLG in feldspars can develop at ~ 450 – 600 °C, while

Table 2
Analytical results for Pb-Pb evaporation geochronology.

Zircon	Temp.	Ratios	$^{204}\text{Pb}/^{206}\text{Pb}$	2σ	$(^{208}\text{Pb}/^{206}\text{Pb})$	2σ	$(^{207}\text{Pb}/^{206}\text{Pb})$	2σ	Age	2σ
AMP27/2	1550	16/16	0.000055	0.000007	0.32924	0.02766	0.1915	0.00036	2755.4	3.1
AMP27/3	1500	36/36	0.00006	0.000004	0.30835	0.00393	0.19171	0.00025	2757.2	2.1
AMP27/7	1500	10/18	0.000044	0.00002	0.36544	0.00145	0.19148	0.00037	2755.2	3.2
AMP27/23	#1450	0/8	0.00109	0.000062	0.15454	0.00217	0.17711	0.00106	2626.2	9.9
	*1500	0/36	0.000212	0.000016	0.17906	0.00253	0.18873	0.00067	2731.6	5.9
	1550	34/34	0.000181	0.000013	0.18215	0.00044	0.19111	0.00024	2752.1	2.1
AMP27/27	*1450	0/22	0.00012	0.000013	0.13495	0.00198	0.18493	0.00033	2698	2.9
	1500	36/36	0.000078	0.000005	0.23529	0.00053	0.19111	0.00023	2752	2
MD01/3	*1450	0/12	0.000879	0.000019	0.23663	0.00142	0.17986	0.00199	2652	18
	1500	22/22	0.000272	0.000008	0.25250	0.00654	0.19067	0.00056	2748	5
	1550	32/32	0.000271	0.000008	0.26816	0.00115	0.19015	0.00043	2744	4
MD01/4	1500	08/08	0.000094	0.000031	0.30565	0.00471	0.19119	0.00141	2753	12
MD01/13	*1450	0/36	0.000195	0.000013	0.25544	0.00232	0.18741	0.00033	2720	3
	1500	36/36	0.000171	0.000017	0.28003	0.00144	0.19095	0.00023	2751	2
MD01/16	1500	30/30	0.000181	0.000011	0.59212	0.00905	0.19049	0.0005	2747	4
MYF40/1	1500	24/24	0.000057	0.000008	0.2417	0.002	0.1915	0.0002	2755	2
MYF40/3	1500	36/36	0.000142	0.000007	0.2161	0.0053	0.1907	0.0003	2749	3
MYF40/4	1450	0/6	0.000178	0.000088	0.3035	0.0039	0.1901	0.0011	2744	10
MYF40/7	1500	0/6	0.000103	0.000082	0.1397	0.0028	0.1914	0.0035	2754	30

(#) – Evaporation stage eliminated for present $^{204}\text{Pb}/^{206}\text{Pb}$ ration higher than 0,0004.

(*) – Evaporation stage eliminated subjectively.

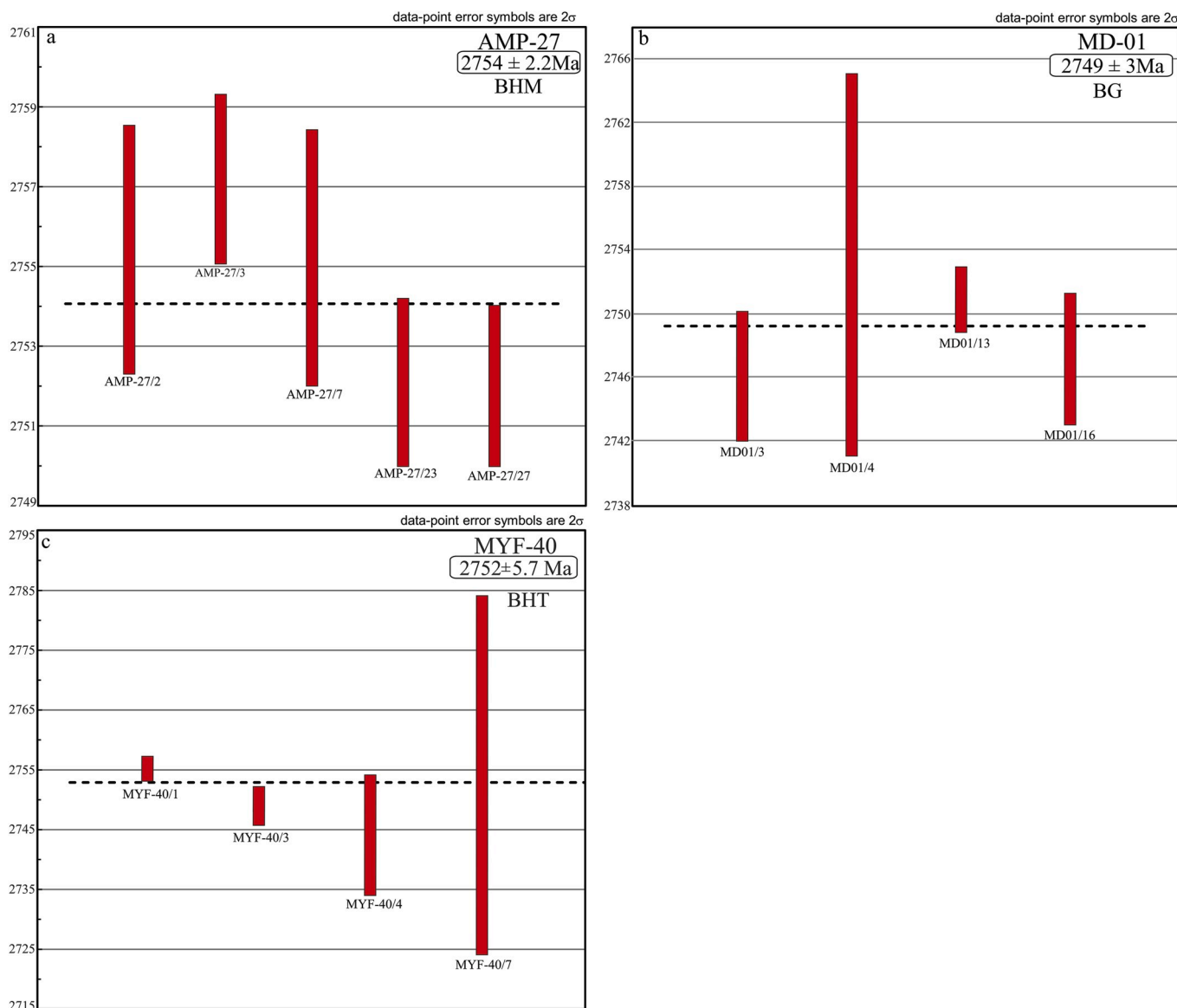


Fig. 8. Pb-Pb mean ages of the dated samples from: a) Seriated biotite-hornblende monzogranite, b) porphyritic biotite monzogranite and c) biotite-hornblende tonalite.

myrmekite and dynamic recrystallization via SGR occur at temperatures above 600 °C (Gapais, 1989; Tullis and Yund, 1991). Therefore, in accordance with the microstructural observations in quartz, the microstructural analysis of feldspars of the studied granitoids indicates moderate to high-temperature deformation (>500 °C).

Ferromagnesian minerals show a different deformational behavior. According to experimental studies (Kronenberg et al., 1990; Wilson, 1980), at temperatures above 250 °C, biotite is ductile and frequently recrystallizes to form fine-grained crystals. Accordingly, biotite is commonly found as aggregates of recrystallized grains. On the other hand, hornblende grains, as well as accessory minerals, are deformed dominantly by brittle-ductile mechanisms. Hornblende with undulatory extinction and subgrain patterns is found only locally in the high-strain domains suggesting the local occurrence of relatively high deformation temperature (>650–700 °C according to experimental studies of amphibole deformation; Allison and Latour, 1977; Imon et al., 2002).

The common occurrence, in the low-strain domain of the plutons, of microstructures such as microfractures in feldspar phenocrysts, filled with quartz-feldspathic matrix indicating that they were “healed” by melt (Fig. 7d), and a preferred orientation of feldspar crystals with

magmatic shape suggest that submagmatic flow operated during the final stage of crystallization of the granitoids. This is evidence that emplacement and deformation of the studied rocks were coeval (Passchier and Trouw, 2005; Nedelec and Bouchez, 2015).

In short, the microstructures reveal a deformational history of the granitoids involving progressive cooling in the presence of a volatile-rich phase, from the (sub)magmatic to the solid state (Fig. 9a–e). Emplacement and, final crystallization were thus synchronous with deformation in the Vila Jussara suite.

6.2. Magma interaction mechanisms in the Vila Jussara plutons

The Vila Jussara plutonic complex belongs to a series of A-type Neoarchean plutons described in the Carajás province and is composed of rocks with different FeO/(FeO + MgO) ratios, reduced ferroan, oxidized ferroan and magnesian granitoids according to Dall'Agnol et al. (2017). However, its petrology is more complex than previously thought. In particular, the magnesian granitoids are not a single group of rocks, but consist of porphyritic granitoids and tonalites. Also, extensive hybridization between the different granitoids occurred at the time of

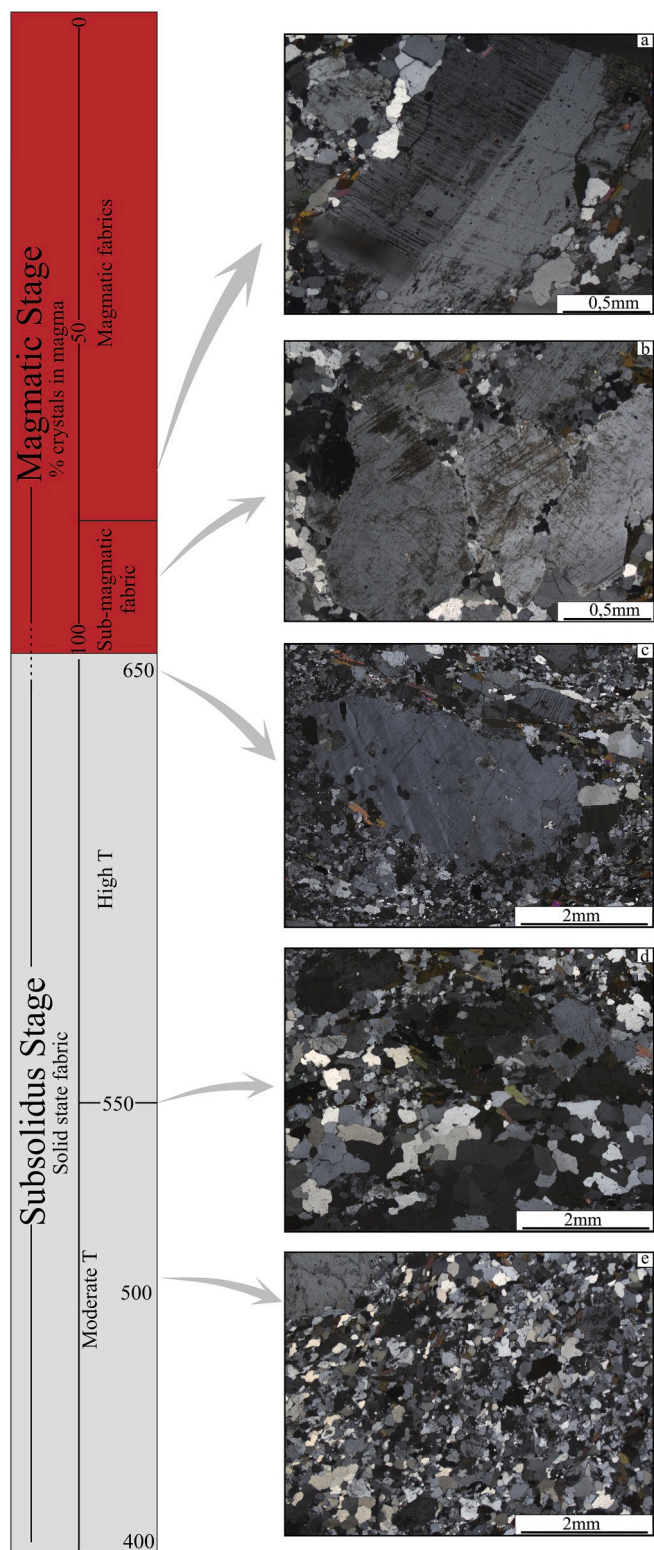


Fig. 9. Summary of the wide range of microstructures observed in the Vila Jussara granitoids. The microstructures reveal progressive cooling in the presence of a water-rich volatile phase and progressive deformation from the (sub) magmatic to the solid state.

their emplacement (Fig. 5). The presence of enclaves of the BHM variety partially digested by porphyritic granitoids suggests a weak rheological contrast between these two components.

Hibbard (1995) considers that a magmatic mixing system should

consist of a magma and a partially crystallized magma that may be either more felsic or more mafic than the other. Such magmas can be: (i) primitive, (ii) evolved, or (iii) hybridized by some previous magma mixing event (Hibbard and Watters, 1985), and may be mixed in different ways, generating a virtually infinite number of hybridized magmas. Generally, the process involves magmas with different temperatures, which often generate thermal disequilibrium features. In the most extreme case, instantaneous injection of mafic magma into a felsic magma chamber with temperatures of approximately 1200 °C and 700 °C, respectively, are catastrophic events, with immediate cooling of the mafic magma and a corresponding overheating of the felsic magma (Hibbard, 1995).

In most magmatic systems where mixing occurs, the less differentiated magmas are not introduced only at the beginning of the plutonic history: they are usually injected at different stages of crystallization of the more differentiated magma. Diverse types of interactions are produced depending on the degree of crystallization of the most differentiated magma at the time of injection of the mafic magma (Barbarin and Didier, 1992). As already stated, the viscosity contrast between the magmas that formed the Vila Jussara granitoids was weak, mainly because they had similar compositions, hence thermal disequilibrium due to mixing was limited.

6.3. Insights on the construction and emplacement of the Vila Jussara plutons

A set of criteria (see e.g. Paterson and Vernon, 1995) may help to determine whether the ascent and emplacement of magmas were controlled by shear zones: (i) evidence of shear zone-assisted extraction of melt in the source region; (ii) plutons fed by diking in the shear zone; (iii) magmatic contacts crosscut by mylonitic foliation in the country rock; (iv) extensive deformation of the country rock showing evidence of pre- and post-emplacement mylonitization; (v) xenoliths of mylonite within the magmatic rocks that are free of solid-state deformation; (vi) less deformation in the mylonitic igneous rock than in the mylonitic country rock; (vii) plutons displaying large aspect ratios, although they do not show intense solid-state deformation; (viii) magmatism restricted to the vicinity of the shear zone; and (ix) alignment of plutons along the shear zone. Some of these criteria are clearly observed in the Vila Jussara plutons, and together with extensive steeply-dipping foliations and shallowly-plunging to oblique mineral lineations (Fig. 6), point to a model that supports both shear zone-assisted melt collection and magma emplacement favored by tranpressive movement.

The estimated pressures of emplacement of these plutons are 3–5 kbar (Dall'Agnol et al., 2017), which correspond to depths of ~11–18 km (mesozone conditions). Emplacement at such moderated crustal depths took place within older, hence colder and more rigid granitoids, as shown by the field relationships (sharp contacts and occurrence of angular xenoliths of TTG country rocks; Fig. 2b) and by the contrast of ages between the country rocks (2.87–2.93 Ga; Silva et al., 2014) and granites (~2.75–2.73 Ga; this work; Dall'Agnol et al., 2017).

Field relationships and geochemical data suggest that the different granitoid varieties of the Vila Jussara suite are not comagmatic (Dall'Agnol et al., 2017): there is increasing evidence that BHM, BG and BHT crystallized from three distinct magmas, and that the HBG resulted from mixing. However, the crystallization ages of the BHM, BG and BHT varieties are quite similar at 2754 ± 2.2 Ma, 2749 ± 3 Ma and 2752 ± 5.7 Ma, showing that the plutons were formed during a single thermal event. Based on these considerations, and admitting the existence of three independent magmas, equivalent to BHM, BG and BHT, a model of syntectonic pluton construction involving three main stages is proposed (Fig. 10):

- 1) The granitic (BG) and tonalitic (BHT) magmas were generated at the same time (at ~2.75). Due to the compressive regime that the area experienced in these Neoarchean times, old Mesoarchean structures

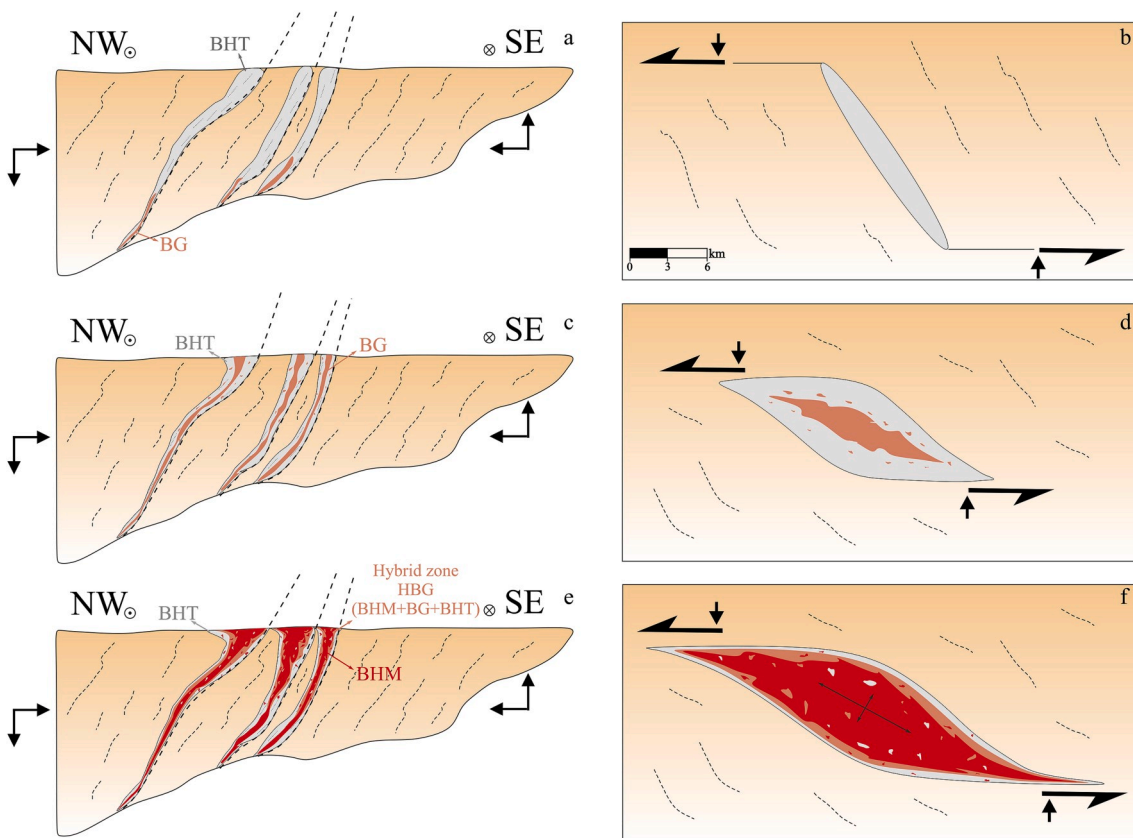


Fig. 10. Model of syntectonic ascent and emplacement of the Vila Jussara magmas. a) and b) Stage one. Generation of the granite (BG) and tonalite (BHT) magmas, with ascent and emplacement of the BHT magma; c) and d) Stage two. Ascent of large amounts of BG magma with subsequent enlargement of the pluton; e) and f) Stage three. Injection of larger volume of felsic magma (BHM) and interaction between the successive magmatic pulses forming a porphyritic hybrid granitoid, the HBG variety.

were reactivated, generating a large number of sinistral, transpressive shear zones. These ductile shear zones served as conduits for magmas to ascend to shallower crustal levels. In the first stage (Fig. 10a and b), the tonalitic magma was likely able to ascend more efficiently than the granitic magma due to its lower viscosity. This first pulse of (tonalitic) magma initiated the pluton construction through space opening possibly, at least locally, owing to injection into extensional zones.

- 2) The BG magma ascended in a similar way and was emplaced in the space opened by the BHT magma. The BHT and BG magmas showing low contrast of temperature and viscosity, the granitic magma interacted with the surrounding tonalitic magma and was partially disintegrated, giving rise to numerous granitic enclaves in the tonalite as well as enclaves of tonalite in the granite, in addition to interdigitated contact zones between the two rocks (Fig. 10c and d).
- 3) The last stage was characterized by the intrusion of a larger volume of granitic magma (BHM) compared to the two first pulses (BHT, BG), which enlarged the open space in the crust. Due to syn-emplacement shearing, the plutons acquired a sigmoidal shape. Along the large contact zones between the successive pulses, the BG and BHT magmas, and to a lesser extent the BHM magma, continuously interacted until a hybrid zone was formed. Granitoids from this zone (HBG) show a distinct porphyritic texture and remarkable micro-to macroscopic similarities with both the BG and BHT varieties (Fig. 10e and f).

We have introduced our model of magma ascent and emplacement favored by shear zone activity in the regional structural interpretation made by Araújo and Maia (1991) (Fig. 11a). Hence, it is shown that migration of the Vila Jussara magmas occurred through a channel

network made of active translithospheric shear zones (Fig. 11b). As already detailed in the model of Fig. 10, the successive magmatic pulses, mostly the BHT and BG magmas, interacted continuously in the thin border zones, leading to considerable compositional changes, with formation of a hybrid granitoid (HBG). It is suggested here in addition that a turbulent convective flow induced by the rising BHM magma was responsible for ripping off and stretching globules from partially crystallized border zones (Fig. 11c) now found as elongated enclaves in the BHM (Fig. 5c).

6.4. Tectonic implications

The complex deformational history of the Neoarchean granitoids of the Carajás province led to often-controversial interpretation of their emplacement conditions. These granitic bodies are usually classified as syntectonic A-type granitoids that were deformed during the closure of the Carajás basin at approximately 2.75 to 2.73 Ga (Barros et al., 2001, 2009; Feio et al., 2012, 2013; Dall'agnol et al., 2017). However, Tavares (2015) stated that these rocks were formed in a distensional rift setting at ~2.73 Ga and were deformed later during the closure of the basin at 2.68 to 2.63 Ga.

It is shown here that magmas of the Vila Jussara Suite were channeled through the crust via reactivated Mesoarchean shear zones forming the ~E-W Itacaiúnas belt, in a context of pure shear-dominated sinistral transpression. It is likely that closure of the Carajás basin occurred during the event of regional deformation responsible for the formation of the Itacaiúnas belt that triggered emplacement of the Vila Jussara suite in the Neoarchean (Dall'Agno et al., 2017). Hence, it is concluded that the Neoarchean magmatism of the Carajás province was generated in a transpressional tectonic regime at 2.75 Ga. Other

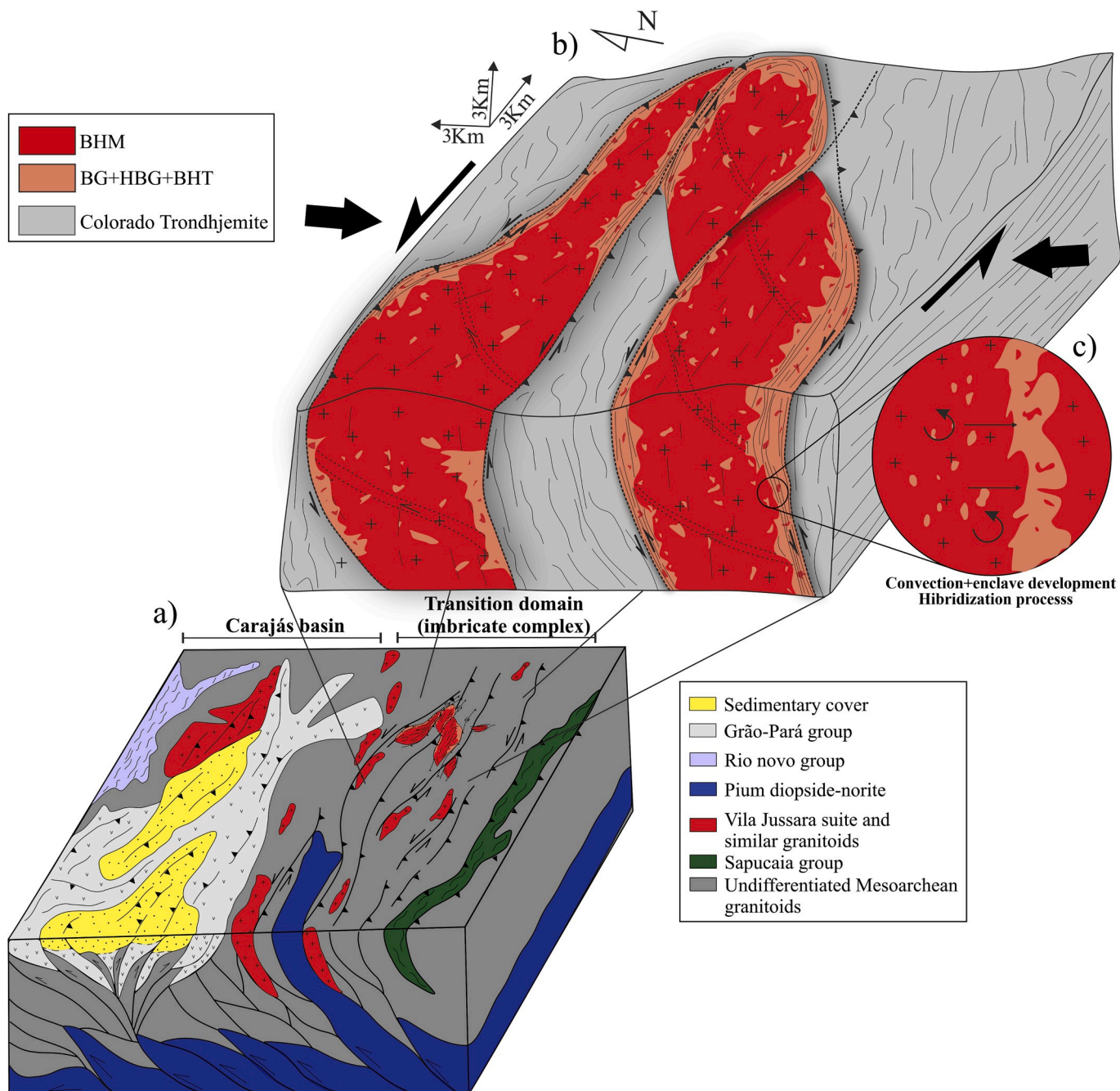


Fig. 11. Emplacement model of the Vila Jussara suite. a) Regional structural interpretation of Araújo and Maia (1991) modified to fit the syntectonic interpretation of the Vila Jussara granitoids; b) Pervasive flow and syntectonic emplacement of the Vila Jussara suite through injection of multiple magmatic pulses controlled by large-scale transpressive sinistral shear zones; c) Detail of the interaction between the BHT, BG and BHM magmas giving rise to extensive hybridization and formation of the HBG magma.

Neoarchean granitoids from the Carajás domain (e.g. the Vila União suite; Marangoanha et al., 2019, 2020) and worldwide (Shukla and Mohan, 2019; Polat et al., 2018; Mvondo et al., 2017; Tang and Santosh, 2018; Zibra et al., 2017; Laurent et al., 2014) despite their own particularities present regional tectonic history at ~2.7 Ga similar to what is suggested here for the Vila Jussara suite.

7. Conclusions

The geological picture of the Neoarchean granitoids in the Vila Jussara area is more complex than previously admitted. Identification of various lithotypes in the Vila Jussara suite with contrasted textures and

mineralogies, however similar crystallization ages (~2.75 Ga) allows to propose a model of pluton building during a single thermal event by multiple injections of magmas, generating extensive hybridization. It is also proposed that ascent and emplacement of the Vila Jussara plutons were controlled by imbricated E-W sinistral transpressive shear zones of the Itacaiúnas belt. These shear zones resulted from high-temperature reactivation of Mesoarchean megastructures (translithospheric shear zones) during oblique collision.

Declaration of competing interest

The authors declare that they have no known competing financial

interests or personal relationships that could have appeared to influence the work reported in this paper.

CRediT authorship contribution statement

Fernando Fernandes da Silva: Writing - original draft, Conceptualization, Methodology, Investigation. **Davis Carvalho de Oliveira:** Writing - review & editing, Methodology. **Roberto Dall'Agnol:** Supervision. **Luciano Ribeiro da Silva:** Formal analysis. **Ingrid Viana da Cunha:** Validation.

Acknowledgments

The authors would like to thank the Research Group on Granitoid Petrology (GPPG) for its support in the various stages of this work, the Institute of Geosciences (IG) of the Universidade Federal do Pará (UFPA), the Post-Graduate Program in Geology and Geochemistry (PPGG) and F.V Guimarães for the Pb-Pb data acquisition and M.L.T. Silva for the collect and organization of prior samples and petrographic data. We are also grateful to M.T. Galarza for assistance during the acquisition of Pb-Pb evaporation geochronology data at the Laboratório de Geologia de Isotópica (PARAISO-UFPA). We also wish to express our gratitude to the anonymous reviewers for the careful reading and many insight thoughts on the manuscript. The first author (FF) thanks the Conselho Nacional de Desenvolvimento Científico e Tecnológico (CNPq) and Coordenação de Aperfeiçoamento de Pessoal de Nível Superior (CAPES) for a doctoral thesis scholarship (Proc. 140077/2018-9 and finance code 001). Funding for this project came from CNPq (D.C. Oliveira – Proc. 311647/2019-7 and 435552/2018-0; R. Dall'Agnol - Proc. 306108/2014-3) and PROPESP (PAPQ)/UFPA.

Appendix A. Supplementary data

Supplementary data to this article can be found online at <https://doi.org/10.1016/j.jsames.2020.102696>.

References

- Allison, I., Latour, T.E., 1977. Brittle deformation of hornblende in a mylonite: a direct geometrical analogue of ductile deformation by translation gliding. *Can. J. Earth Sci.* 14, 1953–1958.
- Almeida, F.F.M., Hasui, Y., Brito Neves, B.B., Fuck, R.A., 1981. Brazilian Structural provinces: an introduction. *Earth Sci. Rev.* 1–29.
- Almeida, J.A.C., Dall'Agnol, R., Leite, A.A.S., 2013. Geochemistry and zircon geochronology of the Archean granite suites of the Rio Maria granite-greenstone terrane, Carajás Province, Brazil. *J. S. Am. Earth Sci.* 42, 103–126.
- Almeida, J.A.C., Dall'Agnol, R., Oliveira, M.A., Macambira, M.J.B., Pimentel, M.M., Rämö, O.T., Guimarães, F.V., Leite, A.A.S., 2011. Zircon geochronology, geochemistry and origin of the TTG suites of the Rio Maria granite-greenstone terrane: implications for the growth of the Archean crust of the Carajás province, Brazil. *Precambrian Res.* 187 (1), 201–211.
- Althoff, F.J., Barbey, P., Boullier, A.M., 2000. 2.8–3.0 Ga plutonism and deformation in the SE Amazonian craton: the Archean granitoids of Marajoara (Carajás Mineral province, Brazil). *Precambrian Res.* 104, 187–206.
- Araújo, O.J.B., Maia, R.G.N., Silva, J.J.X.D.A., Costa, J.B.S., 1988. A megaestruturação arqueana da folha Serra dos Carajás. *Anais VII Congresso Latino-Americano de Geologia* 1, 324–338 (Belém).
- Araújo, O.J.B., Maia, R.G.N., 1991. Projeto especial mapas de recursos minerais, de solos e de vegetação para a área do Programa Grande Carajás; Subprojeto Recursos Minerais; Folha SB.22-Z-A Serra dos Carajás - Estado do Pará. DNPM/CPRM, Brasília, p. 136.
- Bandyopadhyay, P.K., Chakrabartil, A.K., DeoMurari, M.P., Misra, S., 2001. 2.8 Ga oldanorogenic granite-acid volcanics association from western margin of the Singhbhum-Orissa Craton, Eastern India. *Gondwana Res.* 1, 465–475.
- Barbarin, B., Didier, J., 1992. Genesis and evolution of mafic magmatic enclaves through various types of interactions between coeval felsic and mafic magmas. *Earth and Environmental Science Transactions of the Royal Society of Edinburgh* 83, 145–153.
- Barbosa, A.A., Lafon, J.M., Neves, A.P., Vale, A.G., 1995. Geocronologia Rb-Sr e Pb-Pb do Granito Redenção, SE do Pará: implicações para a evolução do magmatismo proterozóico da região de Redenção. *Boletim do Museu Paraense Emílio Goeldi, Série Ciências da Terra* 7, 147–164.
- Barros, C.E.M., Sardinha, A.S., Barbosa, J.P., Krimski, R., Macambira, M.J., 2001. Pb-Pb and zircon ages of Archean sytectonic granites of the Carajás metallogenic province, Northern Brazil. In: Servicio Nacional de Geología Y Minería, Simposio Sudamericano de Geología Isotópica, 3, Resumos Expandidos (Pucon, Chile, CD-ROM).
- Barros, C.E.M., Sardinha, A.S., Barbosa, J.P., Macambira, M.J., Barbey, P., Boullier, A.M., 2009. Structure, petrology, geochemistry and zircon U/Pb and Pb/Pb geochronology of the synkinematic archean (2.7 Ga) a-type granites from the Carajás metallogenic province, northern Brazil. *Can. Mineral.* 47, 1423–1440.
- Behr, W.M., Platt, J.P., 2011. A naturally constrained stress profile through the middle crust in an extensional terrane. *Earth Planet Sci. Lett.* 303, 181–192.
- Bodorkos, S., Cawood, P.A., Oliver, N.H.S., 2000. Timing and duration of synmagmatic deformation in the Mabel Downs Tonalite, northern Australia. *J. Struct. Geol.* 22, 1181e1198.
- Brown, M., Solar, G.S., 1998. Granite ascent and emplacement during contractional deformation in convergent orogens. *Journal of Structural Geology* 20 (9), 1365e1393.
- Costa, J.B.S., Araújo, O.J.B., João, X.S.J., Macambira, M.J.B., Lafon, J.M., 1995. A Província Mineral de Carajás: aspectos tectono-estruturais, estratigráficos e geocronológicos. *Boletim do Museu Paraense Emílio Goeldi, Série Ciências da Terra* 7, 199–235.
- Cunha, I.R.V., Dall'Agnol, R., Feio, G.R.L., 2016. Mineral chemistry and magnetic petrology of the archean Planalto suite, Carajás province – amazonian craton: implications for the evolution of ferroan archean granites. *J. S. Am. Earth Sci.* 67, 100–121.
- Dall'Agnol, R., Cunha, I.R., Guimarães, F.V., Oliveira, D.C., Feio, G.R., Lamarão, C.N., 2017. Mineralogy, geochemistry, and petrology of Neoarchean ferroan to magnesian granites of Carajás Province, Amazonian Craton: the origin of hydrated granites associated with charnockites. *Lithos* 277, 3–32.
- Dall'Agnol, R., Oliveira, D.C., Guimarães, F.V., Lamarão, C.N., Althoff, F.J., 2013. Geologia do Subdomínio de Transição do Domínio Carajás – implicações para a evolução arqueana da Província Carajás – pará. In: Simpósio de Geologia da Amazônia, vol. 13. Belém (PA), CD-rom.
- D'lemos, R.S.D., Brown, M., Strachan, R.A., 1992. Granite magma generation, ascent and emplacement within a transpressional orogen. *J. Geol. Soc.* 149, 487–490.
- Dunlap, W.J., Hirth, G., Teyssier, C., 1997. Thermomechanical evolution of a ductile duplex. *Tectonics* 16, 983–1000.
- Essene, E.J., 1989. The current status of thermobarometry in metamorphic rocks. In: Daly, J.S., Cliff, R.A., Yardley, B.W.D. (Eds.), *Evolution of Metamorphic Belts*, vol. 43. Geological Society, London, Special Publications, pp. 1–44.
- Feio, G.R., Dall'Agnol, R., Dantas, E.L., Macambira, M.J., Gomes, A.C., Sardinha, A.S., Santos, P.A., 2012. Geochemistry, geochronology, and origin of the Neoarchean Planalto Granite suite, Carajás, Amazonian craton: a-type or hydrated charnockitic granites? *Lithos* 151, 57–73.
- Feio, G.R., Dall'Agnol, R., Dantas, E.L., Macambira, M.J., Santos, J.O., Althoff, F.J., Soares, J.E., 2013. Archean granitoid magmatism in the Canaã dos Carajás area: implications for crustal evolution of the Carajás province, Amazonian craton, Brazil. *Precambrian Research* 227, 157–185.
- Florisbal, L.M., Bitencourt, M.F., Janasi, V.A., Nardi, L.V.S., Heaman, L.M., 2012. Petrogenesis of syntectonic granites emplaced at the transition from thrusting to transcurrent tectonics in post-collisional setting: whole-rock and Sr-Nd-Pb isotope geochemistry in the Neoproterozoic Quatro Ilhas and Mariscal Granites, Southern Brazil. *Lithos* 153, 53–71.
- Gabriel, E.O., Oliveira, D.C., 2014. Geologia, petrografia e geoquímica dos granitoides arqueanos de alto magnésio da região de Água Azul do Norte, porção sul do Domínio Carajás, Pará. *Boletim do Museu Paraense Emílio Goeldi, Cienc. Nat.* 9 (3), 533–564.
- Gapais, D., 1989. Shear structures within deformed granites: mechanical and thermal indications. *Geology* 17, 1144–1147.
- Gleason, G.C., Tullis, J., 1995. A flow law for dislocation creep of quartz aggregates determined with the molten-salt cell. *Tectonophysics* 247, 1–23.
- Hacker, B.R., Yin, A., Christie, J.M., Snook, A.W., 1990. Differential stress, strain rate, and temperatures of mylonitization in the Ruby Mountains, Nevada: implications for the rate and duration of uplift. *J. Geophys. Res.* 95, 8569–8580.
- Hibbard, M.J., 1995. Petrography and Petrogenesis. Prentice Hall, New Jersey.
- Hibbard, M.J., Watters, R.J., 1985. Fracturing and dikeing in incompletely crystallized granitic plutons. *Lithos* 18, 1–12.
- Hirth, G., Tullis, J., 1992. Dislocation creep regimes in quartz aggregates. *J. Struct. Geol.* 14, 145–159.
- Hodges, K., 1991. Pressure-temperature-time paths. *Annu. Rev. Earth Planet Sci.* 19, 207–236.
- Holdsworth, R.E., Pinheiro, R.V.L., 2000. The anatomy of shallow-crustal transpressional structures: insights from the Archaean Carajás fault zone, Amazon, Brazil. *J. Struct. Geol.* 22, 1105–1123.
- Hutton, D.H.W., Dempster, T.J., Brown, P.E., Becher, S.M., 1990. A new mechanism of granite emplacement: intrusion in active extensional shear zones. *Nature* 343, 452–455.
- Hutton, D.H.W., Reavy, R.J., 1992. Strike-slip tectonics and granites petrogenesis. *Tectonics* 11, 960–967.
- Hutton, D.H.W., 1988. Granite emplacement mechanisms and tectonic controls: inferences from deformation studies. *Earth and Environmental Science Transactions of the Royal Society of Edinburgh* 79, 245–255.
- Imon, R., Okudaira, T., Fujimoto, A., 2002. Dissolution and precipitation processes in the deformed amphibolites: an example from the ductile shear zone of the Ryoke metamorphic belt, SW Japan. *Journal of Metamorphic Geology* 20, 297–308.
- Karlstrom, K.E., Miller, C.F., Kingsbury, J.A., Wooden, J.L., 1993. Pluton emplacement along an active ductile thrust zone, Piute Mountains, Southeastern California: interaction between deformational and solidification processes. *Geol. Soc. Am. Bull.* 105, 213e230.

- Kober, B., 1987. Single grain evaporation combined with Pb emitter bedding $^{207}\text{Pb}/^{206}\text{Pb}$ investigations using thermal ion mass spectrometry and implications to zirconology. *Contribution Mineralogy and Petrology* 96, 63–71.
- Kohlstedt, D.L., Evans, B., Mackwell, S.J., 1995. Strength of the lithosphere — constraints imposed by laboratory experiments. *Journal of Geophysical Research Atmospheres* 100, 17587–17602.
- Kronenberg, A.K., Kirby, S., Pinkston, J., 1990. Basal slip and mechanical anisotropy of biotite. *Journal of Geophysical Research Atmospheres* 95, 19257–19278.
- Kruhl, J.H., 1998. Reply: prism- and basal-plane parallel subgrain boundaries in quartz: a microstructural geothermobarometer. *Journal of Metamorphic Petrology* 16, 142–146.
- Larin, A.M., Kotov, A.B., Sal'nikova, E.B., Glebovitskii, V.A., Sukhanov, M.K., Yakovleva, S.Z., Kovach, V.P., Berezhnaya, N.G., Velikoslavinskii, S.D., Tolkachev, M.D., 2006. The Kalar Complex, Aldan-Stanovoi Shield, an ancient anorthosite–mangerite–charnockite–granite association: geochronologic, geochemical, and isotopic-geochemical characteristics. *Petrology* 14, 2–20.
- Laurent, O., Raposo, M., Stevens, G., Moyen, J.F., Martin, H., Doucelance, R., Bosq, C., 2014. Contrasting petrogenesis of Mg–K and Fe–K granitoids and implications for post-collisional magmatism: case study from the Late-Archean Matok pluton (Pietersburg block, South Africa). *Lithos* 196–197, 131–149.
- Law, R.D., 2014. Deformation thermometry based on quartz c-axis fabrics and recrystallization microstructures: a review. *J. Struct. Geol.* 66, 129–161.
- Le Maître, R.W., 2002. A Classification of Igneous Rocks and Glossary of Terms, 2 ed. Cambridge University Press, London.
- Leite-Santos, P.J., Oliveira, D.C., 2014. Trondhjemites da área de Nova Canadá: novas ocorrências de associações magmáticas tipo TTG no Domínio Carajás. *Boletim do Museu Paraense Emílio Goeldi, Cienc. Nat.* 9 (3), 635–659.
- Leite-Santos, P.J., Oliveira, D.C., 2015. Leucogranitos arqueanos de Água Azul do norte – província Carajás. In: Simpósio de Geologia da Amazônia, vol. 14. Marabá (PA), CD-rom.
- Luan, F.C., Paterson, M.S., 1992. Preparation and deformation of synthetic aggregates of quartz. *J. Geophys. Res.* 97, 301–320.
- Macambira, J.B., Moura, C.A.V., Lafon, J.M., Scheller, T., 1994. O método Pb-Pb por Evaporação em Zircão: avaliação dos Dados Obtidos no Laboratório de Geologia Isotópica da UFPA. In: Congresso brasileiro de geologia, 38. Camboriú, pp. 404–406, 1994. Anais SBG.
- Machlin, E.S., 2007. An Introduction to Aspects of Thermodynamics and Kinetics Relevant to Materials Science, 3rd edn. Elsevier, Oxford, pp. 461–pp.
- Marangoanha, B., Oliveira, D.C., Oliveira, V.E., Galarza, M.A., Lamarão, C.N., 2019. Neoarchean A-type granitoids from Carajás province (Brazil): new insights. *Precambrian Res.* 324, 86–108.
- Misra, S., Sankar, S.S., Ghosh, S., 2002. Evolution of Mayurbhanj granite pluton, eastern Singhbhum, India: a case study of petrogenesis of an A-type granite in bimodal association. *J. Asian Earth Sci.* 20, 965–989.
- Moore, M., Davis, D.W., Robb, L.J., Jackson, M.C., Grobler, D.F., 1993. Archean rapakivi granite-anorthosite-rhyolite complex in the Witwatersrand basin Hinterland, southern Africa. *Geology* 21, 1031–1034.
- Moreto, C.P.N., Monteiro, L.V.S., Xavier, R.P., Amaral, W.S., Santos, T.J.S., Juliani, C., Souza Filho, C.R., 2011. Mesoarchean (3.0 and 2.86 Ga) host rocks of the iron oxide–Cu–Au Bacaba deposit, Carajás Mineral Province: U–Pb geochronology and metallogenetic implications. *Miner. Deposita* 46, 789–811.
- Mvondo, H., Lentz, D.R., Bardoux, M., 2017. Crustal shortening and thickening in Neoarchean granite-greenstone belts: a case study from the link between the ~2.7 Ga Elu and Hope Bay belts, northeast Slave craton, Canada. *J. Struct. Geol.* 104, 6–20.
- Nedelec, A., Bouchez, J.L., 2015. Granites: Petrology, Structure, Geological Setting, and Metallogeny. Oxford University Press, New York.
- Neves, S.P., Vauchez, A., Archanjo, C.J., 1996. Shear-zone controlled magma emplacement or magma-assisted nucleation of shear-zones? Insights from northeast Brazil. *Tectonophysics* 262, 349–365.
- Oliveira, D.C., Santos, P.J., Gabriel, E.O., Rodrigues, D.S., Faresin, A.C., Silva, M.L., Macambira, M.J., 2010. Aspectos geológicos e geocronológicos das rochas magmáticas e metamórficas. Congresso Brasileiro de Geologia 45. CDrom, Belém (in Portuguese).
- Oliveira, M.A., Dall'Agnol, R., Althoff, F.J., Leite, A.A.S., 2009. Mesoarchean sanukitoid rocks of the Rio Maria granite-greenstone terrane, Amazonian craton, Brazil. *J. S. Am. Earth Sci.* 27 (2), 146–160.
- Paiava Jr., A.L.D.P., Lamarão, C.N., Lima, P.H.A., 2011. Geologia, Petrografia e Geoquímica do Batólito Seringa, Província Carajás, SSE do Pará. *Braz. J. Genet.* 41 (2), 185–202.
- Passchier, C.W., Trouw, R.A.J., 2005. Microtectonics, 2 ed. Springer-Verlag, Germany.
- Paterson, S.R., Tobisch, O., 1992. Rates of processes in magmatic arcs: implications for the timing and nature of pluton emplacement and wall rock deformation. *J. Struct. Geol.* 14, 291–300.
- Paterson, S.R., Vernon, R.H., Tobisch, O.T., 1989. A review of criteria for the identifications of magmatic and tectonic foliations in granitoids. *J. Struct. Geol.* 11, 349–363.
- Paterson, S.R., Vernon, R.H., 1995. Bursting the bubble of ballooning plutons: a return to nested diapirism emplaced by multiple processes. *Geol. Soc. Am. Bull.* 107, 1356–1380.
- Petford, N., Cruden, A.R., McCaffrey, K.J.W., Vigneresse, J.L., 2000. Granite magma formation, transport and emplacement in the Earth's crust. *Nature* 408, 669e673.
- Philpotts, A., Ague, J., 2009. Principles of Igneous and Metamorphic Petrology, 2nd edn. Cambridge University Press, Cambridge, pp. 684–pp.
- Polat, A., Frei, R., Longstaffe, F.J., Woods, R., 2018. Petrogenetic and geodynamic origin of the neoproterozoic doré lake complex, Abitibi subprovince, Superior province, Canada. *Int. J. Earth Sci.* 107 (3), 811–843.
- Post, A.D., Tullis, J., Yund, R.A., 1996. Effects of chemical environment on dislocation creep of quartzite. *J. Geophys. Res.* 101, 22143–22155.
- Powell, R., Holland, T.J.B., 2008. On thermobarometry. *J. Metamorph. Geol.* 26, 155–179.
- Rajesh, H.M., Mukhopadhyay, J., Beukes, N.J., Gutierrez, J., Belyanin, G.A., Armstrong, R.A., 2009. Evidence for an early Archean granite from Bastar craton, India. *J. Geol. Soc.* 166, 193–196.
- Rodrigues, D.S., Oliveira, D.C., Macambira, M.J.B., 2014. Geologia, geoquímica e geocronologia do Granito Mesoarqueano Boa Sorte, município de Água Azul do Norte, Pará - província Carajás. Boletim do Museu Paraense Emílio Goeldi, Cienc. Nat. 9 (3), 597–633.
- Ronaib, C., Oliveira, D.C., 2013. Geologia, petrografia e geoquímica das associações TTG e leucogranodioritos do extremo norte do Domínio Rio Maria. Boletim do Museu Paraense Emílio Goeldi - Ciências Naturais 8 (3), 383–415.
- Rosenberg, C.L., 2004. Shear zones and magma ascent: a model based on a review of the Tertiary magmatism in the Alps. *Tectonics* 23 (3), n/a. -n-a.
- Santos, J.O., 2003. Geotectônica do Escudo das Guianas e Brasil-Central. In: Bizzi, L.A., Schobbenhaus, C., Vidotti, R.M., Gonçalves, J.H. (Eds.), *Geologia, Tectônica e Recursos Minerais do Brasil*. CPRM, Brasília, pp. 169–226 (s.n.).
- Santos, P.A., Feio, G.R., Dall'Agnol, R., Costi, H.T., Lamarão, C.N., Galarza, M.A., 2013. Petrography, magnetic susceptibility and geochemistry of the Rio Branco granite, Carajás province, southeast of Pará, Brazil. *Braz. J. Geol.* 43 (1), 2–15.
- Sardinha, A.S., Barros, C.E.M., Krymsky, R., 2006. Geology, geochemistry, and U–Pb geochronology of the Archean (2.74 Ga) Serra do Rabo granite stocks, Carajás Province, northern Brazil. *J. S. Am. Earth Sci.* 20, 327–339.
- Shukla, S., Mohan, M.R., 2019. Magma mixing in Neoproterozoic granite from Nalgonda region, Eastern Dharwar Craton, India: morphological, mineralogical and geochemical evidences. *Journal of Earth System Science*. <https://doi.org/10.1007/s12040-019-1095-8> (in press).
- Silva, A.C., Dall'Agnol, R., Guimarães, F.V., Oliveira, D.C., 2014. Geologia, petrografia e geoquímica de Associações Tonalíticas e Trondhjemíticas Arqueanas de Vila Jussara, Província Carajás, Pará. Boletim do Museu Paraense Emílio Goeldi. Boletim do Museu Paraense Emílio Goeldi - Ciências Naturais 9 (1), 13–45.
- Souza, S.Z., Dall'Agnol, R., Althoff, F.J., Leite, A.A.S., Barros, C.E.M., 1996. Carajás mineral province: geological, geochronological and tectonic constraints on the archean evolution of the Rio Maria granite-greenstone terrain and the Carajás block. *Extended Abstracts of the Symposium on Archean Terranes of South America Platform 1*, 31–32.
- Smithies, R.H., Champion, D.C., 1999. Late Archean felsic alkaline igneous rocks in the Eastern Goldfields, Yilgarn Craton, Western Australia: a result of lower crustal delamination? *J. Geol. Soc.* 156, 561–576.
- Stacey, J.S., Kramers, J.D., 1975. Approximation of terrestrial lead isotope evolution by two-stage model. *Earth and Planetary Science Letters* 26 (2), 207–221.
- Tang, L., Santos, M., 2018. Neoarchean granite-greenstone belts and related ore mineralization in the North China Craton: an overview. *Geoscience Frontiers* 9 (3), 751–768.
- Tassinari, C.G., Macambira, M.J.B., 2004. Evolução Tectônica Do Cráton Amazônico. São Paulo: S.I. S.B.G.
- Tavares, F.M., 2015. Evolução geotectônica do nordeste da Província Carajás. Tese de Doutorado – Universidade Federal do Rio de Janeiro, Rio de Janeiro, p. 115 (in Portuguese).
- Teixeira, M.F.B., Dall'Agnol, R., Silva, A.C., 2013. Geologia, petrografia e geoquímica do Leucogranodiorito Pantanal e dos leucogranitos arqueanos da área a norte de Sapucaia, Província Carajás, Pará: implicações petrogeológicas. *Boletim do Museu Paraense Emílio Goeldi - Ciências Naturais* 8 (3), 291–323.
- Teixeira, M.F.B., Dall'Agnol, R., Santos, J.O.S., Oliveira, D.C., Lamarão, C.N., McNaughton, N.J., 2018. Crystallization ages of paleoproterozoic A-type granite suites and related granites of Carajás province, Amazon craton: constraints from U–Pb geochronology of zircon and titanite. *J. S. Am. Earth Sci.* 88, 312–331.
- Teixeira, M.F.B., Dall'Agnol, R., Santos, J.O.S.S., Kemp, A., Evans, N., 2019. Petrogenesis of the paleoproterozoic (orosirian) A-type granites of Carajás province, Amazon craton, Brazil: combined in situ Hf isotope of zircon. *Lithos* 323–333, 1–22.
- Tullis, J., 1983. Deformation of feldspars. In: Ribbe, P.H. (Ed.), *Feldspar Mineralogy*, vol. 2. Mineralogical Society of America, pp. 297–323.
- Tullis, J., Yund, R.A., 1985. Dynamic recrystallisation of feldspar: a mechanism for ductile shear zone formation. *Geology* 13, 238–241.
- Tullis, J., Yund, R.A., 1987. Transition from cataclastic flow to dislocation creep of feldspar: mechanisms and microstructures. *Geology* 15, 606–609.
- Tullis, J., Yund, R.A., 1991. Diffusion creep in feldspar aggregates: experimental evidence. *J. Struct. Geol.* 13, 989–1000.
- Vasquez, L.V., Rosa-Costa, L.R., Silva, C.G., Ricci, P.F., Barbosa, J.O., Klein, E.L., Lopes, E.S., Macambira, E.B., Chaves, C.L., Carvalho, J.M., Oliveira, J.G., Anjos, G. C., Silva, H.R., 2008. Escala 1:1.000.000. In: Vasquez, M.L., Rosa-Costa, L.T. (Eds.), *Geologia e Recursos Minerais do Estado do Pará: Sistema de Informações Geográficas e SIG: texto explicativo dos mapas Geológico e Tectônico e de Recursos Minerais do Estado do Pará*. CPRM, Belém, p. 328 (in Portuguese).
- Vigneresse, J.L., Barbe, P., Cuney, M., 1996. Rheological transitions during partial melting and crystallization with application to felsic magma segregation and transfer. *J. Petrol.* 37, 1579–1600.
- Weinberg, R.F., Sial, A.N., Mariano, G., 2004. Close spatial relationship between plutons and shear zones. *Geology* 32, 377–380.
- Wilson, C.J., 1980. Shear zones in a pegmatite: a study of albite-mica-quartz deformation. *J. Struct. Geol.* 2, 203–209.

- Zhou, G., Wu, Y., Gao, S., Yang, J., Zheng, J., Qin, Z., Wang, H., Yang, S., 2015. The 2.65 Ga A-type granite in the northeastern Yangtze craton: petrogenesis and geological implications. *Precambrian Res.* 258, 247–259.
- Zibra, I., Clos, F., Weinberg, R.F., Peternell, M., 2017. The ~2730 Ma onset of the neorarchean yilgarn orogeny. *Tectonics* 36, 1787–1813.
- Zozulya, D.R., Bayanova, T.B., Eby, G.N., 2005. Geology and age of the Late Archean Keivy alkaline province, northeastern Baltic shield. *J. Geol.* 113, 601–608.

3 GEOCHEMISTRY, SHRIMP U-PB ZIRCON GEOCHRONOLOGY, AND Hf-Nd ISOTOPE COMPOSITION ON THE NEOARCHEAN VILA JUSSARA GRANITOID COMPLEX FROM CARAJÁS PROVINCE, AMAZONIAN CRATON: PETROGENESIS AND TECTONIC IMPLICATIONS.

Autores:

Fernando Fernandes da Silva
Davis Carvalho de Oliveira
Roberto Dall'Agnol
João Orestes Schneider Santos
Marco Antonio Galarza Toro
Fabriciana Vieira Guimarães
Luan Alexandre Martins de Souza

Artigo submetido para publicação em revista A *Qualis CAPES* (Lithos)

This is an automated message.

Journal: LITHOS

Title: Geochemistry, SHRIMP U-Pb Zircon geochronology, and Hf-Nd isotope composition on the Neoarchean Vila Jussara granitoid complex from Carajás Province, Amazonian Craton: petrogenesis and tectonic implications.

Corresponding Author: Mr Fernando Fernandes da Silva

Co-Authors: Davis Carvalho de Oliveira; Roberto Dall'Agnol; João Orestes Schneider Santos;

Marco Antonio Galarza Toro; Fabriciana Vieira Guimarães; Luan Alexandre Martins de Souza

Manuscript Number:

Geochemistry, SHRIMP U-Pb Zircon geochronology, and Hf-Nd isotope composition on the Neoarchean Vila Jussara granitoid complex from Carajás Province, Amazonian Craton: petrogenesis and tectonic implications.

Fernando Fernandes da Silva¹, Davis Carvalho de Oliveira¹, Roberto Dall'Agnol^{1,2}, João Orestes Schneider Santos³, Marco Antonio Galarza Toro¹, Fabriciana Vieira Guimarães⁴, Luan Alexandre Martins de Souza¹

¹ Grupo de Pesquisa Petrologia de Granitoides (GPPG) - Instituto de Geociências (IG) Programa de Pós-Graduação em Geologia e Geoquímica Universidade Federal do Pará (UFPA). CEP-66075-900, Belém, Pará. (PPGG) – IG – UFPA.

²Instituto Tecnológico Vale (ITV), Belém, PA, Brazil

³University of Western Australia, Centre for Exploration Targeting, Crawley, WA, 6009, Australia.

⁴Universidade Federal do Oeste do Pará, (UFOPA), Instituto de Engenharia e Geociências/Curso de Geologia. Rua Vera Paz Salé 68040255 - Santarém, PA – Brasil.

ABSTRACT

Neoarchean granitoids of the Vila Jussara complex are located in the Sapucaia subdomain from Carajás Province, where they appear as a series of coalescing sigmoidal-shaped plutons along the E-W direction with high angle foliations ($75\text{--}85^\circ$) that follow a regional trend. These plutons are formed mainly by seriated biotite-hornblende monzogranite (BHM). Subordinated varieties are biotite-hornblende tonalite (BHT); biotite granite (BG); and hornblende-biotite granite (HBG). As regards the geochemical features, these granitoids can be distinguished by Fe* index [FeOt/(FeOt/MgO) ratio]. The BHM present in general, moderate to high values of this ratio, and can be characterized as oxidized and reduced ferroan A-type granites. The BG and HBG are porphyritic granitoids and transitional between oxidized granites and slightly magnesian granites. In contrast, the BHT have lower and restricted FeOt/(FeOt/MgO) ratios and magnesian character. The SHIRMP U-Pb dating resulted in ages of 2743 ± 11 Ma for the BHM, 2742 ± 14 Ma for HBG and 2766 ± 9.6 Ma for BHT. The isotopic data of Nd and Hf suggest that the magmas of the Vila Jussara suite are not juvenile [ε Nd mostly between -3.5 and 0.24 and ε Hf between -3.5 and -1.2] and were derived from rocks of Mesoarchean age ($TDM > 3.0$ Ga). The petrogenetic model adopted to generate the primary magmas of this suite admits as source rocks geochemically similar to Mesoarchean granulites from the Ouro Verde area of the Canaã dos Carajás subdomain. The emplacement of Neoarchean granites occurred by multiple injections of magmas, generating extensive hybridization under a transpressional/transtensional tectonic regime dominated by pure shear, attributing a syn-tectonic post-collisional setting to these rocks.

1. Introduction

The different processes that formed the Archean continental crust are still the subject of extensive discussion and a lack of consensus (De Wit 1998, Moyen et al. 2006, Hamilton 2011, Bédard et al. 2013). Almost all Archean cratons exhibit variable field aspects, ranging from homogeneous gneisses to highly heterogeneous migmatites as a direct product of post-magmatic metamorphic overprinting (Martin 1994). Crustal reworking due to the successive tectono-thermal events that these terrains undergo ultimately hampers geodynamic reconstruction. The best attempt to reconstruct a crustal history and the different events that may have occurred is through granitoids, especially syntectonic plutons. From magma generation in the source to complete crystallization, syntectonic plutons may record short-lived geological events related to crustal melting and continental crust deformation (Paterson and Tobisch 1992, Karlstrom et al. 1993, Bodorkos et al. 2000, Petford et al. 2000, Rosemberg 2004, Florisbal et al. 2012).

In the Carajás province of the Amazonian craton, various deformed Neoarchean granite plutons with magnesian to ferroan A-type geochemical characteristics have been described (Dall'Agnol et al. 2017). Their origin has been associated with partial melting of mafic-to-intermediate lower crustal rocks, and they are classified as ‘deformed’ A-type, alkaline, metaluminous-to-weakly-peraluminous granitoids (Sardinha et al. 2006; Barros et al. 2009, Feio et al. 2012, Marangoanha et al. 2019). Understanding the internal fabric of these granitoids, as well as their relationship with the regional structure and solid-state deformation, is critical to constrain space-time-temperature-deformation relationships during pluton crystallization. In this case, shear zones are major channels for magma transport, providing an important emplacement mechanism for many syntectonic plutons related to transpressive deformation regime in Carajás province (Silva et al. 2020).

In the Sapucaia subdomain (northern portion of the Carajás province), Silva et al. (2020) recognized a singular geological-structural scenario, with ferroan granites crystallized under distinct oxidation states spatially associated with magnesian tonalites. This indicates a complex magmatic evolution involving liquids produced under different oxygen fugacity (fO_2) that was accentuated by mixing processes (Silva et al. 2020). The area investigated in this study is a relatively well-preserved section of the Meso- and Neoarchean continental crust forming the Carajás province. This paper presents the results of an integrated approach applied to a Neoarchean granitoid complex formed by several plutons emplaced along the Itacaiúnas shear belt. The evidence of successive multiple liquid injections, the sources of these granitoid magmas, the role played by transcurrent tectonics during their emplacement,

and the relationships between plutonism and tectonism are discussed. To that end, a detailed study was conducted, integrating petrography, structural observation, geochemistry, whole-rock Sm-Nd isotopes and combined U-Pb and Lu-Hf isotopic analyses in zircon. In addition, modeling of melt and residue compositions will make it possible to test the possible sources and quantify the role of each magma in processes involving the origin of these granitoids. Finally, a model for the origin and evolution of Neoarchean granitoids from Carajás is proposed.

2. Regional geology

Carajás Province, located in the southeast of the Amazonian craton (Figure 1a,c) (Almeida et al. 1981), represents its preserved Archean core (Machado et al. 1991). The Amazonian craton is composed of different geochronological provinces, and Santos (2003) considers the Carajás Province geochronologically independent, while Tassinari and Macambira (2004) deem it to be part of the Central Amazon province, which is subdivided into two blocks (Carajás and Xingu-Iricoumé) (Figure 1a). The province was subdivided by Santos (2003) and Vasquez et al. (2008) into two mainly tectonic domains: Rio Maria domain (3.0 – 2.86 Ga) and Carajás domain (3.0 – 2.73 Ga). Dall’Agnol et al. (2013), using a wide overview of geophysical and geological data, showed that the Carajás domain is not tectonically homogeneous, which led to the designation of the subdomains Canaã dos Carajás in the center and Sapucaia in the south, with the Carajás basin to the north (Figure 1c).

The Rio Maria Domain is composed of supracrustal greenstone belt sequences (3.0 to 2.9 Ga) and four granitoid suites, aged between 2.98 and 2.86 Ga (Althoff et al. 2000, Oliveira et al. 2009, Almeida et al. 2011, 2013, Ronaib and Oliveira 2013). The granitoid suites include: (i) TTG associations represented by Arco Verde, Caracol and Mariazinha tonalites and Mogno trondhjemite, formed during two main magmatic events at 2.96 Ga and 2.93 Ga; (ii) the Rio Maria sanukitoid suite, aged 2.87 Ga, consisting of granodiorites with associated mafic-to-intermediate rocks forming enclaves or locally, layered rocks; (iii) the 2.87 Ga Guarantã suite formed by high Ba-Sr calc-alkaline leucogranodiorite; and (iv) the 2.87-2.86 Ga potassic biotite leucogranites of calc-alkaline affinity, represented by Xinguara and Mata Surrão granites and small stocks. These rocks are weakly deformed, showing a WNW-ESE planar fabric (magmatic and tectonic), and intruded by 1.88 Ga Paleoproterozoic anorogenic granites (Barbosa et al. 1995, Paiva Jr. et al. 2011, Teixeira et al. 2018).

The Canaã dos Carajás subdomain is composed of 2.87-2.85 Ga high-K calc-alkaline granites (Boa Sorte, Bom Jesus, Cruzadão and Serra Dourada granites) and 2.74 Ga enderbite-

charnockite-granites (diopside norite Pium and Planalto suite) with subordinate occurrences of TTG (Rio Verde trondhjemite, ~2.93 Ga), amphibole-bearing tonalite represented by Bacaba tonalite (3.0 Ga) and the Campina Verde tonalitic complex (2.87-2.85 Ga), sodic leucogranites of calc-alkaline affinity (Canaã dos Carajás granite, ~2.93 Ga) and 1.88 Ga anorogenic plutons (Feio et al. 2012, 2013, Santos et al. 2013; Rodrigues et al. 2014). The Ouro Verde area exhibits Mesoarchean granulites with protolith crystallization and metamorphism ages of 3.05-2.93 Ga and 2.89-2.84 Ga, respectively (Marangoanha et al., 2019). A summary of the age distribution for the Meso- and Neoarchean geologic units from the Canaã dos Carajás and Sapucaia subdomains is shown in Figure 2.

The Sapucaia subdomain is largely dominated by Mesoarchean TTG associations similar to those of the Rio Maria domain, but these were intensely deformed and intruded by granite plutons during the Neoarchean. It consists of TTG (Colorado and Agua Fria trondhjemites) and amphibole-bearing tonalites (Sao Carlos tonalite). It also exhibits sanukitoid associations denominated Agua Azul and Agua Limpa, high Ba-Sr calc-alkaline leucogranodiorite-granites (Pantanal and Nova Canada), and Neoarchean high-K, A-type granites represented by the Vila Jussara suite (Teixeira et al. 2013, Silva et al. 2014, Gabriel and Oliveira 2014, Leite-Santos and Oliveira 2014, 2016, Dall'Agnol et al. 2017) (Figure 1c). The structural pattern identified in the SS and CCS is marked by moderate-to-strong heterogeneous deformation when compared to Rio Maria. Both domains are composed of E-W oriented plutonic bodies, which show E-W magmatic tectonic foliations and subvertical dip.

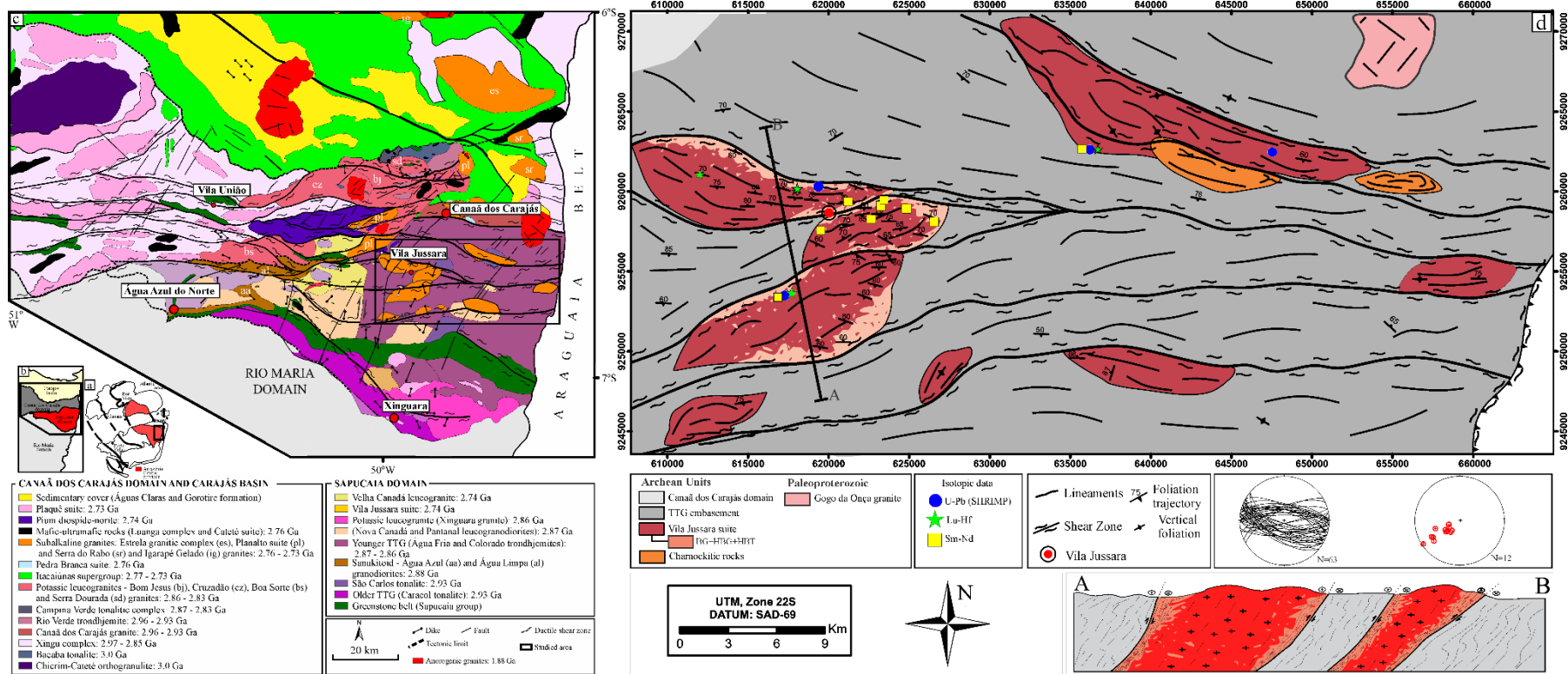


Figure 1. a) map of the Amazonian Craton showing the location of the Carajás province (black rectangle); b) detailed geological map of part of the Carajás Province, highlighting the work area. Modified from Vasquez et al. (2008), Oliveira et al. (2010), Feio et al. (2013), Santos & Oliveira (2012), Gabriel (2012); c) Detailed map of the Vila Jussara granitoids. The main granitic variety is often at the core of the plutons, while the porphyritic and tonalitic varieties are in the edges forming an interdigitate pattern within and with the main granitic facies as represented by pink color in some of these plutons. Besides that is shown a N-S section across the plutons and lower hemisphere, equal-area projection of foliation and mineral lineation.

References: 1, Marangoanha et al. (2019); 2, Delinardo et al. (2014); 3, Pigdeon et al. (2000) 4, Avelar et al. (1999); 5, Huhn et al. (1999); 6, Feio et al. (2013); 7, Morcto et al. (2011); 8, Rodrigues et. al. (2014); 9, Santos et al. 2013; 10, Barros et al. (2009); 11, Melo et al. (2016); 12, Oliveira et al. (2010); 13, Feio et al. (2012); 14, Galarza et al. (2017); 15, Sardinha et al. (2004) 15, Vasquez et al. (2008). * refers to ages obtained in this work

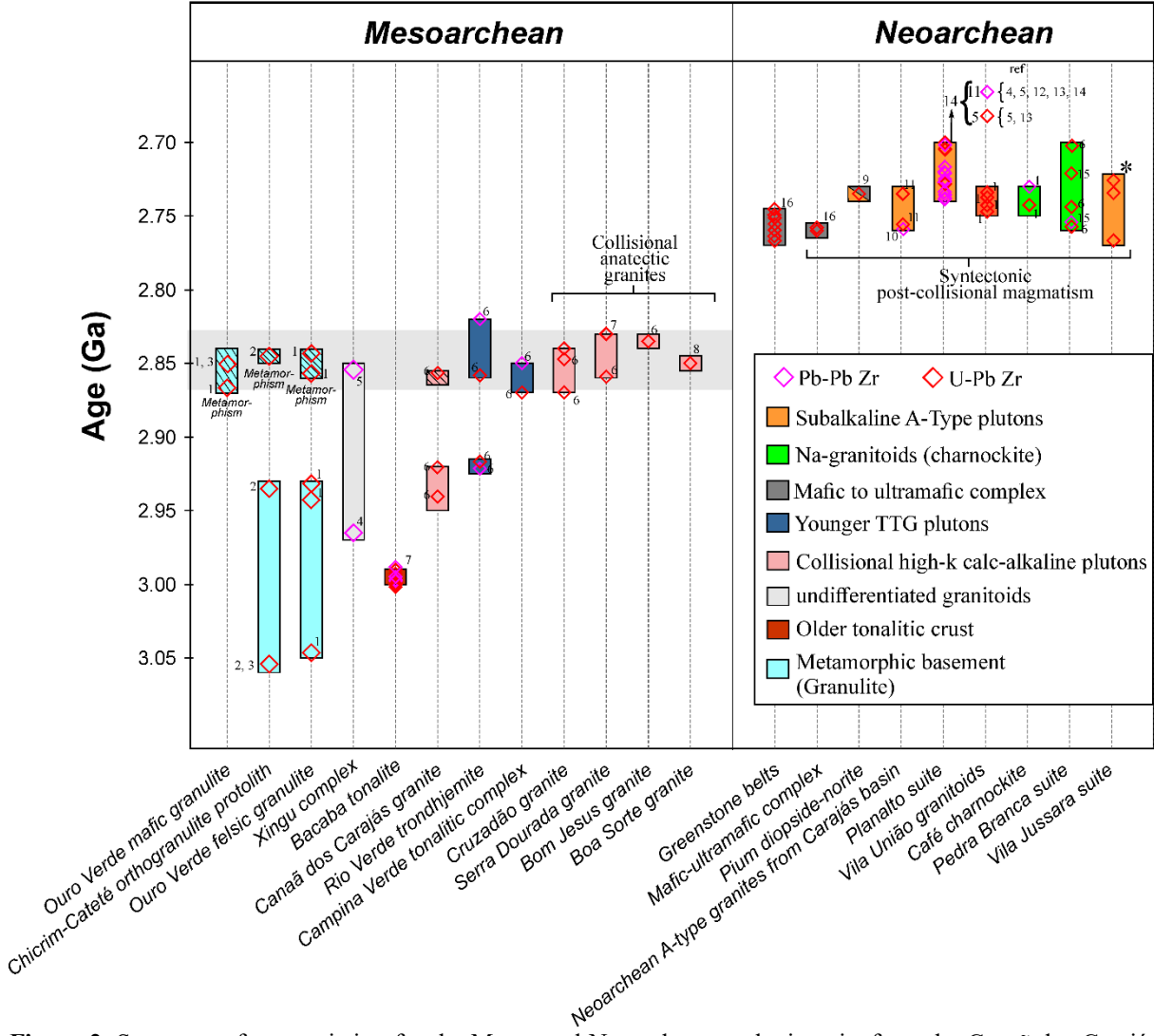


Figure 2. Summary of age variation for the Meso- and Neoarchean geologic units from the Canaã dos Carajás and Sapucaia subdomains, Carajás province. The gray field represents the Mesoarchean anatexitic granite crystallization age range (between 2.87 and 2.83 Ga). The asterisk symbols indicate the geochronological data obtained in this work. Modified from Marangoanha et al. (2019).

3. Analytical methods

3.1. Whole rock geochemistry

A total of 28 rock samples were selected for whole-rock chemical analysis (ALS Geochemistry Laboratories), and analyzed for major and trace elements, including rare earth elements (REE). The former were analyzed by ICP-AES, and the latter by ICP-MS. In addition, the rocks of the Vila Jussara complex analyzed by Dall'Agnol et al. (2017) were reclassified according to the textural terms predicted above and then cataloged for this study, resulting in a total of 50 samples of the plutons studied. Geochemical diagrams were generated by GCDkit software (Janoušek et al. 2003). Detailed information about analytical procedures can be found at www.alsglobal.com

3.2. Zircon U-Pb dating

The representative samples from Vila Jussara were crushed, ground and sieved into fractions between 125–175 µm at Pará-Iso/UFPA. Zircon grains were separated using the conventional heavy-liquid (bromoform) and magnetic techniques. Representative zircon grains were handpicked under a binocular microscope (ca. 60–80 grains/sample), mounted on epoxy resin discs and then polished to about half their thickness to expose crystal interiors.

To perform SHRIMP (Sensitive High-Resolution Ion Microprobe), U-Pb zircon analysis was conducted using a SHRIMP IIe system installed at the Geochronology High Resolution Laboratory of São Paulo University, Brazil (GeoLab/USP) and at Curtin University (Perth, Western Australia), whose instrumental performance and analytical procedures for the former are documented by Sato et al. (2014) and the later by Compston et al. (1992). The standards used for the Brazilian SHRIMP were SL 13 for U composition reference (238 ppm; Sato et al. 2014), and TEMORA-2 zircon (416.78 ± 0.33 Ma) and for the Australian SHRIMP zircons standards were BR266 (559 Ma, 903 ppm U; Stern 2001) and M257 (561 Ma, 840 ppm U; Nasdala et al. 2008).

The spot size of the primary ion beam was 30µm. Raw data were corrected for background signal, common Pb, laser-induced elemental fractionation, instrumental mass discrimination, and time-dependent Pb/U elemental fractionation using an Excel (Microsoft) in-house spreadsheet program. The common Pb correction was based on the Pb composition model (Stacey & Kramers 1975). The criteria for selecting the zircon crystals analyzed to calculate the ages involved were as follows: (i) common lead content (204Pb), excluding analyses containing $204\text{Pb} / 206\text{Pb}$ ratios greater than 0.0004; (ii) analytical precision, excluding isotopic ratios with errors greater than 3.0%; and (iii) degree of disagreement, with values closer to zero considered fit. The results were analyzed with the samples, under the same conditions. The analytical data were calculated and plotted using Isoplot 4.15 (Ludwig 2008). The isotope ratio errors are 2σ .

3.3. Whole-rock Sm-Nd isotope

For Sm-Nd isotopic analyses, 17 representative samples previously prepared for whole-rock major and trace elements analyses were used. The analyses were conducted using a Thermo Finnigan Neptune MC-ICP-MS with Faraday collectors at the Isotopic Geology Laboratory of the Federal University of Pará (Pará-Iso/UFPA). For each sample, ~100mg of rock powder was weighed in a Teflon high-pressure vessel, mixed with a 150Nd/149Sm

tracer solution and HF + HNO₃ acids, and reacted at 150°C for one week, following the procedures described by Oliveira et al. (2008). After 7 days of digestion, the solution was evaporated to dryness and then redissolved in HF + HNO₃ acids. This solution is then dried and dissolved in 6N HCl, followed by sequential drying and added with 2N HCl. After evaporation, rare earth elements (REE) were isolated by chromatographic exchange using *BioRad Dowex 50WX-8* cationic resin, 2N HCl and 3N HNO₃. Sm and Nd were separated from the other REE and collected by passing the solution through a further set of ion exchange columns loaded with *Dowex AGI-X4*, 7N HNO₃ and methanol. After evaporation, each Sm and Nd fraction was diluted with 1 ml HNO₃** (2%), and then analyzed in the MC-ICP-MS. During the course of this study, mass fractionation correction for 143Nd/144Nd was carried out with 146Nd/144Nd of 0.7219, using the exponential law. The La Jolla standard obtained an average 143Nd/144Nd value of 0.511834 (± 5).

3.4. Zircon Lu-Hf isotope

Lu-Hf isotopic analyses were carried out at the Isotopic Geochemistry Laboratory of the Federal University of Ouro Preto (UFOP), Brazil, using a multi-collector ICP-MS Thermo Scientific Neptune Plus system coupled to a Photon-Machines 193 ArF Excimer laser ablation system, following the methods suggested by Gerdes and Zeh (2006, 2009). Hf isotopic data were obtained from the zircon grains with U-Pb data. Laser spots for Lu-Hf analyses were drilled on or immediately beside the previous U-Pb spots.

Data were collected in static mode during 60 seconds of ablation with a spot size of 50 μm . Nitrogen (~0.080 l/min) was introduced into the Ar sample carrier gas. Typical signal intensity was ca. 10 V for ^{180}Hf . The isotopes ^{172}Yb , ^{173}Yb and ^{175}Lu were simultaneously monitored during each analysis step to allow for correction of isobaric interferences of Lu and Yb isotopes on mass 176. The ^{176}Yb and ^{176}Lu were calculated using a $^{176}\text{Yb}/^{173}\text{Yb}$ of 0.796218 (Chu et al., 2002) and $^{176}\text{Lu}/^{175}\text{Lu}$ of 0.02658 (JWG in-house value). The correction for instrumental mass bias applied an exponential law and a $^{179}\text{Hf}/^{177}\text{Hf}$ value of 0.7325 (Patchett and Tatsumoto, 1980) in order to correct Hf isotopic ratios. The mass bias of Yb isotopes generally differs slightly from that of the Hf isotopes, with a typical offset of ca. 1.04 to 1.06 for $\beta\text{Hf}/\beta\text{Yb}$ when using the $^{172}\text{Yb}/^{173}\text{Yb}$ value of 1.35274 from Chu et al. (2002). This offset was determined for each analytical session by averaging the $\beta\text{Hf}/\beta\text{Yb}$ of multiple analyses of the JMC 475 solution doped with variable Yb amounts and all laser ablation analyses (typically $n > 50$) of zircon with a ^{173}Yb signal intensity of > 60 mV. The

mass bias behavior of Lu was assumed to follow that of Yb. The Yb and Lu isotopic ratios were corrected using the β_{Hf} of the individual integration steps ($n = 60$) of each analysis.

3.5. Geochemical Modelling

In order to generate a petrogenetic model for the Vila Jussara rocks, we present geochemical modeling involving partial melting and mixing models. The mass-balance calculations for major elements were performed by applying the least-squares approximation using GENESIS 4.0 software (Teixeira 2005). Trace element modeling was carried out on an Excel spreadsheet created by the authors, which was based on the equilibrium partial melting equation (Wilson 1989). The mineral/liquid partition coefficients (K_d) used in the modeling were obtained from Rollinson (1993) and the online database <https://earthref.org/KDD/>. A Microsoft Excel spreadsheet program was used to build a mixing model (PETROMODELER Ersoy 2013).

4. Results

4.1. Geology of the vila Jussara plutons

4.1.1. Field and compositional aspects

Granitic magmatism in the Vila Jussara area is characterized by the occurrence of at least eight coalescing, elongated and amalgamated granite plutons, showing intense deformation near E-W and high-angle dips (75 to 85°) that follow the regional trend, and is marked by extensive shear zones. These plutons show the presence of several different enclaves, some of which indicate their intrusive nature (TTG's xenoliths). Due to the geometric and kinematic partition of the deformation, the central portions and borders of the bodies contain low and high-strain domains, respectively, indicating that these plutons were affected by large-scale shear zones (Figure 1c). The framework identified in both deformation domains (low and high strain) shows a main direction consistent with the long axes of the batholiths and defines a continuous arrangement with the tectonic foliation developed in the country rock. However, the intensity and orientation of both the submagmatic and mylonitic frames vary locally.

The Vila Jussara granitoids cover a large compositional spectrum and were named according to their dominant composition and textural aspects: coarse-to medium-grained seriated amphibole-biotite monzogranite (**BHM**); biotite-amphibole tonalite (**BHT**); porphyritic biotite granite (**BG**), porphyritic amphibole-biotite monzogranite to granodiorite (**HBG**) (Figures 3a and 4a-d). All granitoids are predominantly leucocratic rocks, with colors

ranging from reddish gray to whitish gray due to variations in the plagioclase/microcline ratio, and dark spots corresponding to mafic mineral aggregates. With respect to mafic content, the granite varieties contain $5 < M' < 34\%$ and the granodiorites $11 < M' < 27\%$, while the tonalites are slightly more enriched in mafic minerals ($15 < M' < 38\%$) (Figure 3b). Hornblende and biotite (\pm titanite) are the dominant mafic minerals in all the varieties (except the BG variety). The primary accessory minerals are opaques (ilmenite \pm magnetite; cf. Martins et al., 2022), apatite, zircon, titanite, allanite and epidote, while the secondary mineral assemblage consists of sericite, chlorite, epidote, scapolite, titanite, goethite and albite.

Mingling relationships occur all along the plutons, which exhibit complex interactions such as interdigitated contacts between the porphyritic granitoids (HBG) and the dominant BHM, and more restrictedly, tonalite rocks (Figure 4e). In addition, contemporaneous features with magma emplacement are the presence of feldspar xenocrysts or even partially digested granite fragments contained in porphyritic granitoids (Figure 4f).

4.1.2. Microstructural aspects

Some of the varieties exhibit euhedral to subhedral equigranular texture with relatively well-preserved igneous characteristics, as evidenced by preserved feldspar crystals with magmatic shape and oscillatory zoning in euhedral plagioclase grains, in addition to euhedral to subhedral mafic minerals (biotite, hornblende, and primary accessory minerals). However, we observe microstructures that arose from both cataclastic and intracrystalline plasticity mechanisms, such as the preferred orientation of euhedral to subhedral feldspar crystals, mafic minerals and elongated aggregates of recrystallized quartz, which may indicate continuity between (sub) magmatic and solid-state flow (Figures 5a-d). Undulatory extinction, deformation bands in feldspar porphyroclasts and quartz, deformation twins in feldspars and hornblende, and elongated aggregates of quartz grains with sutured or straight grain boundaries are additional clues of ductile straining and evidence of dynamic recrystallization through grain boundary migration (GBM) and subgrain rotation (SGR) (To a deep description an interpretation of the microstructural features see Silva et al. 2020). Hornblende grains are euhedral to subhedral with predominantly brittle deformational behavior, they may show undulatory extinction and, less rarely, a subgrain pattern (Figure 5e). Although primary biotite crystals may occur, due to its high deformation intensity, biotite is more commonly observed as aggregates of small, recrystallized grains, with irregular to straight grain boundaries (Figure 5f).

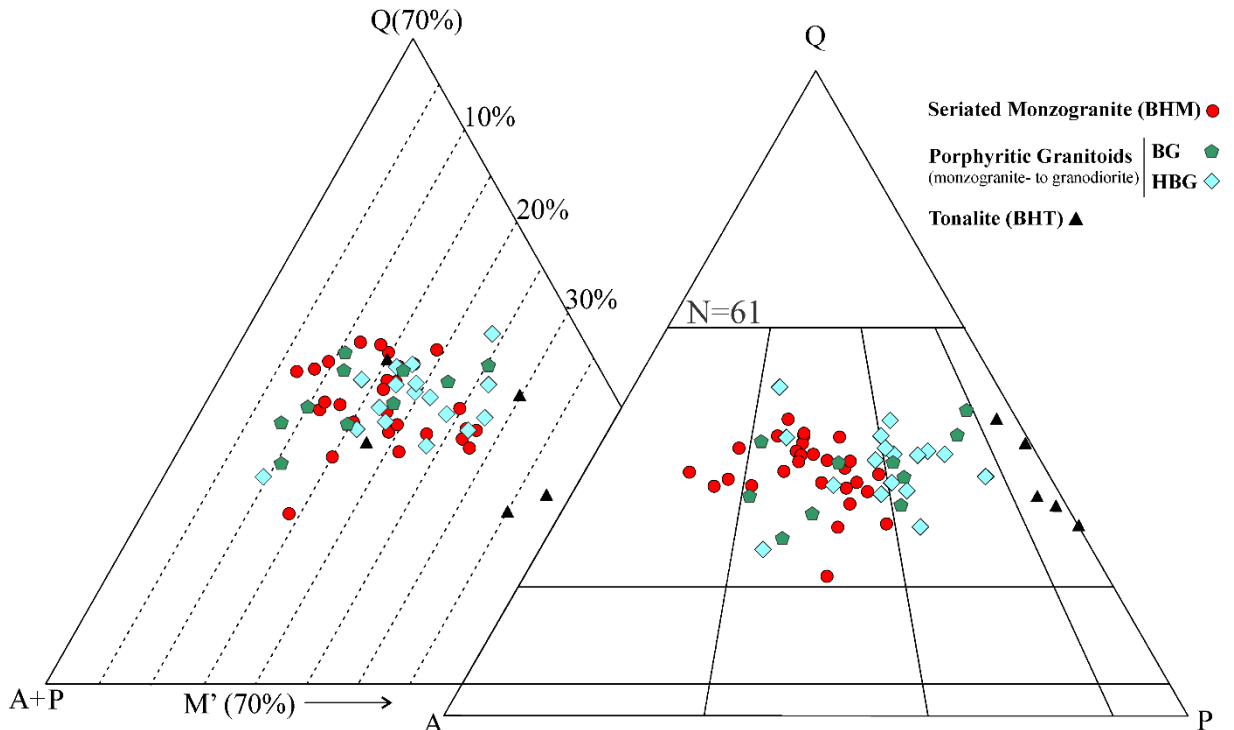


Figure 3. Q-A-P and Q-(A+P)-M' plots (Le Maitre et al. 2002) and petrographic classification of the Vila Jussara complex granitoids. The Vila Jussara granitoids were named following the recommendations of the International Union of Geological Sciences (IUGS) Subcommission on the Systematics of Igneous Rocks (Le Maitre et al., 2002). Red circles: Coarse-to medium-grained seriated amphibole-biotite monzogranite (BHM); black triangles: biotite-amphibole tonalite (BHT); cyan diamonds: porphyritic biotite granite (BG), green pentagons: porphyritic amphibole-biotite monzogranite to granodiorite (HBG). The modal compositions of 61 samples (=N) were determined in thin sections under a Zeiss microscope using the Endeeper Hardledge software; 2000 points were counted per section on a grid of 0.4 mm.

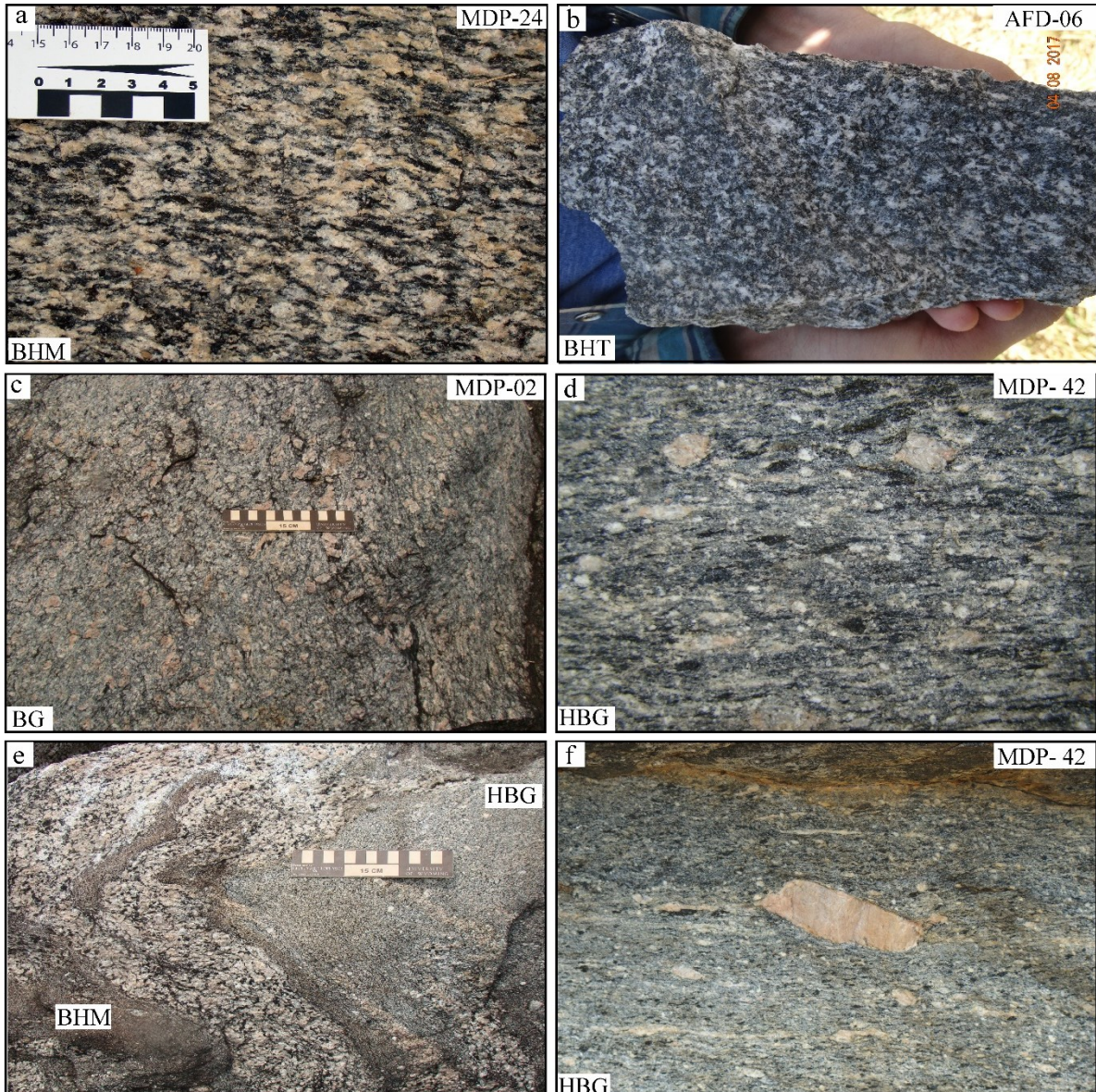


Figure 4. The central portions of the plutons (low-strain domains) are dominantly composed of BHM (a). The marginal portions of the plutons (high-strain domains) expose mainly tonalites (BHT) (b) and porphyritic granitoid (BG and HBG) (c and d) showing complex interactions, such as a mingling/mixing relationship occurs all along the plutons between BHM magma and that of granodioritic composition (HBG), as evidenced by the presence of partially digested granite fragments in the latter with interdigitated contacts with porphyritic granitoid (e) or even feldspar xenocrysts (f).

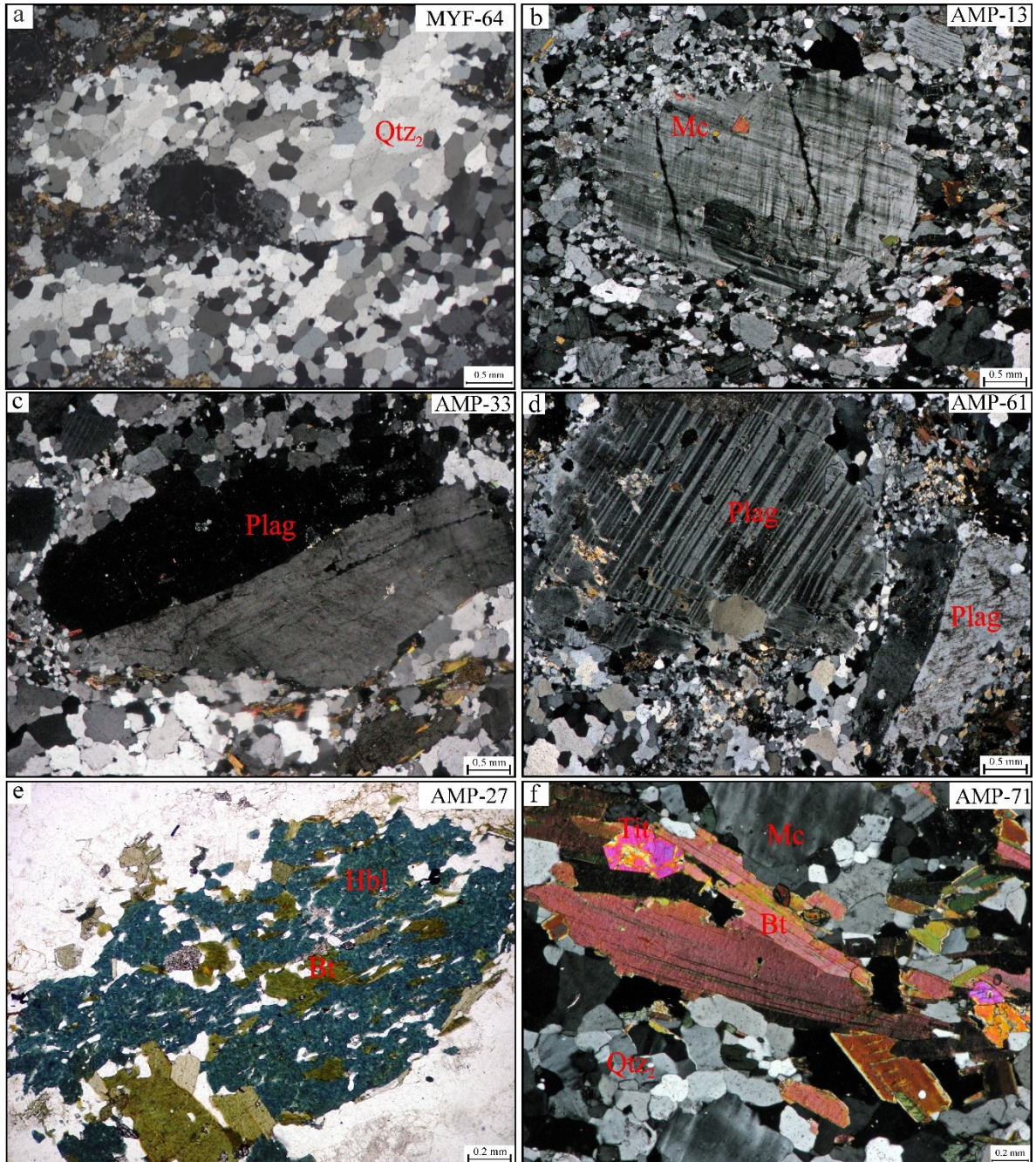


Figure 5. Microphotographs in crossed polars showing microstructures of the Vila Jussara granitoids. a) Elongated aggregates of quartz micrograins resulting from dynamic recrystallization via GBM and SGR; b) Microcline macrocryst showing core-mantle microstructure. The mantle is very fine-grained and contains domains of coarser new grains with, indicating dynamic recrystallization via SGR and migration of low grain boundary temperature (bulging – BLG); c) Serrated plagioclase macrocryst showing a slightly plastic deformation; d) Plagioclase with a core mantle texture; e) Aspect of the amphibole and associated biotite; f) Biotite aggregates associated with euhedral epidote and zircon. *Qtz = quartz; Mc = Microcline; Plag = Plagioclase; Hbl = Hornblende; Bt = Biotite; Tit = Titanite.

4.2. Whole-Rock Geochemistry

4.2.1. Geochemical classification and typology

Despite their multiple affinities and the geologic evidence that they are essentially part of a same magma event, the Vila Jussara granitoids show significant differences that are indicated by some geochemical contrasts. The Fe* index [FeOt/(FeOt/MgO) ratio in whole rock] shows large variation in these granitoids (cf. the oxidized and reduced ferroan and magnesian granitoid groups described by Dall'Agnol et al. 2017). **BHM** exhibit moderate-to-high values of this ratio (0.74 to 0.98) and are characterized as oxidized and reduced ferroan granites (Figures 6 a and b). They differ in this respect from the reduced granites of the Planalto suite because they display larger FeOt/(FeOt/MgO) ratio variations. **BG** and **HBG** (porphyritic granitoids), on the other hand, show affinities with both the slightly oxidized magnesian granites, which also reflects their wide variation for this ratio. By contrast, **BHT** have lower and restricted FeOt/(FeOt/MgO) ratios (0.74-0.79), demonstrating their magnesian character and calc-alkaline trend. In the PQ diagram (Debon & Le Fort, 1983), these granitoids vary from tonalites to granites (Figure 6c). In the Whalen et al. (1987) classification, the overall granitoids are mostly A-type granites (Figure 6d). The AFM diagram (Irvine and Baragar 1971) shows that the granitoids form two parallel trends, where the ferroan granitoids are aligned to those defined by the tholeiitic series and the biotite granite and tonalites are akin to the calc-alkaline series (Figure 6e). The Vila Jussara granitoids are predominantly post-collisional according to the classification of Pearce et al. 1984 (Figure 6f).

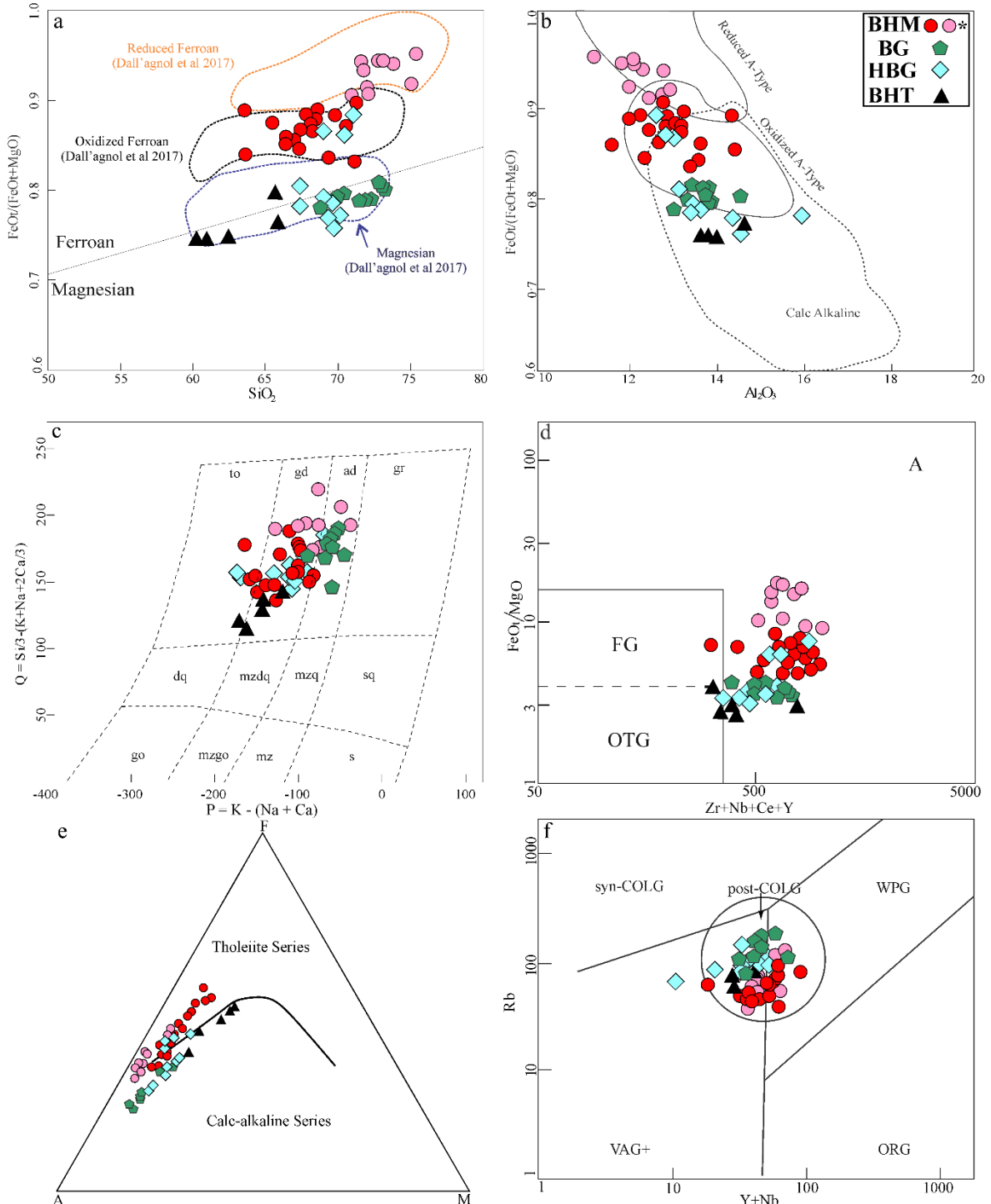


Figure 6. Classification diagrams for the Vila Jussara rocks. a) SiO_2 vs $\text{FeOt}/(\text{FeOt}+\text{MgO})$ diagram; (Frost et al. 2001); b) Dall’Agnol & Oliveira (2007) diagram to show series affinity; c) P-Q diagram (Debon & Le fort 1983); d) Whalen et al. (1987) diagram for the series affinity; e) AFM diagram (Irvine and Baragar, 1971) f) Tectonic classification diagrams of Pearce et al. (1984). *Red circles are the oxidized monzogranite and pink circles are the reduced one.

4.2.2. Major and trace elements

The Vila Jussara granitoids show a wide variation in silica values (SiO_2 from 60.0 to 75.2 wt%), with **BHM** rocks encompassing the widest range of SiO_2 contents (63.3 to 75.2 wt%) in relation to the other groups (Table 1). In this group, the reduced ferroan BHM

($\text{Fe}^* \geq 0.90$) exhibit the highest SiO_2 contents (70.7 to 75.2 wt%), while the oxidized ferroan BHM (Fe^* between 0.82 and 0.89) are less evolved (SiO_2 from 63.3 to 70.9 wt%) (Table 1). **BG** and **HBG** exhibit more restricted variation of SiO_2 values in relation to the seriated monzogranites (68.6 to 72.9 wt% and 67.1 to 70.8 wt%, respectively). In the BG and HBG, silica contents are generally slightly lower than those shown by reduced ferroan BHM. The **BHT** variety, in turn, contains the lowest SiO_2 (60.0 to 65.7 wt%) among the four granitoid groups. The overall arrangement of the rocks analyzed in the Harker variation diagrams (SiO_2 vs. compatible oxides) show a linear reduction in TiO_2 , Al_2O_3 , MgO , FeO and CaO contents with an increase in SiO_2 content (Figures 7a-d and f).

The reduced BHM show more uniform and lower content (11.2 to 13.0 wt%) of Al_2O_3 compared to the oxidized BHM samples (11.7 to 14.5 wt%) and also to the other varieties [BHT (13.63 to 14.67%), BG (13.15 to 14.64%) and HBG (12.8 to 16.05%)] (Table 1; Figure 7b). Contents of the ferromagnesian oxides and CaO clearly distinguish the different Vila Jussara granitoids. Despite the overlap of values between granitoid groups, the **BHT** variety shows the highest MgO (1.62 to 2.82 wt%) and CaO (3.65 to 5.56 wt%) contents, which decreases while passing through porphyritic granitoids (HBG and BG) and oxidized-BHM until they reach the lowest values in the reduced-BHM variety [MgO (0.20 to 0.6 wt%) and CaO (1.45 to 2.88 wt%)]. FeOt and TiO_2 exhibit similar behavior and their highest contents are found in oxidized-BHM (4.96 to 10.25 wt% and 0.63 to 1.22 wt%, respectively) and BHT samples (5.74 to 9.21 wt% and 0.92 to 1.06 wt%, respectively), with lower contents attributed to the reduced-BHM (4.24 to 6.22 wt% and 0.32 to 0.63 wt%, respectively) and BG rocks (2.79 to 4.95 wt% and 0.37 to 0.79 wt%, respectively).

The negative correlation of the above oxides with SiO_2 would not necessarily be the product of magmatic evolution from a single magmatic series, since the arrangement of the sample sets sometimes shows parallel trends, that allow a distinction mainly between the BHM varieties and porphyritic granitoids (**HBG** and **BG**), suggesting that these rocks are not comagmatic (see Figures 7c and d). This behavior could be explained by the internal fractionation of the magma forming each rock group, provoked by the early crystallization of hornblende, magnetite, ilmenite and apatite. Plagioclase fractionation may play a significant role in the apparent decline in Al_2O_3 and CaO . On the other hand, the $\text{K}_2\text{O}/\text{Na}_2\text{O}$ ratio increases in more evolved rocks (Figure 7e), indicating that K feldspar was not a fractionating phase during the evolution of these magmas.

With respect to the variation of trace elements, the Ba/Sr ratio shows a wide variation for all varieties, except for the BG, where this ratio exhibits a shorter interval (4.09 to 6.69) in

relation to the other varieties (Figure 7g). The Ba/Sr ratio tend to be higher in the reduced ferroan granites (5.06 to 9.31). The BHT variety has a lower overall interval for Ba/Sr (1.88 to 4.49). In the Rb/Zr x SiO₂ diagram, all varieties can be classified as high HFSE granitoids, where the magnesian rocks, including BHT, BG and HBG, tend to show the highest Rb/Zr ratios (Figure 7h).

Table 1. Whole rock geochemical analyses of the Vila Jussara granitoids.

Unit	VILA JUSSARA																											
Facies	Oxidized BHM												Reduced BHM															
Sample	MDP 16A	AMP 47A*	PFA 39 *	MDP 43	AMP 39*	MDP 06	MYF 64*	MDP 39	AMP 43B*	AMP 61*	MAR 23*	MYF 77*	AMP 27*	MDP 34	MDP 14A	MDP 33C	MDP 35	MDP 37	AMP 88A*	PFR 16A*	MDP 57A	MAR 16*	PFR 14*	AMP 88C*	MDP 44	PFA 77*	AMP 23*	
SiO ₂	63.30	65.18	66.20	66.20	66.66	67.10	67.12	67.60	68.03	68.21	68.33	69.07	69.40	69.60	70.90	70.70	71.10	71.80	71.42	71.44	71.90	72.51	72.82	73.54	74.80	75.02	75.24	
TiO ₂	1.22	1.04	1.40	0.92	0.82	1.08	0.78	0.87	0.81	0.79	0.76	0.63	0.70	0.77	0.80	0.63	0.61	0.47	0.40	0.36	0.64	0.40	0.32	0.34	0.45	0.21	0.33	
Al ₂ O ₃	13.30	13.13	11.70	12.80	13.70	12.55	14.49	14.45	12.97	13.16	12.91	13.64	12.90	12.30	13.50	12.55	12.85	13.00	12.31	12.89	12.85	12.19	12.21	11.89	12.10	12.19	11.24	
FeOt	10.25	8.14	8.67	6.80	6.22	7.89	5.25	6.77	6.60	5.63	6.48	4.96	5.52	6.21	5.33	6.22	5.24	4.29	5.34	4.76	5.91	5.07	4.46	4.52	3.93	2.99	4.24	
MnO	0.12	0.10	0.11	0.08	0.08	0.09	0.06	0.09	0.08	0.07	0.08	0.05	0.06	0.09	0.08	0.07	0.08	0.07	0.06	0.06	0.08	0.06	0.05	0.06	0.03	0.05		
MgO	1.15	1.06	1.37	1.02	0.94	1.07	0.86	0.79	0.87	0.78	0.73	0.88	0.77	0.73	0.99	0.59	0.53	0.37	0.30	0.30	0.55	0.26	0.24	0.25	0.32	0.19	0.20	
CaO	4.45	3.50	3.54	3.12	3.51	3.98	3.61	4.04	3.08	2.81	2.94	2.76	2.57	3.20	2.73	2.81	2.88	2.41	2.00	1.91	2.83	1.93	1.45	1.87	1.74	0.94	1.52	
Na ₂ O	4.29	3.85	3.33	3.48	4.31	3.92	3.81	4.11	3.69	3.63	3.58	3.46	3.34	3.62	3.42	3.63	3.49	3.84	3.46	3.94	3.60	3.21	3.93	3.24	3.02	3.58		
K ₂ O	1.53	2.78	2.15	2.80	2.58	2.06	2.72	2.01	3.05	3.62	3.06	3.72	3.75	3.04	3.24	2.71	2.66	3.79	3.47	3.93	2.28	3.34	4.21	3.10	3.96	4.49	3.05	
P ₂ O ₅	0.33	0.29	0.37	0.27	0.20	0.31	0.17	0.25	0.18	0.16	0.17	0.16	0.16	0.22	0.24	0.15	0.17	0.11	0.07	0.07	0.15	0.08	0.05	0.07	0.07	0.03	0.05	
LOI	0.24	0.60	0.80	0.37	0.37	0.60	0.30	0.50	0.47	0.30	0.80	0.60	0.20	0.30	0.50	0.29	0.39	0.47	0.62	0.40	0.50	0.25	0.20	0.70	0.10	0.66	0.70	0.20
Total	100.10	99.67	99.64	97.86	99.60	100.50	99.37	101.40	99.66	99.66	99.69	99.65	99.59	100.00	101.72	100.24	100.22	100.42	99.62	99.68	101.30	99.64	99.72	99.67	101.30	99.80	99.70	
Ba	723	907	1229	1405	1459	899	2067	872	99.72	1856	1530	1234	1831	1145	1060	1195	1480	1595	2180	1480	1815	2015	1123	1813	1655	397	1704	
Rb	37.90	82.90	49.80	59.90	47.60	41.30	49.30	47.00	87.50	68.20	75.70	93.60	89.40	95.60	83.00	54.50	58.90	100.00	75.50	114.60	38.80	60.20	118.60	77.50	81.50	242.60	53.40	
Sr	322	233	276	275	375	353	336.80	350	280.90	261.00	263.40	200.80	242.60	226.00	230	236	282	214	234.80	209.30	326	216	154.80	223.70	187	57.10	183.90	
Zr	502	487	746	378	520.10	449.00	757.20	262	520.60	646.20	584.20	616.60	644.90	609	359.00	693	456	366	599.10	361.90	682	547	373.40	474.40	534	209.60	460.30	
Nb	20.80	20.40	16.40	21.70	10.90	13.30	10.40	12.70	12.90	17.80	16.90	13.40	16.40	24.80	11.30	14.00	14.60	14.20	12.50	19.20	11.20	13.40	16.90	11.00	12.60	25.70	13.90	
Y	45.10	74.80	37.80	32.50	26.70	29.80	23.50	33.90	36.50	45.90	46.20	29.60	40.20	41.00	23.20	50.70	32.90	43.20	29	47.70	28.60	27.80	54.50	27.80	29.10	48.00	34.40	
Ga	23.60	-	-	18.30	-	24.90	-	21.60	-	-	-	-	-	-	21.50	17.40	20.70	20.30	23.30	-	-	20.00	-	-	-	17.30	19.10	-
Th	2.67	15.40	1.80	4.61	8.70	10.15	1.60	4.62	10.20	2.40	3.40	11.10	7.70	6.20	9.34	15.80	36.50	7.38	14.20	16.20	13.30	7.30	49.60	5.80	7.40	53.30	9.20	
La	68.80	111.90	51.80	39.00	44.70	57.70	46.10	44.50	73.50	51.50	42.60	39.50	74.80	56.30	46.10	105.00	41.60	50.30	37.60	68.10	56.00	26.60	187.90	22.00	32.90	151.00	36.00	
Ce	161	221	112	90	90.10	117.50	77.50	95.60	142.80	119.80	110.50	83.90	143.70	139.50	88.30	206	95	88.50	80.70	138.10	106	65.70	330.40	51.60	65.50	286.70	88.30	
Pr	19.55	29.76	14.20	11.15	10.59	12.55	10.09	11.30	16.21	16.53	12.66	10.11	16.90	16.15	9.57	23.60	11.75	12.30	9.93	16.48	11.80	6.57	38.36	6.81	7.66	30.33	10.65	
Nd	71.60	113.50	53.50	47.80	40.80	47.80	38.90	45.70	59	67.80	50.20	39.50	64.60	58.80	35.00	85.80	46.20	46.20	40.40	57.90	43.10	24.90	124.10	29.00	30.00	99.50	44.70	
Sm	12.50	18.95	10.10	9.24	7.47	8.60	6.89	8.41	10.21	12.13	9.71	7.42	11.25	10.75	5.97	14.85	8.28	8.39	7.23	10.56	7.50	5.50	17.84	6.05	5.18	13.97	9.14	
Eu	2.37	2.20	2.00	1.95	2.25	2.23	2.37	2.08	2.00	1.96	2.07	1.32	1.90	1.83	1.05	2.09	2.24	2.19	2.32	2.12	2.67	2.00	2.08	1.92	1.90	0.67	1.76	
Gd	12.00	16.23	9.15	8.84	6.39	7.14	6.29	7.81	8.33	10.78	8.63	6.65	9.62	8.93	4.94	13.05	6.70	8.55	6.34	9.59	6.54	5.07	12.62	5.53	4.84	10.41	8.64	
Tb	1.60	2.23	1.20	1.17	0.85	1.21	0.81	1.14	1.11	1.61	1.32	0.96	1.40	1.42	0.75	1.78	1.02	1.25	0.87	1.33	0.98	0.80	1.70	0.79	0.64	1.45	1.21	
Dy	9.27	12.76	6.75	6.63	5.07	5.72	4.14	6.15	6.50	8.48	7.34	5.47	7.68	7.50	3.84	9.88	5.99	6.88	5.05	8.20	5.34	4.33	9.49	4.87	4.18	7.63	6.68	
Ho	1.81	2.51	1.22	1.19	0.92	1.12	0.79	1.18	1.20	1.50	1.01	1.49	1.45	0.80	1.91	1.16	1.42	1.02	1.49	1.02	0.86	1.73	0.96	0.82	1.56	1.26		
Er	5.29	6.94	3.48	3.06	2.68	3.20	2.14	3.44	3.43	4.76	4.30	2.83	4.17	4.58	2.18	5.21	3.45	4.27	3.06	4.53	2.80	2.47	5.22	2.65	1.94	4.72	3.57	
Tm	0.68	0.99	0.47	0.41	0.36	0.49	0.34	0.48	0.50	0.65	0.66	0.42	0.60	0.59	0.30	0.70	0.48	0.63	0.42	0.66	0.42	0.39	0.71	0.40	0.33	0.76	0.50	
Yb	4.61	6.39	3.03	2.26	2.36	2.96	2.06	3.09	2.53	3.86	3.99	2.69	3.69	3.95	2.04	4.09	2.98	3.65	2.77	4.82	2.70	2.48	5.11	2.72	2.05	4.49	3.01	
Lu	0.70	0.89	0.43	0.37	0.34	0.46	0.31	0.46	0.45	0.56	0.62	0.40	0.52	0.61	0.32	0.70	0.43	0.57	0.45	0.69	0.43	0.40	0.70	0.43	0.29	0.74	0.48	
A/CNK	0.79	0.83	0.82	0.88	0.84	0.86	0.91	0.88	0.86	0.87	0.88	0.91	0.84	0.93	0.91	0.91	0.91	0.89	0.96	0.91	0.93	0.97	0.89	0.94	1.06	0.94		
K ₂ O/Na ₂ O	0.36	0.72	0.65	0.80	0.60	0.53	0.71	0.49	0.83	1.00	0.84	1.04	1.08	0.91	0.89	0.79	0.73	1.09	0.90	1.14	0.58	0.93	1.31	0.79	1.22	1.49	0.85	
FeO/(FeO+MgO)	0.89	0.87	0.85	0.86	0.86	0.87	0.85	0.89	0.87	0.87	0.89	0.84	0.87	0.88	0.82	0.90	0.90	0.91	0.94	0.93	0.91	0.95	0.94	0.94	0.92	0.93	0.95	
Mg#%	0.18	0.21	0.24	0.23	0.23</td																							

Table 1 (cont.).

Unit	VILA JUSSARA															BHT									
Facies	BG								HBG								BHT								
Sample	LIF 04A	MDP 03A	AMP 77*	MDP 02A	MD 01*	MDP 55	MAR 30*	MDP 05	MDP 03B	MDP 02D	MDP 14CH	MDP 57B	AFD 08*	MDP 14E	ADE 01D*	MDP 06B	MDP 33A	MDP 42B	MDP 36	MDP 02E	MDP 02C	AFD 11B 11B*	AFD 06*	MYF 40*	
SiO ₂	68.60	69.60	70.10	71.20	71.50	72.00	72.49	72.80	72.90	67.10	67.20	68.60	68.86	69	69.07	69.70	69.90	70.30	70.80	60.00	62.20	60.67	65.22	65.70	
TiO ₂	0.79	0.65	0.46	0.49	0.41	0.40	0.37	0.50	0.49	0.87	0.75	0.83	0.71	0.81	0.49	0.52	0.38	0.79	0.62	1.06	0.92	0.97	1.02	0.92	
Al ₂ O ₃	13.15	13.80	14.64	13.90	13.80	13.55	13.53	13.85	13.70	13.25	13.50	13.10	13.54	13.70	14.47	14.65	16.05	12.90	12.80	13.90	13.75	14.03	13.63	14.67	
FeOt	4.95	4.46	3.19	3.30	2.91	2.79	2.94	3.43	3.43	6.70	5.30	6.20	4.92	5.50	3.66	4.17	3.45	5.67	5.93	9.09	8.24	9.21	7.16	5.74	
MnO	0.09	0.06	0.05	0.03	0.03	0.04	0.03	0.04	0.04	0.08	0.08	0.10	0.06	0.08	0.04	0.06	0.05	0.07	0.06	0.12	0.11	0.12	0.09	0.07	
MgO	1.25	1.04	0.74	0.80	0.70	0.66	0.63	0.75	0.76	1.48	1.33	0.87	1.18	1.36	0.98	1.19	0.91	0.82	0.69	2.78	2.49	2.82	1.63	1.62	
CaO	2.64	2.67	1.86	2.23	1.92	2.12	1.66	2.04	2.01	3.47	3.41	3.16	2.75	3.48	2.54	3.19	3.40	2.74	2.27	5.56	4.86	5.49	4.17	3.65	
Na ₂ O	3.16	3.56	3.87	3.42	3.35	3.41	3.70	3.33	3.27	3.36	3.61	3.99	3.61	3.69	4.11	4.79	4.77	3.57	3.25	3.38	3.34	3.46	3.79	3.65	
K ₂ O	3.74	3.26	4.58	3.91	4.45	4.06	3.93	4.04	3.99	2.88	3.23	2.68	3.55	3.26	3.35	1.89	1.72	3.32	3.57	1.75	2.27	2.01	2.51	2.89	
P ₂ O ₅	0.22	0.18	0.12	0.13	0.01	0.09	0.08	0.12	0.12	0.25	0.26	0.23	0.23	0.29	0.13	0.13	0.11	0.23	0.15	0.31	0.28	0.29	0.31	0.25	
LOI	0.91	0.28	0.10	0.50	0.70	0.68	0.40	0.55	0.61	0.44	0.64	0.44	0.30	0.56	0.90	0.75	0.55	0.39	0.45	0.75	0.55	0.70	0.20	0.70	
Total	99.50	99.56	99.71	99.91	99.78	99.80	99.76	101.45	101.32	99.88	99.31	100.20	99.71	101.70	99.74	101.04	100.80	100.59	98.70	99.01	99.77	99.73	99.86		
Ba	1725	1135	1240	1205	1029	997	699	1200	1220	1010	1065	2430	1117	1090	1093	475	514	1560	1145	599	681	769	970	1349	
Rb	110.50	76.10	144.60	128.50	163	147	190.2	96.20	105	101	92.50	40.10	90.00	104	145.20	82.20	63	93.90	96.50	71.30	85.10	75.40	54.90	80.00	
Sr	258	261	259.90	264	219	219	171	231	244	243	285	335	260.40	243	267.40	276	442	277	161	318	247	301.40	340.80	300.20	
Zr	436	401	323.30	481	268	300	234.7	501	393	381	454	459	435.30	290	295.90	378	225	486	668	268	221	238.40	205.50	420.30	
Nb	17.60	10	10.90	12.20	13.60	11	19.30	9.60	9.80	15.40	12.40	21.30	11.20	11.80	10.40	7.60	6.30	17.50	13.60	9.80	7.00	7.30	11.10	12.20	
Y	58.10	28.70	24.10	37	34.40	30.40	40.90	25.80	32.10	42.60	33.70	24.70	24.00	24.40	25.10	14.10	4.60	40.20	44.60	30.20	30.90	25.80	20.70	37.80	
Ga	17.80	16.90	-	18.10	-	18.30	-	14.50	16.70	19.60	22.50	16.50	-	23.10	-	22.30	24.90	20.20	17.80	19.30	17.60	-	-	-	
Th	18.80	4.12	12.80	4.60	31.70	13.85	26.30	8.29	5.67	10.95	5.42	1.81	4.20	16.80	8.90	2.70	14.05	7.69	7.74	7.60	13.25	6.90	5.50	26.90	
La	104.50	55.30	68.00	27.20	75.60	69.40	40.20	49.30	42.60	91.20	70.80	34.90	37.50	50.50	43.70	20.90	61.70	40.70	66.30	39.40	48.70	32.60	37.70	160.90	
Ce	182.00	104.50	131.90	69.50	153.00	133.50	84.60	107.50	91.70	169.00	135.50	68.10	81.80	101.50	91.10	42.20	107.50	92.40	130	86.30	97.10	71.20	77.40	266.90	
Pr	19.85	11.60	14.27	9.35	16.40	14.55	10.99	12.10	11.40	18.85	16.00	8.65	10.19	11	11.07	4.95	9.70	11.85	15.25	10.05	13.70	9.27	9.27	26.36	
Nd	66.60	42.40	49.80	37.50	60.40	50.80	41.50	44.90	46.60	67.90	57.90	36.30	39.70	38.00	42.10	19.10	30.20	48.40	57.90	39	36.70	36.40	34.80	87.10	
Sm	11.30	7.13	7.79	6.97	8.99	8.95	8.63	7.95	8.57	11.20	10.15	7.27	6.82	6.81	7.31	3.69	3.57	9.57	11.10	6.83	6.57	6.37	5.97	11.26	
Eu	1.49	0.99	0.85	1.03	0.93	0.93	0.83	1.03	1.09	1.63	1.50	3.01	1.03	1.10	0.96	0.64	0.85	1.93	1.68	1.64	1.18	1.43	1.32	1.66	
Gd	9.75	5.73	5.64	6.33	7.19	7.90	7.85	6.58	8.48	8.93	8.23	5.93	5.59	5.29	5.78	3.47	1.82	8.37	10.15	6.15	5.36	5.42	4.70	8.69	
Tb	1.48	0.79	0.79	0.83	0.90	1.07	1.31	0.99	1.18	1.34	1.15	0.95	0.86	0.77	0.88	0.52	0.20	1.25	1.51	0.89	0.86	0.83	0.73	1.14	
Dy	8.46	5.11	4.20	5.11	5.87	5.50	7.68	4.58	6.32	7.27	6.46	4.65	4.80	4.28	4.62	2.84	1.06	6.56	8.56	5.35	4.72	4.85	3.69	6.58	
Ho	1.85	0.93	0.79	0.99	1.07	1.10	1.52	0.96	1.09	1.40	1.17	0.88	0.84	0.86	0.87	0.55	0.18	1.36	1.66	1.10	0.94	0.91	0.73	1.16	
Er	5.03	2.22	2.21	2.91	2.87	2.93	4.65	2.51	2.80	3.88	3.45	2.16	2.44	2.49	2.45	1.37	0.42	3.35	4.55	2.82	2.61	2.78	2.09	3.38	
Tm	0.69	0.34	0.31	0.40	0.45	0.48	0.67	0.33	0.44	0.65	0.48	0.37	0.38	0.34	0.35	0.19	0.05	0.57	0.67	0.45	0.42	0.43	0.30	0.51	
Yb	4.00	1.85	2	2.15	2.71	2.73	4.29	2.13	2.39	3.33	2.73	2.31	2.21	2.46	1.94	1.37	0.40	3.36	3.85	2.97	2.68	2.57	1.80	3.39	
Lu	0.66	0.35	0.28	0.39	0.38	0.42	0.56	0.33	0.30	0.51	0.47	0.32	0.33	0.35	0.29	0.20	0.07	0.56	0.59	0.42	0.43	0.39	0.28	0.46	
A/CNK	0.93	0.96	0.99	0.99	1.00	0.97	1.01	1.02	1.02	0.88	0.86	0.86	0.91	0.86	0.90	0.93	1.01	0.89	0.95	0.79	0.81	0.78	0.82	0.93	
K ₂ O/Na ₂ O	1.18	0.92	1.18	1.14	1.33	1.19	1.06	1.21	1.22	0.86	0.89	0.67	0.98	0.88	0.82	0.39	0.36	0.93	1.10	0.52	0.36	0.58	0.68	0.66	
FeO/(FeO _t +MgO)	0.78	0.79	0.80	0.79	0.79	0.79	0.81	0.80	0.80	0.80	0.78	0.87	0.79	0.78	0.77	0.76	0.77	0.86	0.89	0.75	0.75	0.75	0.80	0.76	
MgO#	0.33	0.32	0.32	0.33	0.32	0.32	0.30	0.30	0.31	0.30	0.33	0.22	0.32	0.33	0.35	0.36	0.34	0.22	0.19	0.38	0.38	0.38	0.31	0.36	
Rb/Sr	0.43	0.29	0.56	0.49	0.74	0.67	1.11	0.42	0.43	0.42	0.32	0.12	0.35	0.43	0.54	0.30	0.14	0.34	0.60	0.22	0.34	0.25	0.16	0.27	
Ba/Sr	6.69	4.35	4.77	4.56	4.70	4.55	4.09	5.19	5.00	4.16	3.74	7.25	4.29	4.49	4.09	4.09	1.72	1.16	5.63	7.11	1.88	2.76	2.55	2.85	4.49
(La/Yb) N	17.65	20.15	22.92	8.53	18.85	17.14	6.32	15.72	12.02	18.46	17.86	10.19	11.41	13.84	15.22	10.29	103.99	8.17	11.61	8.94	12.25	8.55	14.12	32.00	
Eu/Eu*	0.42	0.47	0.39	0.47	0.34	0.34	0.31	1.11	0.39	0.50	0.50	1.40	0.51	0.56	0.44	0.55	0.12	0.66	0.48	0.77	0.61	0.74	0.61	0.61	

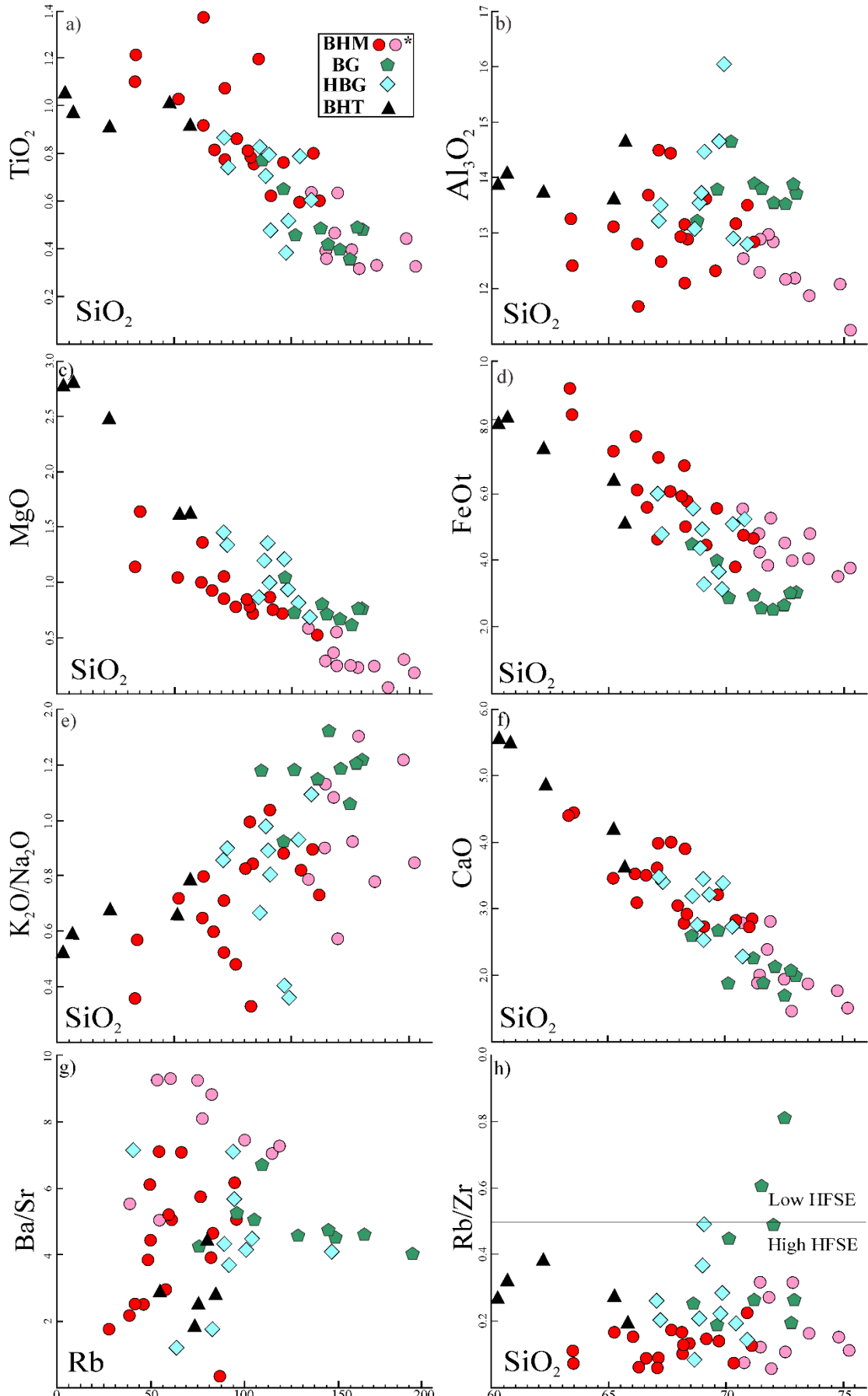


Figure 7: Harker diagrams for major (in wt.%) and trace (in ppm) for the granitoids from Vila Jussara area. *Red circles are the oxidized monzogranite and pink circles are the reduced one.

4.2.3. Rare earth elements and multielemental patterns

Analytical data on REE for representative samples of the Vila Jussara rocks demonstrate that despite the clear textural distinction of the different groups, REE behavior is quite similar (Figures 8a, c, e, g). In general, the associations show higher light REE content when compared to heavy REE (moderate La/Yb ratios). The moderate negative Eu anomalies, as well as the La/Yb ratios, are similar in the different groups; however, they are less pronounced to slightly positive in the tonalite rocks ($\text{Eu/Eu}^* = 0.61$ to 0.77). In the multielement diagrams and ETR patterns, there is marked similarity among the different varieties (Figure 9), all of which exhibit significant negative Sr, Ti and Nb-Ta pair anomalies, ranging from intense monzogranites, declining in the HBT and BG and becoming significantly smaller in the BHT (Figure 9h). These anomalies represent greater or less plagioclase (Sr), rutile, ilmenite and titanite (Ti, Nb and Ta) fractionation. The significant LILE content (Rb, Ba, and K) in relation to HFSE found in these rocks shows that the continental crust may have had an important contribution to the origin of these varieties.

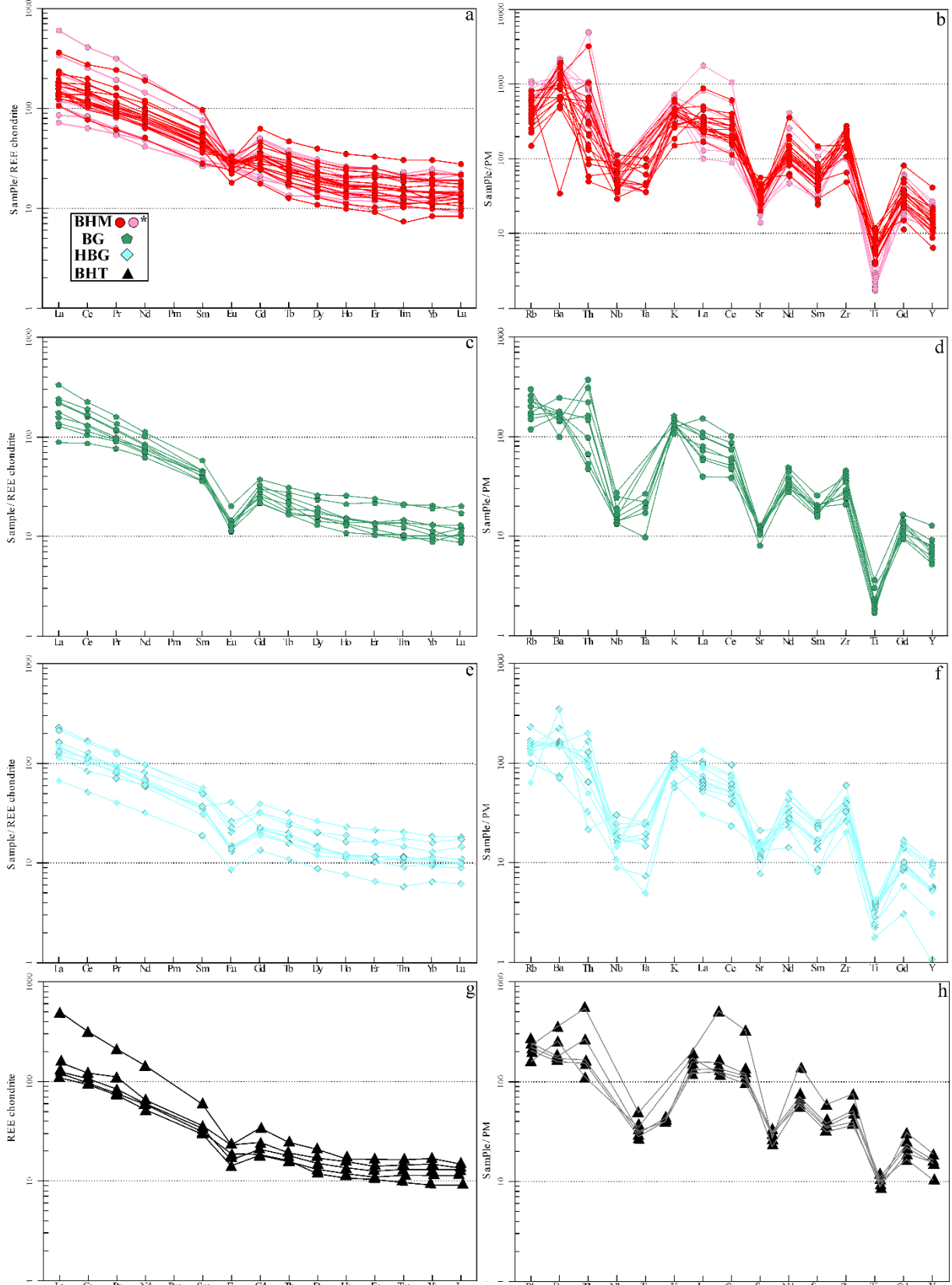


Figure 8: REE pattern and Multielemental pattern for the Vila Jussara rocks normalized for Boynton (1984) and Sun (1980) chondrite respectively. Symbols according to Figure 8. a,b) for the reduced and oxidized BHM; c,d) for the BG; e, f) for the HBG (hybrid granitoids) and g, h) for the BHT. *Red circles are the oxidized monzogranite and pink circles are the reduced one.

4.3. Isotopic data

4.3.1. U-Pb Zircon dating

The 0.3 mm zircon crystals that occur in the ferroan oxidized/reduced monzogranitic varieties are generally associated with the mafic mineral aggregates, occurring in prismatic, colorless, non-inclusional, and fractured forms. The zircons showed prismatic morphologies and concentric oscillatory zoning, as presented in Figures 9a, b. The magnesian variety exhibits subhedral to anhedral zircon grains characterized by the presence of a relatively incipient growth zone with some local resorption (Figure 9c). A total of 11 zircon crystals (Table 3) were analyzed in the oxidized **BHM** variety, and only 8 (AMP 27 - 2.1, 4.1, 6.1, 7.1, 8.1, 9.1, 10.1, 11.1) were used to calculate Concordia age, obtaining 2743 ± 11 Ma (MSWD = 1.7 - Figure 10a). A total of 6 (PFA 77 - 4.1, 5.1, 6.1, 7.1, 8.2 9.1) were used to calculate the concordant age of crystallization for the reduced **BHM** sample (2745 ± 20 Ma) (MSWD = 2.3 - Figure 10b), 4 (LIF 29 - 1.1, 2.1, 3.2, 14.1) for the **HBG** sample (2742 ± 14 Ma) (MSWD = 0.38 - Figure 10c) and a total of 3 (MYF 40 - 1-4, 1-1, 8-1) for the **BHT** variety (2766 ± 9.6 Ma) (MSWD = 0.51 - Figure 10d).

4.3.2. Sm-Nd whole-rock isotope

Samarium-neodymium isotopic compositions were determined for 15 samples, which comprise the different varieties of the Vila Jussara granitoids. Full details regarding analytical procedures are given in section 3.3. Sm-Nd data are listed in Table 3 and plotted in Figure 11. All samples display similar values, where $^{147}\text{Sm}/^{144}\text{Nd}$ ratios vary from 0.09469 to 0.12836. Initial $\epsilon\text{Nd}(t)$ values range between -3.58 and 1.56, and TDM from 3.27 to 2.81 Ga. In spite of their similarities, $\epsilon\text{Nd}(t)$ values of **BHM** are slightly higher than the other varieties and **HBG** displays wide dispersity compared to the others, which may have been due to the hybridization nature of this rock. **BG** values vary from negative to positive and **BHT** has one of the lowest values among all varieties.

4.3.3. Zircon Lu-Hf isotope

Hf-isotope data of zircon grains from four granitoid samples are presented in Table 4 and plotted in Figure 12, revealing a number of similarities. Forty-eight and 9 zircon grains from the reduced monzogranite sample (MDP-57 and PFA-77) show initial Hf isotopes ranging from 0.280924 to 0.280987 and 0.280936 to 0.280959 respectively, negative $\epsilon\text{Hf}(t)$ values of -3.5 to -1.2 and -3.8 to -2.2, with TDM ages of 3.24 to 3.38 and 3.31 to 3.36 Ga,

respectively. Eleven zircon grains from the AMP-27 sample (oxidized monzogranite) display a narrow range of initial $^{176}\text{Hf}/^{177}\text{Hf}$ ratios, varying from 0.280925 to 0.280980. The $\epsilon\text{Hf}(t)$ values range between -3.4 and -1.5 and TDM from 3.26 to 3.38 Ga. In the ADE-01 sample belonging to the hornblende-bearing granitoid (**HBG**), analyses of 9 zircon grains yielded $^{176}\text{Hf}/^{177}\text{Hf}$ ratios between 0.281090 and 0.280906, negative $\epsilon\text{Hf}(t)$ values from -4.77 to -1.78, and TDM from 3.04 to 3.45 Ga.

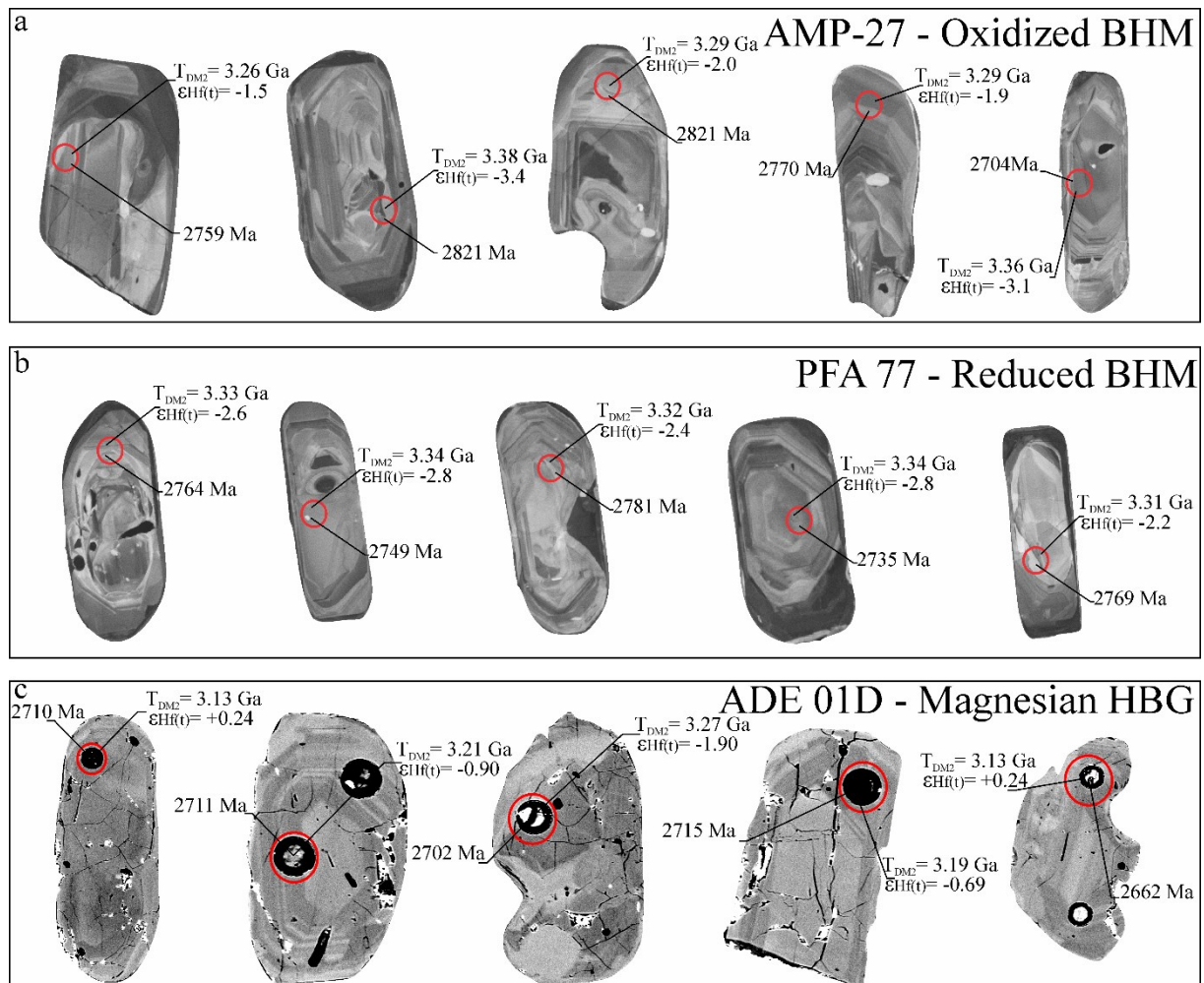


Figure 9. BSE images of representative zircon grains from the granitic ferroan oxidized (a) and reduced (b) variety and c) to representative zircons from the magnesian variety.

Table 2: U-Pb SHRIMP data for the zircons of the Vila Jussara area. Errors are in 1σ

Spot	U	Th	Th/U	$^{206}\text{Pb}_{\text{c}}$	Isotopic ratios					Age		Discordance	
	(ppm)	(ppm)	(%)		$^{207}\text{Pb}/^{235}\text{U}$	2 σ (%)	$^{206}\text{Pb}/^{238}\text{U}$	2 σ (%)	ρ	$^{207}\text{Pb}/^{206}\text{Pb}$	2 σ (%)	(%)	
AMP-27 (Oxidized BHM)													
2.2	128	102.2	0.8	3.9	13	1.9	0.5	1.5	0.774	2735.3	19.7	5.4	
3.1	46.5	37.2	0.8	2.6	14.2	2.4	0.5	2.1	0.894	2821.1	17.6	5.6	
5.1	56.9	33.3	0.6	1.3	13.7	2.2	0.5	2	0.898	2758.4	15.7	2.7	
1.1	57.8	60.6	1.1	1.9	13.8	3.1	0.5	1.9	0.606	2759.5	40	2.4	
4.1	57.2	51.3	0.9	1.2	13.7	2.2	0.5	2	0.883	2747.6	17.1	2.2	
11.1	101.2	125.5	1.3	0.7	13.6	1.7	0.5	1.6	0.917	2736.6	11.4	1.3	
10.1	58.9	33.5	0.6	0.6	13.3	2.3	0.5	2	0.864	2704.8	19.1	0.2	
9.1	41.6	37.6	0.9	1	13.5	2.8	0.5	2.3	0.845	2722.5	24.3	0.4	
6.1	109.8	79.2	0.7	0.6	13.7	1.7	0.5	1.5	0.909	2740.8	11.7	1	
7.1	68.9	39.7	0.6	1	14.1	2.1	0.5	1.9	0.892	2770.2	15.5	1.5	
2.1	43.3	30.1	0.7	-0.3	14.2	2.3	0.5	2.1	0.913	2760.7	15.4	-0.5	
8.1	61.1	57.8	1	-0.5	14.5	2.1	0.5	1.9	0.916	2772.5	14	-0.9	
PFA-77 (Reduced BHM)													
6.2	51	39	0.78	3.52	12.88	4.1	0.4965	2.2	0.53	2726	57	6	
10.1	46	57	1.28	3.08	13.42	3.1	0.5038	2.3	0.74	2769.4	34	6	
1.1	36	38	1.07	2.63	13.41	3	0.5049	2.6	0.87	2764.7	24	6	
2.1	40	38	0.99	2.19	13.16	2.8	0.5067	2.3	0.85	2728.4	24	4	
3.1	53	53	1.03	2.03	13.46	2.4	0.5115	2.1	0.87	2749.2	19	4	
8.1	31	23	0.75	1.89	13.44	3.1	0.5132	2.7	0.86	2742.1	26	3	
6.1	24	39	1.71	2.67	13.18	4.6	0.5142	3	0.66	2706	56	1	
4.1	71	115	1.69	1.85	13.44	2.2	0.5153	1.9	0.85	2735	19	2	
9.1	41	37	0.94	1.56	13.87	2.9	0.5229	2.4	0.85	2762.6	25	2	
8.2	23	23	1.02	1.15	13.25	4	0.5216	3.1	0.79	2690.9	41	-1	
7.1	24	20	0.85	1.01	14.47	3.9	0.5392	3.2	0.83	2781.2	35	0	
5.1	43	29	0.71	0.47	14.45	2.6	0.5387	2.3	0.89	2781	20	0	
LIF-29 (HBG)													
1.1	135	88	0.65	0.6	13.8	1.7	0.53	1.1	0.63	2735	22	0	
2.1	115	150	1.31	0.93	13.8	1.3	0.528	1.1	0.84	2742	12	0	
3.2	135	195	1.44	--	14	1.4	0.537	1.1	0.79	2733	14	-2	
4.1	233	379	1.63	2.27	12.6	1.2	0.497	1	0.81	2695	11	4	
5.1	89	73	0.83	6.73	12.4	2	0.476	1.2	0.61	2725	26	9	
6.1	88	148	1.69	2.35	14.4	3.1	0.542	1.3	0.42	2768	46	-1	
7.1	223	369	1.65	5.4	12.4	1.2	0.475	1	0.81	2730	12	10	
8.1	85	110	1.29	3.89	13.4	1.7	0.508	1.2	0.74	2748	19	4	
9.1	347	146	0.42	13.07	4.5	1.7	0.213	0.9	0.55	2382	24	52	
10.1	122	234	1.93	4.47	12.8	1.7	0.492	1.1	0.68	2735	20	7	
11.1	93	155	1.66	4.16	13.6	2.1	0.518	1.2	0.59	2747	27	3	
12.1	33	45	1.35	11.76	14	4.2	0.502	1.9	0.45	2846	60	9	
13.1	130	89	0.69	3.02	13.8	1.4	0.515	1.1	0.82	2776	13	4	
14.1	49	62	1.27	0.98	13.9	2.1	0.531	1.5	0.7	2748	25	0	
MYF-40 (BHT)													
1-4	51	57	1.16	0	14.27	2.52	0.534	2.16	0.86	2774	21	0.5	
2-1	73	81	1.16	0.45	13.84	2.2	0.520	1.92	0.87	2769	18	2.5	
1-1	211	46	0.23	0	14.22	1.57	0.539	1.33	0.85	2755	14	-0.8	
1-3	316	75	0.25	0	13.53	1.39	0.511	1.21	0.87	2762	11	3.7	
6-2	88	100	1.17	0	14.06	2.04	0.522	1.7	0.83	2787	18	2.8	
7-1	84	50	0.61	0.14	13.62	1.97	0.516	1.75	0.89	2754	15	2.6	
8-1	106	102	0.99	0.06	14.10	1.91	0.527	1.75	0.91	2777	13	1.7	
10-1	82	67	0.85	0.18	13.78	2.06	0.515	1.84	0.90	2777	15	3.6	
10-2	266	48	0.19	0	13.7138	1.52	0.5202	1.4	0.923	2753	10	1.9	

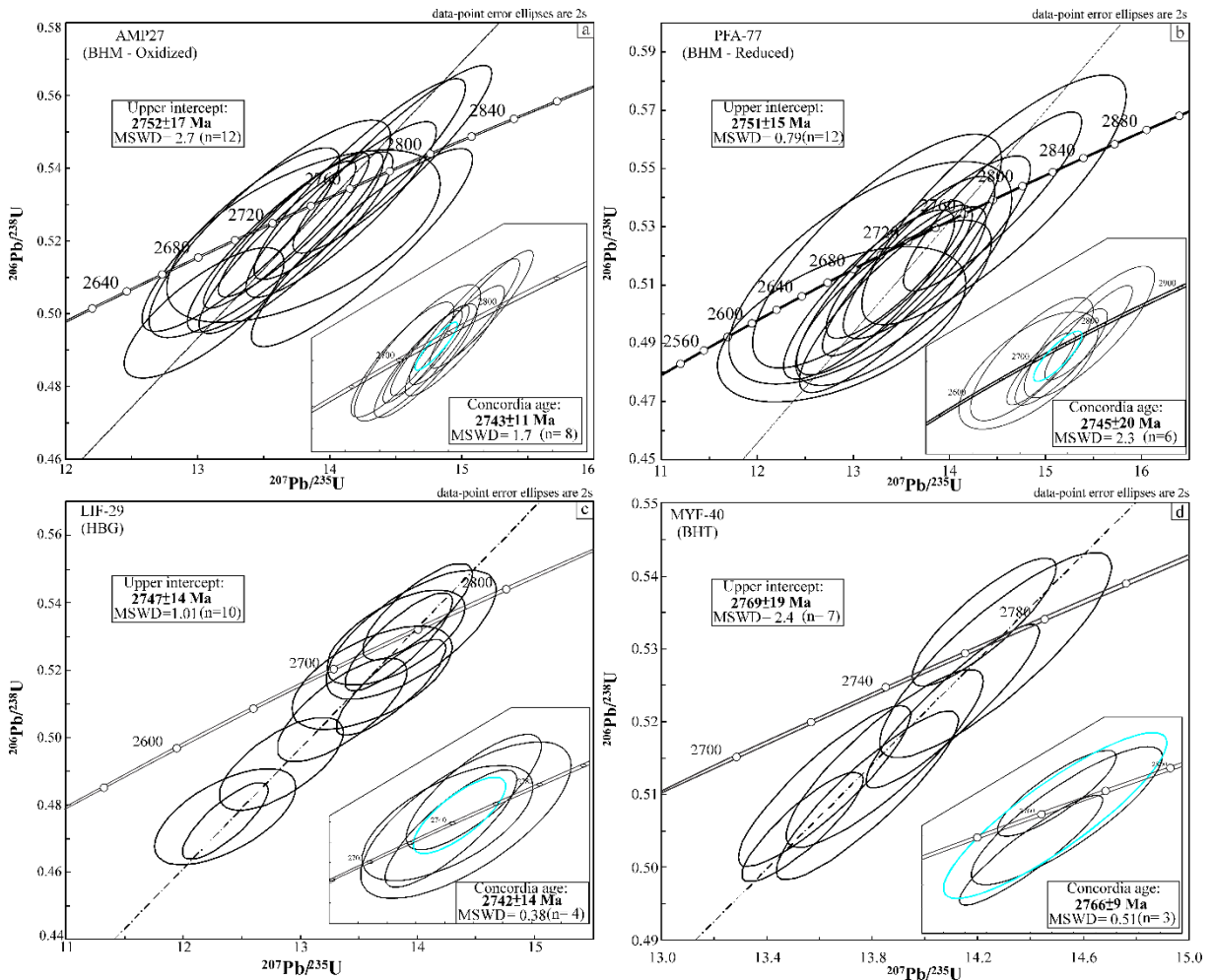


Figure 10. U-Pb SHRIMP Concordia plots of the granitoids from Vila Jussara area. Plots for the Monzogranite variety oxidized (a), reduced (b) for the HBG variety (c) and tonalite (d).

Table 3: Whole-rock Sm-Nd isotopic data for the granitoids from Vila Jussara area.

Sample	Sm (ppm)	Nd (ppm)	$^{147}\text{Sm}/^{144}\text{Nd}$	2σ	$^{143}\text{Nd}/^{144}\text{Nd}$	2σ	$f(\text{Sm/Nd})$	$\epsilon_{\text{Nd}}(0)$	$T_{(\text{DM})} \text{ Ga}$	$\epsilon_{\text{Nd}}(t)$	U-Pb (Ma)
BHM											
AMP-27	15.79	74.35	0.12836	0.00320	0.511346	0.000009	-0.3475	-25.20	3.078	-1.08	2743
LIF-14A	12.22	61.7	0.11977	0.00679	0.511063	0.000019	-0.3911	-30.72	3.270	-3.58	2743
MDP-14A	5.85	35.45	0.09984	0.00283	0.510880	0.000013	-0.4924	-34.29	2.926	-0.09	2743
MDP-57A	7.06	38.35	0.11123	0.00173	0.511017	0.000010	-0.4345	-31.62	3.054	-1.45	2743
MDP-16A	5.98	34.92	0.10361	0.00243	0.510885	0.000022	-0.4732	-34.20	3.024	-1.34	2743
PFA-77	6.85	41.04	0.10096	0.00207	0.510812	0.000012	-0.4867	-35.62	3.054	-1.83	2743
HBG											
LIF-18A	8.49	54.2	0.09469	0.00139	0.510700	0.000008	-0.5186	-37.80	3.036	-1.70	2750
MDP-02D	9.61	55.97	0.10379	0.00247	0.510799	0.000011	-0.4724	-35.87	3.155	-3.00	2750
LIF-16B	10.11	54.35	0.11243	0.00553	0.510929	0.000021	-0.4284	-33.34	3.233	-3.53	2750
LIF-14C	8.26	44.82	0.11135	0.00530	0.511038	0.000021	-0.4339	-31.21	3.024	-1.00	2750
MDP-14C2	9.44	51.09	0.11172	0.00295	0.510933	0.000014	-0.4321	-33.26	3.202	-3.20	2750
MDP-14E	6.22	36.26	0.10361	0.00243	0.510961	0.000025	-0.4732	-32.71	2.914	0.24	2750
BG											
AMP-77	13.43	77.69	0.11978	0.00123	0.511325	0.000019	-0.3910	-25.61	2.818	1.56	2743
MDP-02A	6.27	31.22	0.12148	0.00222	0.511181	0.000016	-0.3824	-28.42	3.125	-1.81	2750
BHT											
MDP-02E	6.29	32.79	0.11597	0.00440	0.511003	0.000021	-0.4104	-31.89	3.234	-3.34	2750

T_{DM} and $\epsilon_{\text{Nd}}(t)$ were calculated relative to CHUR and Depleted Mantle (DM) with present-day values of $^{143}\text{Nd}/^{144}\text{Nd} = 0.512638$ and $^{147}\text{Sm}/^{144}\text{Nd} = 0.1967$, following De Paolo and Wasserburg (1976) and De Paolo (1981) models, respectively, for Nd isotopic evolution of depleted mantle.

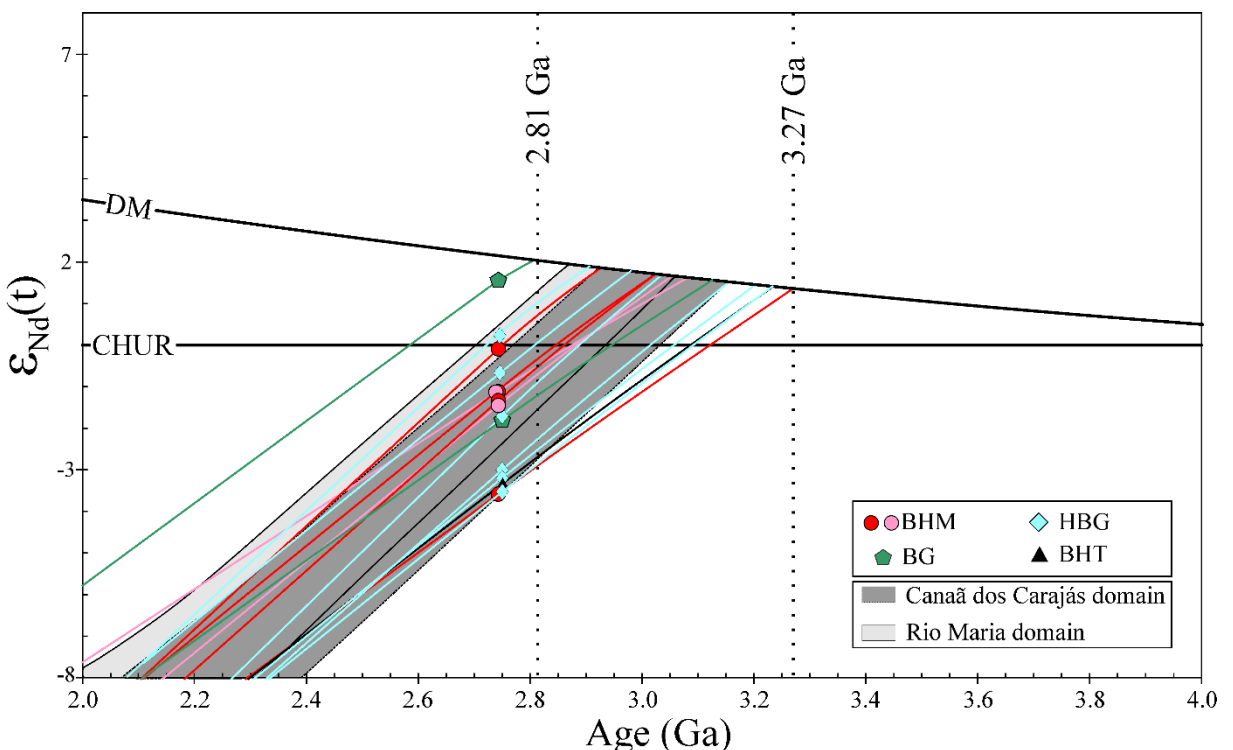
Figure 11. Plot of time vs. ϵ_{Nd} values for the granitoids from Vila Jussara area (dataset in table 3).

Table 4. LA-MC-ICP-MS Lu-Hf isotopic data of zircon grains for the granitoids from Vila Jussara area.

Zircon	$^{176}\text{Hf}/^{177}\text{Hf}$	2s	$^{176}\text{Lu}/^{177}\text{Hf}$	2s	$^{176}\text{Yb}/^{177}\text{Hf}$	2s	$^{178}\text{Hf}/^{177}\text{Hf}$	ϵ_{H} (t0)	$t(\text{U-Pb})$ (Ga)	$^{176}\text{Hf}/^{177}\text{Hf}$	ϵ_{Hf} (t)	T_{DM}^{c} (Ma)*
MDP-57												
seq0021	0.280968	21	0.000284	2	0.007182	6	1.467181	-64.3	2.74	0.280953	-2.4	3323
seq0022	0.280962	19	0.000394	2	0.010058	8	1.467202	-64.5	2.74	0.280941	-2.9	3350
seq0023	0.280983	25	0.000369	3	0.009467	9	1.467195	-63.7	2.74	0.280964	-2.0	3299
seq0024	0.281004	20	0.000631	4	0.016749	15	1.467261	-63.0	2.74	0.280971	-1.8	3284
seq0025	0.280984	26	0.000405	2	0.010337	8	1.467187	-63.7	2.74	0.280962	-2.1	3302
seq0026	0.280977	22	0.000763	5	0.019884	16	1.467167	-63.9	2.74	0.280937	-3.0	3359
seq0027	0.280998	19	0.000906	5	0.023927	19	1.467150	-63.2	2.74	0.280950	-2.5	3330
seq0028	0.280988	21	0.000603	4	0.015980	13	1.467196	-63.5	2.74	0.280956	-2.3	3316
seq0029	0.280973	20	0.000634	4	0.016803	13	1.467213	-64.1	2.74	0.280940	-2.9	3353
seq0030	0.280989	24	0.000842	5	0.019810	16	1.467165	-63.5	2.74	0.280944	-2.7	3342
seq0031	0.280991	25	0.000554	3	0.014730	12	1.467196	-63.4	2.74	0.280962	-2.1	3303
seq0032	0.280987	19	0.000984	6	0.026257	21	1.467229	-63.6	2.74	0.280935	-3.1	3362
seq0033	0.280991	23	0.000376	2	0.009650	8	1.467207	-63.4	2.74	0.280971	-1.8	3283
seq0034	0.280990	20	0.000409	2	0.010393	8	1.467229	-63.5	2.74	0.280969	-1.9	3287
seq0035	0.281016	25	0.000590	4	0.015308	12	1.467284	-62.6	2.74	0.280985	-1.3	3253
seq0036	0.280964	16	0.000313	2	0.007950	6	1.467176	-64.4	2.74	0.280948	-2.6	3334
seq0037	0.281004	22	0.000837	9	0.022543	28	1.467176	-63.0	2.74	0.280960	-2.2	3308
seq0038	0.280993	16	0.000486	3	0.012667	11	1.467188	-63.4	2.74	0.280967	-1.9	3291
seq0039	0.280999	14	0.000346	2	0.008825	7	1.467220	-63.2	2.74	0.280980	-1.5	3262
seq0040	0.280977	17	0.000400	3	0.010193	9	1.467158	-63.9	2.74	0.280956	-2.3	3317
seq0041	0.280988	19	0.001219	7	0.034662	28	1.467187	-63.6	2.74	0.280924	-3.5	3388
seq0042	0.281001	16	0.000319	2	0.008246	8	1.467216	-63.1	2.74	0.280984	-1.3	3254
seq0043	0.280986	14	0.000625	4	0.016613	14	1.467240	-63.6	2.74	0.280953	-2.4	3323
seq0044	0.281011	16	0.000681	4	0.016969	14	1.467278	-62.7	2.74	0.280975	-1.7	3274
seq0045	0.281003	18	0.000354	2	0.009076	7	1.467216	-63.0	2.74	0.280984	-1.3	3254
seq0046	0.281003	15	0.001022	7	0.024470	22	1.467183	-63.0	2.74	0.280950	-2.6	3331
seq0059	0.280988	26	0.001111	8	0.030237	27	1.467200	-63.5	2.74	0.280930	-3.3	3375
seq0060	0.280966	26	0.000382	2	0.009870	8	1.467215	-64.3	2.74	0.280946	-2.7	3338
seq0061	0.280983	17	0.000445	4	0.011611	14	1.467184	-63.7	2.74	0.280959	-2.2	3309
seq0062	0.280985	17	0.000655	8	0.017463	25	1.467141	-63.6	2.74	0.280951	-2.5	3327
seq0063	0.280991	18	0.000817	5	0.021890	19	1.467213	-63.4	2.74	0.280948	-2.6	3334
seq0064	0.280969	22	0.000522	3	0.013613	11	1.467223	-64.2	2.74	0.280941	-2.8	3349
seq0065	0.280995	18	0.000501	3	0.013109	11	1.467205	-63.3	2.74	0.280968	-1.9	3289
seq0066	0.280969	18	0.000505	3	0.013097	10	1.467169	-64.2	2.74	0.280942	-2.8	3347
seq0067	0.280977	22	0.000478	3	0.012520	10	1.467246	-63.9	2.74	0.280952	-2.5	3325
seq0068	0.280993	19	0.000445	3	0.011541	9	1.467205	-63.4	2.74	0.280969	-1.9	3287
seq0069	0.280992	24	0.000460	3	0.011526	9	1.467179	-63.4	2.74	0.280968	-1.9	3289
seq0070	0.281027	20	0.001217	7	0.029824	24	1.467235	-62.2	2.74	0.280963	-2.1	3301
seq0071	0.281000	19	0.000822	5	0.021383	17	1.467218	-63.1	2.74	0.280957	-2.3	3313
seq0072	0.280970	20	0.000326	2	0.008329	7	1.467245	-64.2	2.74	0.280953	-2.5	3324
seq0073	0.280998	24	0.000478	3	0.012377	10	1.467196	-63.2	2.74	0.280973	-1.7	3279
seq0074	0.280981	21	0.000345	2	0.008618	7	1.467130	-63.8	2.74	0.280963	-2.1	3301
seq0075	0.280988	15	0.000390	2	0.008270	7	1.467172	-63.5	2.74	0.280968	-1.9	3290
seq0076	0.280971	16	0.000506	3	0.013106	11	1.467159	-64.1	2.74	0.280945	-2.7	3341
seq0077	0.280999	18	0.000233	1	0.005866	5	1.467183	-63.2	2.74	0.280987	-1.2	3248
seq0078	0.280979	21	0.000606	4	0.015810	14	1.467216	-63.9	2.74	0.280947	-2.6	3336
seq0079	0.280998	18	0.000593	4	0.015129	12	1.467236	-63.2	2.74	0.280967	-1.9	3292
seq0080	0.280988	18	0.000776	5	0.020723	17	1.467205	-63.5	2.74	0.280947	-2.6	3336
PFA-77												
seq0241	0.280966	22	0.000354	2	0.009034	7	1.467190	-64.3	2.74	0.280948	-2.6	3335
seq0242	0.280968	18	0.000507	3	0.013250	11	1.467184	-64.3	2.74	0.280941	-2.8	3349
seq0243	0.280962	18	0.000495	3	0.013060	10	1.467182	-64.5	2.74	0.280936	-3.1	3362
seq0244	0.280976	14	0.000427	3	0.011172	9	1.467261	-64.0	2.74	0.280953	-2.4	3322
seq0245	0.280976	22	0.000653	4	0.017026	14	1.467254	-64.0	2.74	0.280942	-2.8	3348
seq0246	0.280983	20	0.000556	4	0.014594	13	1.467205	-63.7	2.74	0.280954	-2.4	3321
seq0247	0.280962	28	0.000359	2	0.009164	7	1.467211	-64.5	2.74	0.280943	-2.8	3346
seq0248	0.280958	20	0.000331	2	0.008521	7	1.467172	-64.6	2.74	0.280941	-2.9	3350
seq0249	0.280984	19	0.000473	3	0.012563	10	1.467212	-63.7	2.74	0.280959	-2.2	3310
AMP-27												
seq0262	0.281011	21	0.000595	4	0.015584	13	1.467234	-62.7	2.74	0.280980	-1.5	3263
seq0263	0.280982	19	0.000825	5	0.022360	18	1.467271	-63.8	2.74	0.280939	-3.0	3355
seq0264	0.280975	21	0.000305	2	0.007664	6	1.467249	-64.0	2.74	0.280959	-2.2	3310
seq0265	0.280950	24	0.000474	3	0.012425	11	1.467193	-64.9	2.74	0.280925	-3.4	3386
seq0266	0.280980	20	0.000252	2	0.006425	5	1.467254	-63.8	2.74	0.280966	-2.0	3293
seq0267	0.280998	26	0.000627	4	0.016741	14	1.467232	-63.2	2.74	0.280965	-2.0	3297
seq0268	0.280985	23	0.000452	4	0.011598	11	1.467214	-63.6	2.74	0.280962	-2.1	3304
seq0269	0.280997	29	0.000553	7	0.014289	19	1.467226	-63.2	2.74	0.280968	-1.9	3290
seq0270	0.280985	21	0.000433	3	0.011326	9	1.467193	-63.7	2.74	0.280962	-2.1	3303
seq0271	0.280999	28	0.000380	2	0.009844	8	1.467158	-63.2	2.74	0.280979	-1.5	3266

seq0272	0.280955	19	0.000421	3	0.010883	9	1.467191	-64.7	2.74	0.280933	-3.1	3367
ADE-01D												
1.1	0.281091	21	0.000846	7	0.008329	7	1.467245	-59.9	2712	0.281047	0.2	3133
1.3	0.281055	15	0.000653	2	0.012377	10	1.467196	-61.2	2712	0.281021	-0.69	3191
6.4	0.280967	22	0.001180	3	0.012667	11	1.467188	-64.3	2712	0.280906	-4.77	3447
6.3	0.280986	20	0.000521	5	0.008825	7	1.467220	-63.6	2712	0.280959	-2.87	3328
5.2	0.281042	23	0.000535	3	0.010193	9	1.467158	-61.6	2712	0.281014	-0.91	3206
4.3	0.281044	29	0.000566	2	0.034662	28	1.467187	-61.6	2712	0.281015	-0.90	3205
4.4	0.281017	21	0.000596	3	0.011326	9	1.487193	-62.5	2712	0.280986	-1.90	3268
3.4	0.281123	28	0.000639	1	0.009650	8	1.467207	-58.8	2712	0.281090	1.78	3036
1.4	0.280980	23	0.000399	4	0.008618	7	1.467130	-63.8	2712	0.280960	-2.9	3327

*Calculate from the value of 0.015 (Griffin et al., 2002) for the average continental crust

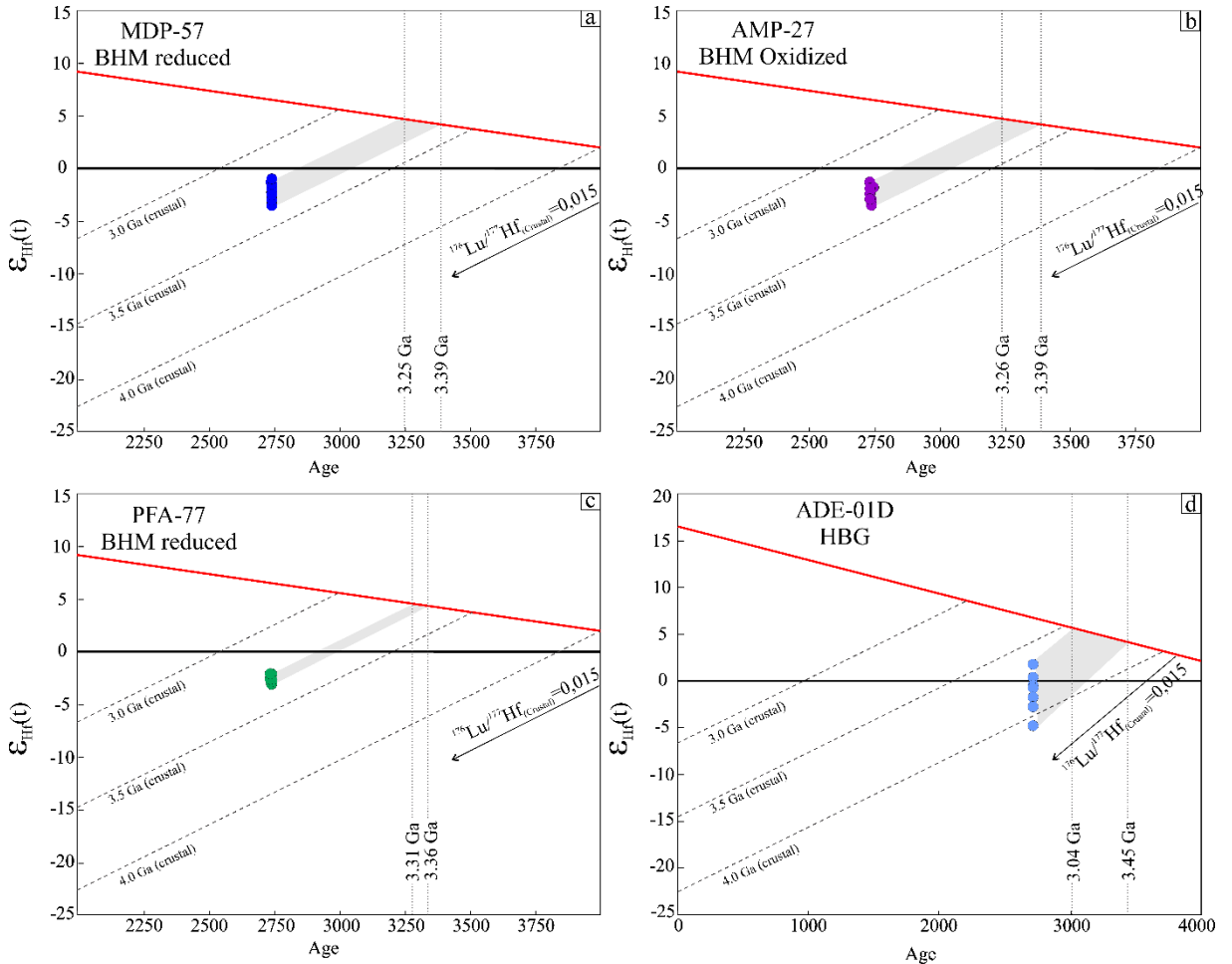


Figure 12. Plots of time vs. $\epsilon_{\text{Hf}}(t)$ values for the granitoids from Vila Jussara area (dataset in Table 4).

5. Implications of the isotopic signatures

One of the goals of this study is to use isotopic data (Nd and Hf) to identify a more precise geological scenario related to the formation of the Vila Jussara granitoids. Nd-isotope data show that BHM (oxidized and reduced ferroan monzogranites) have very similar isotopic characteristics, with $\epsilon_{\text{Nd}}(t)$ and TDM values overlapping (ranging from -3.5 to -1.3, and from 3.27 to 2.81 Ga; cf. Table 3 and Figure 10), while the value for the tonalite variety is slightly lower compared to the monzogranite group (-3.34 and TDM of 3.23 Ga). The BG variety

exhibits a value quite similar to that of BHM (-1.81 and TDM of 3.12 Ga), and HBG (hybrid granitoids) show very similar values with a slight trend to more negative ϵ values (ranging from -3.53 to 0.24 , with TDM from 3.23 to 2.91 Ga). The overlapping $\epsilon_{\text{Nd}}(t)$ values between all the varieties indicates some degree of hybridization (as suggested by field and compositional relationships), since their ages are similar and their emplacement via shear zones favored hybridization among the magmas.

Zircon Hf isotopic data show that the behavior of hornblende-bearing monzogranites (oxidized and reduced ferroan) is significantly more homogeneous than that of Nd isotopes, as shown by their restricted variation in $\epsilon_{\text{Hf}}(t)$ and TDM2 (ranging from -1.2 to -3.5 and 3.24 to 3.38 Ga. cf. Table 4 and Figure 11). On the other hand, the hybrid granitoids (BHG) display a more scattered pattern, revealing the heterogeneous nature of these rocks. Their $\epsilon_{\text{Hf}}(t)$ ranges from negative to positive values (-4.7 to 1.7 and TDM2 3.04 to 3.45 Ga). The negative zircon $\epsilon_{\text{Hf}}(t)$ values in all the varieties suggest the involvement of an old crustal source ($\text{TDM2} > 3.0$ Ga). Moreover, the similarities in zircon Hf and Nd isotope signatures among the hybrid granitoids (BHG) could be explained if the BHT and BHM magma sources had similar isotopic compositions or reached isotopic equilibrium during magma interactions. Since it is difficult to reach isotopic equilibrium in zircon Hf during mixing (Hu et al. 2012, Zhang et al. 2016), it is suitable to assume that these rocks may have different or identical crustal sources.

6. Behavior of trace and major elements and magmatic process

6.1. Partial melting

Granitoids akin to A-type magmas are essentially anhydrous and therefore a granulitic source that was hydrated prior to melting is a plausible argument for the generation of water-rich Neoarchean granitoids from Vila Jussara (>4 wt.% Dall'Agnol et al. 2017). The sources were then enriched in amphibole that was entirely consumed, thus generating a relatively high water content in the magmas and enhancing the partial melting process. To evaluate this proposal, we reformulated the geochemical modeling calculations of Neoarchean and Paleoproterozoic A-Type granites from Carajás province, where gabbro and quartz diorite compositions are assumed as source, respectively (Dall'Agnol et al. 1999, Feio et al. 2012). Given mafic granulite as source for their magmas, the multielement diagram (Figure 13) shows that $\sim 17\%$ (F) melting is necessary to generate liquids analogous to those of A-type granites, which is significantly lower than those reported in the original modeling ($\sim 28\%$) of the Planalto and Jamon magmas.

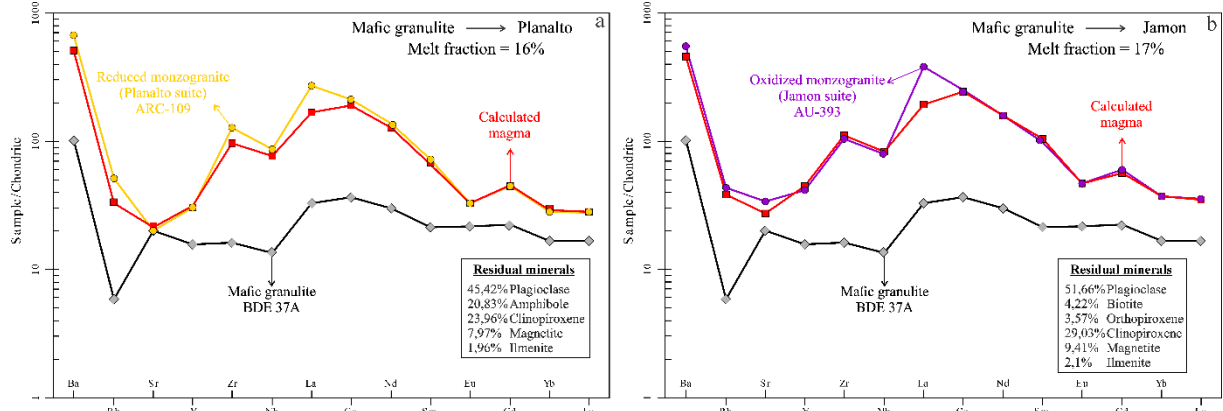


Figure 13. Multielemental diagram normalized by Sun 1980 chondrite to a melting model for the two examples of A-type granites in the Carajás province. (a) The Planalto (Archean A-Type; Feio et al. 2012, 2013) and (b) Jamon (Paleoproterozoic A-Type; Dall'Agnol et al. 1999).

Dall'Agnol et al. (2017) suggested that the occurrence of reduced, oxidized ferroan and magnesian granitoids in the Vila Jussara suite is evidence that an underlying granulitic crust existed in the Sapucaia subdomain in Neoarchean times that was more heterogeneous than in other areas of the province. The near coeval formation of these three distinct magmas probably favored mingling, making the relationships between the resulting granite varieties even more complex (hybrid granitoids). In the Vila Jussara suite, geochemical (cf. the subparallel trends of these varieties in the SiO₂–MgO plot, Fig. 7c; and AFM diagram, Fig. 6e) and oxygen fugacity contrasts demonstrate that the magmas of the reduced and oxidized seriated monzogranite and magnesian tonalite varieties are not derived from each other by fractional crystallization. Even though the REE pattern is slightly different in all samples, the Eu anomaly ranges from slightly positive to negative, since no fractionation process could account for this behavior, we argue that the source rock composition and processes operating during partial melting (e.g., changes in P-T-fO₂) were the most important parameters controlling the chemical compositional heterogeneity observed in the studied pluton.

Nd and Hf isotope data (Tables 3 and 4) suggest that Vila Jussara suite magmas are not juvenile (ϵ Nd and ϵ Hf), but derived from rocks of Mesoarchean age (TDM ages). Thus, to create a petrogenetic model that generates the primary magmas (excluding hybrid granitoids, HBG), the source rock was assumed to be the Mesoarchean granulites of the Ouro Verde area from Canaã dos Carajás subdomain (Marangoanha et al. 2019). Mass balance tests showed that the seriated monzogranite and tonalite granitoids were formed by different degrees of partial melting from a single source (mafic granulite). The results are presented in Table 5 and show that the major element compositions of the liquids are excellent fits for the reduced ($\sum R^2 = 0.9$), oxidized ($\sum R^2 = 0.79$) monzogranites and the magnesian tonalites ($\sum R^2 = 0.84$) with a proportion melt (F): residue (R) ratio of 14:86, 19:81 and 22:78%, respectively. The

residue for these models is formed by plagioclase, clinopyroxene, biotite, magnetite and ilmenite (Table 5). Orthopyroxene is present as residue in reduced-BHM liquid. Thus, the same proportions of melt and residual mineral phases were tested in trace element modeling (Figure 14 a-c), which also provided excellent correspondence between the calculated melt and the representative samples of each proposed model of Vila Jussara granitoids (AMP-88A, MDP-39, MDP-2C).

The BG rocks show mineralogic and geochemical contrasts in relation to the reduced-to -magnesian granitoids due to their more advanced evolution. The mass balance tests applied to these rocks show that a mafic granulitic crust is not related to the origin of the BG variety. Due to its enrichment in incompatible elements, Mesoarchean felsic granulite (sample BVD-39A) is suggested as the source, whose proposed partial melting model results are presented in Table 5. The results of least squares major element modeling with $\sum R^2 = 0.03$ and F:R ratio of 8:92% leave a residue consisting of plagioclase (62.5%), quartz (27.7%), biotite (5.8%) and magnetite (1.8%). In regard to trace element modeling, the correspondence between the composition of the calculated melt and the BG granitoid liquid establishes the felsic granulite crust as source (Figure 14), confirming that a heterogenous crust is responsible for the origin of the Vila Jussara magmas.

Table 5. Liquid composition calculated through modelling.

	BDE-37A (C ₀)	BVD-39A (C ₀)	Calculated Liquid (CL)				AMP 88A	MDP 39	MDP 2C	MD 01
	Mafic Granulite	Felsic Granulite	Reduced	Oxidized	Magnesian	Bt granite	BHM Reduced	BHM Oxidized	HBT Magnesian	BG
SiO ₂	47.5	68.4	72.2	67.3	63.7	72.1	72.4	67.5	63.9	72.1
TiO ₂	0.7	0.3	0.2	0.7	0.8	0.3	0.4	0.8	0.9	0.4
Al ₂ O ₃	15.5	16.3	12.2	14.2	13.9	13.9	12.4	14.4	14.1	13.9
FeOt	12.2	2.7	4.7	5.9	7.4	2.9	4.8	6.0	7.6	2.9
MgO	4.4	0.9	0.2	0.8	2.5	0.7	0.3	0.7	2.5	0.7
CaO	11.90	4.0	1.9	3.9	4.8	1.9	2.0	4.0	4.9	1.9
Na ₂ O	2.9	4.8	4.7	4.9	4.2	3.3	3.8	4.1	3.4	3.3
K ₂ O	0.8	1.0	3.4	1.8	2.2	4.4	3.5	2.0	2.3	4.4
ΣR^2			0.9	0.7	0.8	0.03				
Ba	249	682	1079	859.6	810	886,5	2180	872	681	1029
Rb	13.4	8.8	73.56	57.8	58.9	100,4	75.5	47	85.1	163
Sr	144.5	697	188.2	375.6	212.4	210.8	234.8	350	245	219
Y	24.6	2.5	27.5	38.5	33.7	29.7	29	33.9	30.9	34.4
Zr	62	128	362	281.9	223.4	287,1	559	262	221	268
Nb	3.2	2.6	8.7	13.6	10.7	15.8	12.5	12.7	11.1	16.6
La	7.8	21.4	38.6	34.1	31.6	74,7	37.6	44.5	48.7	75,6
Ce	22.3	34	78.9	97.9	92.3	154,2	80.7	99.6	97.1	153
Nd	13.7	11.4	39.1	34.1	37.3	58,3	40.4	45.7	36.7	60,4
Sm	3.1	1.5	7.8	6.8	6.6	8,6	7.2	8.4	6.5	8,9
Eu	1.2	0.6	2.6	2.3	1.2	0,9	2.3	2.0	1.1	0,9
Gd	4.4	1.0	7.8	7.1	6.8	7,8	6.3	7.8	5.3	7,9
Yb	2.6	0.2	3.3	3.1	3.0	2,6	2.7	3.0	2.6	2,7
Lu	0.4	0.05	0.5	0.5	0.5	0,3	0.4	0.4	0.4	0,3
Residue %										
Plag			51.3	51.2	52	62.5				
Opx			3.0	-	-	-				
Cpx			29.3	32.0	32	-				
Bt			4.7	6.4	5.3	5,8				
Mag			9.2	8.9	9	1.8				
Qtz			-	-	-	27.7				
Ilm			2.1	1.2	1.3	-				
(F)			14%	19%	22%	8%	.			

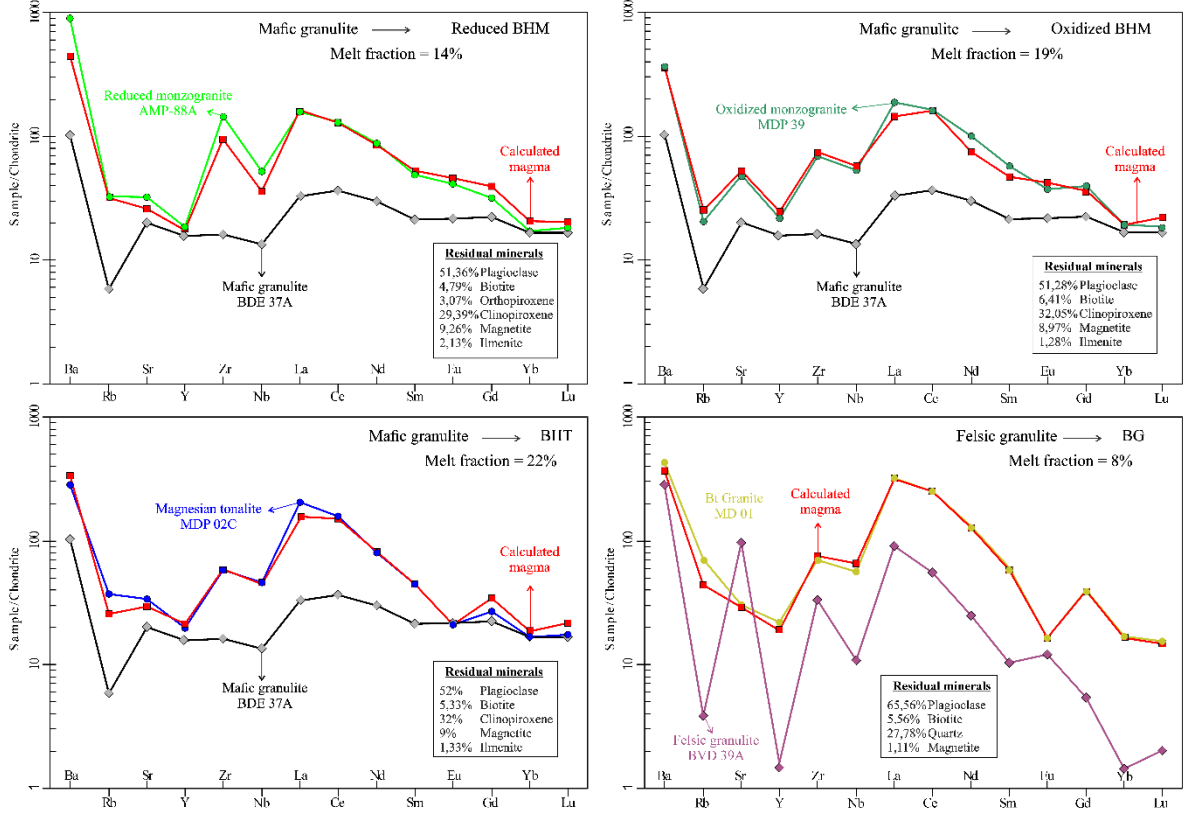


Figure 14. Trace elements models for generation of the (a, b c) monzogranites and tonalites and (d) for the biotite granites by partial melting of a granulitic source (mafic and felsic). Chondrite (C1) normalization values are from McDonough and Sun (1995).

6.2. Hybridization

The porphyritic granitoids (HBG) exhibit a complex relation with other varieties, such as interdigitated contacts with BHM and BHT rocks, where the presence of feldspar xenocrysts or even partially digested granite fragments is common. These features suggest that hornblende-bearing porphyritic granitoids are the product of interaction between different magmas in the Vila Jussara suite, as suggested by Silva et al. (2020) and Dall'Agnol et al. (2017). Considering the hybrid origin of HBG rocks, we constructed a mixing curve to test this hypothesis, where the tonalitic variety shows a lower degree of hybridization and may represent the less evolved end member, while monzogranites and BG correspond to the opposite member. In SiO₂ versus MgO/CaO (Figure 15a) and FeO/MgO (Figure 15b) diagrams, the HBG samples are concentrated largely between the mixing curves, showing that the three components contribute with different degrees in the system. As such, a hyperbolic mixing array is observed, suggesting that each sample represents a hybrid product generated from the mix in variable proportions between a less evolved (BHT) and felsic component (BHM and BG). REE diagrams were built to show that all the varieties participated with different degrees in the mixing systems; however, the tonalite magma appears to be the most

important component (Figures 15c and d). Thus, mixing between the tonalite variety and the BG magma results in an 80:20% ratio, while mixing between tonalite and BHM members produces a 70:30% ratio.

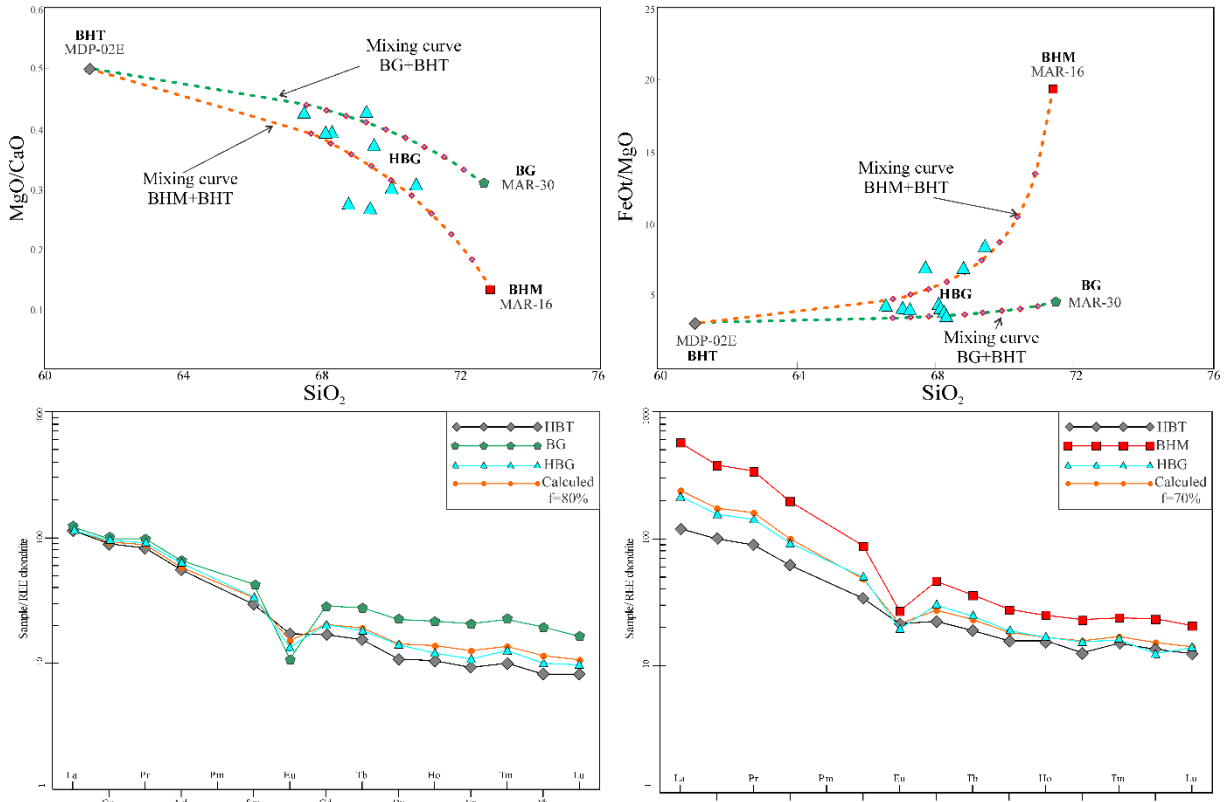


Figure 15. a), b) binary diagram showing a mixing array to the different varieties of Vila Jussara rocks. c, d) REE diagram for the mixing of tonalites and biotite granite c) and for the tonalite and BHM d).

7. Magma emplacement and tectonic implications

The complex deformational history of the Neoarchean granitoids of the Carajás province led to the often controversial interpretation of their emplacement conditions. These granitic plutons are usually classified as syntectonic A-type granitoids that were deformed during the closure of the Carajás basin at approximately 2.75 to 2.73 Ga (Barros et al. 2001, 2009, Feio et al. 2012, 2013, Dall' Agnol et al. 2017). However, Tavares (2015) reported that these rocks were formed in a distensional rift setting at ~2.73 Ga and were deformed later during the closure of the basin between 2.68 and 2.63 Ga. In the Vila Jussara granitoids, the common occurrence of microstructures such as microfractures in feldspar phenocrysts, filled with quartz-feldspathic matrix indicating that they were "healed" by melt and a preferred orientation of magmatic feldspar crystals, suggest that submagmatic flow operated during the final stage of granitoid crystallization. This is evidence that emplacement and deformation of the studied rocks were coeval (Passchier and Trouw 2005, Nedelet and Bouchez 2015). The

microstructures reveal a deformational history of the granitoids involving progressive cooling in the presence of a volatile-rich phase, from the (sub) magmatic to the solid state. Emplacement and final crystallization were thus synchronous with deformation in the Vila Jussara suite.

The genesis and evolution of Vila Jussara rocks is closely linked to the Vila União suite, as described by Marangoanha et al. (2019). The extensive presence of both felsic and mafic granulitic rocks in the Vila União was used in our model as a source for Vila Jussara magmatism. It reveals that these rocks were exposed in different crustal levels, with transpression of exhumed rocks at mid-to-lower crustal levels (20–30 km) with significant underplating and mantle upwelling forming the Vila União suite (Marangoanha et al. 2020). Considering the synchronous emplacement/deformation of their magmas, a geodynamic scenario that favored the formation of the Neoarchean plutonism from Carajás province, demonstrates that the granitoids were emplaced during a N–S transpressional tectonic regime, where the lowermost mafic crust was delaminated after crustal thickening, causing crustal underplating by mantle-derived mafic magma followed by partial melting of the Mesoarchean mafic granulite (2.87–2.84 Ga). These magmas were channeled through the crust via reactivated Mesoarchean shear zones forming the ~E–W Itacaiúnas belt, in a context of pure shear-dominated sinistral transpression (Silva et al. 2020).

The different granitoid varieties of the Vila Jussara suite are cogenetic, corresponding to plutons formed during a single thermal event. Given the existence of at least three distinct magma batches, namely **BHM**, **BG** and **BHT**, a syntectonic pluton model involving three main stages is proposed: (i) the tonalitic magma (BHT) was generated at ~2.75 Ga in a compressive regime related to a large number of sinistral, transpressive and transtensive shear zones, which served as conduits for magmas to ascend, opening space through shear zones at shallower crustal levels; (ii) the most restricted BG magma was emplaced in the space previously opened by the BHT magma. The BHT and BG magmas show low temperature and viscosity contrast, allowing the granitic magma to interact with the surrounding tonalitic magma, giving rise to numerous enclaves and interdigitated contact zones between the two lithologies; (iii) the latter stage was characterized by the intrusion of a larger volume of granitic magma (BHM) compared to the two first pulses (BHT and BG), which enlarged the open space in the crust due to syn-emplacement shearing, where the plutons acquired a sigmoidal shape (Figure 16a). Along the large contact zones between the successive pulses, the BG and BHT magmas, and to a lesser extent BHM magma, continuously interacted until a hybrid zone was formed (Figures 16b, c). Granitoids from this zone (HBG) exhibit a distinct

porphyritic texture and remarkable petrographic similarities with both the BG and BHT varieties.

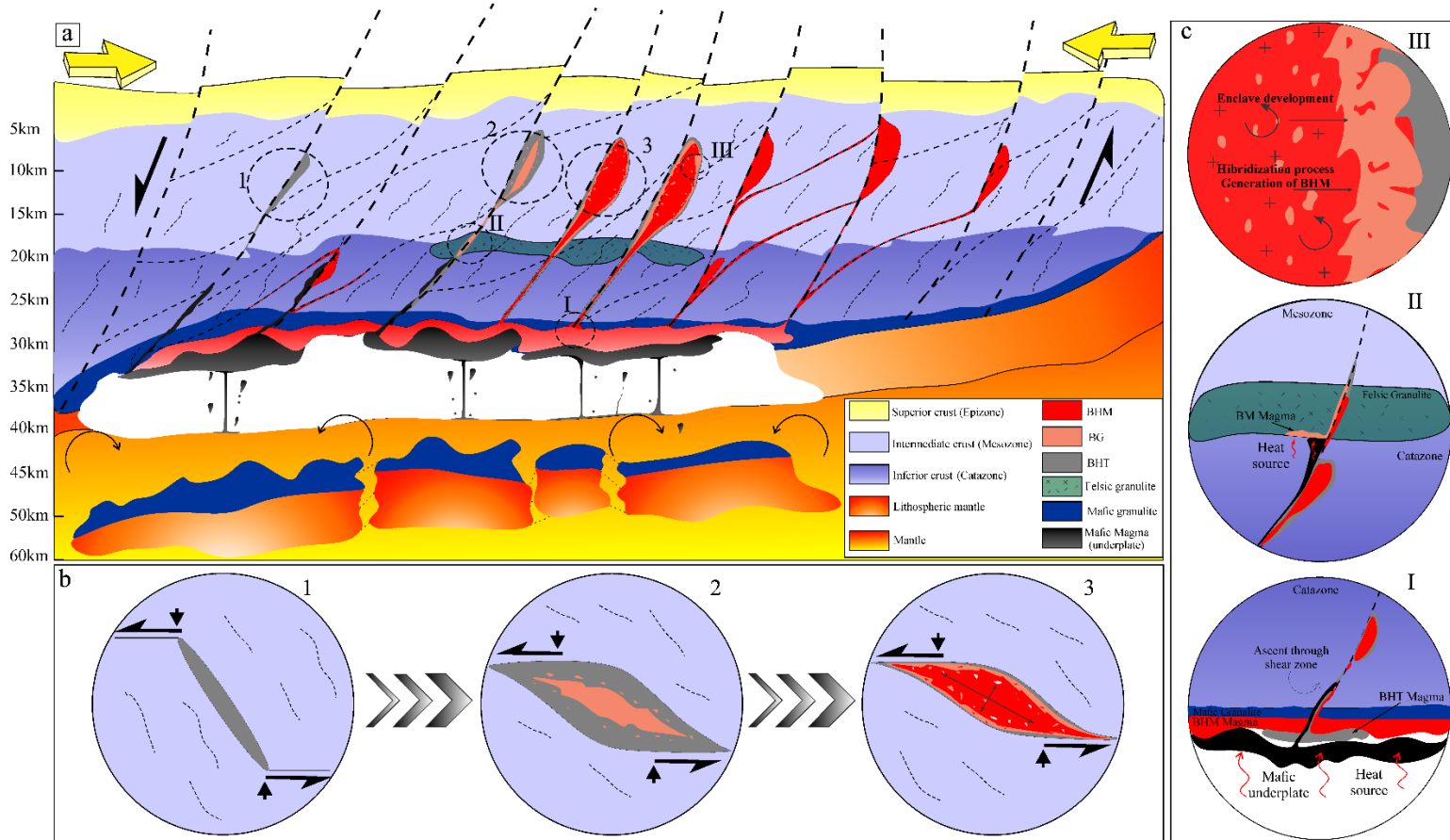


Figure 16. a) Simplified schematic illustration summarizing the petrogenetic/geodynamic model based partial melt and mixing/mingling process between the magmas to generate the granitoids of Vila Jussara area that involved transpressional setting; b) Detail schemes from the different generation process of the Vila Jussara magmas: I) Underplate of mafic magma due to a delamination process which sinking part of the lower crust and the lithospheric mantle. The mafic magma that is stalled into the crustal basis generate enough heat to trigger a partial melt in different degrees (14, 19 and 22%) which lead to the BHM (reduced and oxidized) and the BHT magmas. II) The subsequent rising through shear zones by the BHT-BHM and the mafic magma generates another thermal anomaly into a restricted zone of felsic granulites, leading to the generation of the BG magmas; III) The constant rising of the different magmas generated into the previous process invariably reach the mesozone forming large sigmoidal plutons with a large interaction between these magmas. This interaction lead to generation of hybrid granites which are probable product of a complex mixing system involving different degrees of each cited magma. b) Model of syntectonic ascent and emplacement of the Vila Jussara magmas: 1) Stage one. Generation, ascent, and emplacement of the tonalite (BHT) magmas; 2) Stage two. Ascent of large amounts of BG magma with subsequent enlargement of the pluton; 3) Stage three. Injection of larger volume of felsic magma (BHM) and interaction between the successive magmatic pulses forming a porphyritic hybrid granitoid, the HBG variety.

8. Conclusions

The Neoarchean granite magmatism in the Vila Jussara area is characterized by several coalescent, elongated and amalgamated plutons, which show intense deformation in near E-W directions and high-angle dips that follow the regional trend, and is marked by extensive shear zones linked to the Itacaiúnas belt. SHIRMP U-Pb dating resulted in ages of 2.74 Ga for the BHM and HBG rocks and 2.76 Ga for the tonalite variety, similar to those attributed to other Neoarchean granitoids from Carajás province. The Nd and Hf isotopic data suggest a Mesoarchean crustal source for Vila Jussara magmas [ϵ Nd (-1.5 to -3.5); ϵ Hf (-1.2 to -3.5) and TDM > 3.0 Ga]. In this respect, the petrogenetic model adopted to generate the primary magmas of this suite considers the Mesoarchean granulites from the Ouro Verde area of the Canaã dos Carajás subdomain as source rock. Partial melting (8%) of a felsic granulite has been investigated to generate the BG variety, while partial melting between 14 and 22% of a mafic granulite is required to generate amphibole-bearing granitoids. Successive melting of crustal sources produced the wide compositional spectrum of the Vila Jussara granitoids.

The consolidation (and construction) of the Vila Jussara magmatism is documented by zircon geochronology, field relations, geochemistry and isotopic signatures. These data demonstrate multiple magma injections, repeated melt segregation and evolution with extensive hybridization under a transpressional/transtensional tectonic regime dominated by pure shear. Given the dynamic character of the shear zones that control granite magma emplacement, the syntectonic nature of these granitoids contributes to the hybridization of these systems.

ACKNOWLEDGMENTS

The authors would like to thank the Research Group on Granitoid Petrology (GPPG) for their support in the various stages of this work, the Institute of Geosciences (IG), the Post-Graduate Program in Geology and Geochemistry (PPGG) of Universidade Federal do Pará (UFPA) and the Faculty of Geology of the Universidade Federal do Sul e Sudeste do Pará (UNIFESSPA) for the support of field activities. We are also grateful to M.T. Galarza for assistance during the acquisition of U-Pb, Sm-Nd and Lu-Hf isotope data at the Laboratório de Geologia de Isotópica (PARAISO-UFPA). The first author (FF) thanks the Conselho Nacional de Desenvolvimento Científico e Tecnológico (CNPq) and Coordenação de Aperfeiçoamento de Pessoal de Nível Superior (CAPES) for a doctoral thesis scholarship (Proc. 140077/2018-9).

and finance code 001). Funding for this project came from CNPq (D.C. Oliveira – Proc. 311647/2019-7 and 435552/2018-0; R. Dall’Agnol - Proc. 306108/2014-3), and PROPESP (PAPQ)/UFPA.

References

- Almeida F.F.M., Hasui Y., Brito-Neves B.B., Fuck, R.A., 1981. Brazilian structural provinces: an introduction. *Earth-Science Reviews* 17, 1–29.
- Almeida J.A.C., Dall’Agnol R., Leite A.A.S. 2013. Geochemistry and zircon geochronology of the Archean granite suites of the Rio Maria granite-greenstone terrane, Carajás Province. *Brazil Journal of South American Earth Sciences*, 42: 103–126.
- Almeida J.A.C., Dall’Agnol R., Oliveira M.A., Macambira M.J.B., Pimentel M.M., Rämö O.T., Guimarães F.V., Leite A.A.S. 2011. Zircon geochronology and geochemistry of the TTG suites of the Rio Maria granite-greenstone terrane: implications for the growth of the Archean crust of Carajás Province, Brazil. *Precambrian Research*, 187: 201–221.
- Althoff F.J., Barbey P., Boullier A.M. 2000. 2.8–3.0 Ga plutonism and deformation in the SE Amazonian craton: the Archean granitoids of Marajoara (Carajás Mineral Province, Brazil). *Precambrian Research*, 104: 187–206.
- Avelar V.G., Lafon J.M., Correia Jr. F.C., Macambira E.M.B. 1999. O magmatismo arqueano da região de Tucumã – Província Mineral de Carajás: novos resultados geocronológicos. *Revista Brasileira de Geociências*, 29(4): 453–460.
- Barbosa A.B., Lafon, J.M., Neves A.P., Vale A.G., 1995. Geocronologia Rb-Sr e Pb-Pb do Granito Redenção, SE do Pará: implicações para a evolução do magmatismo proterozoico da Região de Redenção. *Boletim do Museu Paraense Emílio Goeldi, série Ciências da Terra*, Belém, 7:147-164.
- Barros C.E.M., Sardinha A.S., Barbosa J.P.O., Macambira, M.J.B., 2009. Structure, petrology, geochemistry and zircon U-Pb and Pb-Pb geochronology of the synkinematic Archean (2.7 Ga) A-type granites from the Carajas Metallogenic Province, northern Brazil. *Can. Mineral.* 47, 1423e1440.
- Bodorkos S., Cawood P. A., Oliver N.H.S., 2000, Timing and duration of synmagmatic deformation in the Mabel Downs Tonalite, northern Australia: *Journal of Structural Geology*, v. 22, no. 8, p. 1181-1198.
- Boynton W.V. 1984. Cosmochemistry of the rare earth elements: meteorite studies. In: Henderson P. ed. *Rare Earth Element Geochemistry*, pp. 63-114. Elsevier, Amsterdam.

- Chu N.C., Taylor R.N., Chavagnac V., Nesbitt R.W., Boella R.M., Milton J.A., German C.R., Bayon G., Burton K., 2002. Hf isotope ratio analysis using multi-collector inductively coupled plasma mass spectrometry: an evaluation of isobaric interference corrections. *Journal of Analytical Atomic Spectrometry* 17, 1567–1574.
- Compston W., Williams I.S., Kirschvink J.L., Zichao Z., Guoguan M.A., 1992. Zircon U-Pb ages for the Early Cambrian time-scale. *Journal of the Geological Society, London* 149, 171 – 184.
- Dall'Agnol R. & Oliveira D.C. 2007. Oxidized, magnetite-series, rapakivi-type granites of Carajás, Brazil: implications for classification and petrogenesis of A-type granites. *Lithos*, 93: 215–233.
- Dall'Agnol R., Oliveira D.C., Guimarães F.V., Gabriel E.O., Feio G.R.L., Lamarão C.N., Althoff F.J., Santos P.A., Teixeira M.F.B., Silva A.C., Rodrigues D.S., Santos M.J.P., Silva C.R.P., Santos R.D., Santos P.J.L. 2013. Geologia do Subdomínio de Transição do Domínio Carajás – implicações para a evolução arqueana da Província Carajás – Pará. In: SBG, 13º Simpósio de geologia da Amazônia, Belém. Anais. 1 CD-ROM.
- Dall'Agnol R., Cunha I.R.V., Guimarães F.V., Oliveira D.C., Teixeira M.F.B., Feio G.R.L., Lamarão C.N., 2017. Mineralogy, geochemistry, and petrology of Neoarchean ferroan to magnesian granites of Carajas Province, Amazonian Craton: the origin of hydrated granites associated with charnockites. *Lithos* 277, 3-32.
- Delinardo M.A.S., Monteiro L.V.S., Moreto C.P.N., Sousa S.D., Melo G.H.C. 2014. Complexo Xingu: Uma secção da crosta inferior exumada durante a evolução do Domínio Carajás, PA. In: SBG, 47º Congresso brasileiro de geologia, Salvador. Anais. 1 CD-ROM.
- De Paolo D.J., 1981. Neodymium isotope in the Colorado Front Range and crust–mantle evolution in the Proterozoic. *Nature* 291, 193–196.
- De Paolo D.J., Wasserburg, G.J., 1976. Nd isotope variations and petrogenetic models. *Geophysical Research Letters* 3, 249–252.
- De Wit M.J., 1998. On Archean granites, greenstones, cratons and tectonics: does the evidence demand a verdict? *Precambrian Research* 91, 181–226.
- Debon F., Le fort P., 1983. A chemical–mineralogical classification of common plutonic rocks and associations. *Trans Roy Soc Edinb, Earth Sci* 73: 135–149
- Ersoy E.Y., 2013. PETROMODELER (Petrological Modeler): a Microsoft Excel spreadsheet program for modelling melting, mixing, crystallization and assimilation processes in magmatic systems. *Turkish Journal of Earth Sciences* 22, 115–125.

Feio G.R.L., Dall’Agnol R., Dantas E.L., Macambira M.J.B., Gomes A.C.B., Sardinha A.S., Oliveira D.C., Santos R.D., Santos P.A., 2012. Geochemistry, geochronology and origin of the Neoarchean Planalto Granite suite, Carajás, Amazonian craton: atype or hydrated charnockitic granites? *Lithos* 151, 57–73.

Feio G.R.L., Dall’Agnol R., Dantas E.L., Macambira M.J.B., Santos J.O.S., Althoff F.J., Soares J.E.B. 2013. Archean granitoid magmatism in the Canaã dos Carajás area: implications for crustal evolution of the Carajás province, Amazonian craton, Brazil. *Precambrian Research*, 227: 157–185.

Florisbal L.M., Janasi V.A., Bitencourt M.F., Heaman L.M., 2012. Space–time relation of post-collisional granitic magmatism in Santa Catarina, southern Brazil: U–Pb LA-MC ICP-MS zircon geochronology of coeval mafic-felsic magmatism related to the Major Gercino Shear Zone. *Precambrian Research*. 216, 132–15.

Frost B.R., Barnes C., Collins W., Arculus R., Ellis D., Frost C., 2001. A chemical classification for granitic rocks. *Journal of Petrology* 42, 2033–2048

Gabriel E.O., 2012. Geologia, geoquímica e petrologia magnética da porção nordeste de Água azul do norte, Província Carajás. Dissertação (Mestrado). Belém: Instituto de Geociências - Universidade Federal do Pará.

Gabriel E.O. & Oliveira D.C. 2014. Geologia, petrografia e geoquímica dos granitoides arqueanos de alto magnésio da região de Água Azul do Norte, porção sul do Domínio Carajás, Pará. *Boletim do Museu Paraense Emílio Goeldi. Ciências Naturais*, 9(3): 533–564.

Galarza M.A., Oliveira, D.C., Rodrigues E.A., Santos A.C., Marangoanha B., 2017. Granitoides neoarqueanos (2,73 – 2,74 Ga) intrusivos e associados ao Diopsídio Norito Pium, Canaã dos Carajás, Província Carajás (PA). *Contrib. à Geologia da Amaz.* SBG, Belém 10, 225–246.

Gerdes A., Zeh A., 2006. Combined U-Pb and Hf isotope LA-MC-ICP-MS analyses of detrital zircons: Comparison with SHRIMP and new constraints for the provenance and age of an Armorican metasediment in Central Germany. *Earth and Planetary Science Letters* 249, 47–62.

Gerdes A., Zeh A., 2009. Zircon formation versus zircon alteration – New insights from combined U-Pb and Lu-Hf in-situ LA-ICP-MS analyses, and consequences for the interpretation of Archean zircon from the Central Zone of the Limpopo Belt. *Chemical Geology* 261, 230–243.

Griffin W.L., Wang X., Jackson S.E., Pearson N.J., O'Reilly S.Y., 2002. Zircon geochemistry and magma mixing, SE China: in-situ analysis of Hf isotopes, Tonglu and Pingtan igneous complexes. *Lithos* 61, 237–269.

Hamilton W.B., 2011. Plate tectonics began in Neoproterozoic time, and plumes from deep mantle have never operated. *Lithos* 123, 1–20.

Hühn S.B., Macambira M.J.B., Dall'Agnol R. 1999. Geologia e Geocronologia Pb-Pb do granito alcalino arqueano Planalto, Região da Serra do Rabo, Carajás – PA. In: SBG, 6º Simpósio de geologia da Amazônia, Manaus. *Anais*. v. 1, p. 463–466.

Irvine T.N., Baragar W.R.A., 1971. A guide to the chemical classification of the common volcanic rocks. *Canadian Journal Earth Sciences* 8, 523–547.

Janoušek V., Farrow, C.M., Erban V., 2003. GCDkit: New PC software for interpretation of whole-rock geochemical data from igneous rocks. Godschmidt Conference Abstract, A186.

Karlstrom K.E., and Bowring, S.A., 1993, Proterozoic orogenic history in Arizona, in Reed, J.C., Jr., et al., eds., Precambrian: Conterminous U.S.: Boulder, Colorado, Geological Society of America, *Geology of North America*, v. C-2, p. 188–211.

Le Maître R.W., Streckeisen A., Zanettin B., Le Bas M.J., Bonin B., Bateman P., Bellieni G., Dudek A., Efremova J., Keller J., Lameyre J., Sabine P.A., Schmidt R., Sørensen H., Woolley A.R., 2002. Igneous rocks. A classification and glossary of terms. Recommendations of the International Union of Geological Sciences Subcommission on the Systematics of Igneous Rocks. Cambridge University Press, Cambridge, 252 pp.

Leite-Santos P.J. & Oliveira D.C. 2014. Trondhjemites da área de Nova Canadá: novas ocorrências de associações magmáticas tipo TTG no Domínio Carajás. *Boletim do Museu Paraense Emílio Goeldi. Ciências Naturais*, 9(3): 635–659.

Leite-Santos P.J.S. & Oliveira D.C. 2016. Geologia, petrografia e geoquímica das associações leucogranítica arqueanas da área de Nova Canadá: Província Carajás. *Geologia USP. Série Científica*, 16(2): 37–66.

Ludwig K.R., 2008. User's Manual for Isoplot 3.6: a Geochronological Toolkit for Microsoft Excel. Berkeley Geochronology Center Special Publication, Berkeley.

Machado N., Lindenmayer Z., Krogh T.E., Lindenmayer D., 1991. U-Pb geochronology of Archean magmatism and basement reactivation in the Carajás area, Amazon Shield, Brazil. *Precambrian Research*, 49: 329–354.

McDonough W.F., Sun, S.S., 1995. The composition of the Earth. *Chemical Geology* 120(3–4), 223–253.

Marangoanha B., Oliveira D.C., Oliveira V.E., Galarza M.A., & Lamarão C.N., 2019. Neoarchean A-type granitoids from Carajás province (Brazil): New insights. *Precambrian Research*, Volume 324, pp. 86-108.

Martin H. 1994. The Archean grey gneisses and the genesis of continental crust. *Developments in Precambrian Geology*, 11:205-259. [https://doi.org/10.1016/S0166-2635\(08\)70224-X](https://doi.org/10.1016/S0166-2635(08)70224-X).

Melo G.H.C., Monteiro L.V.S., Xavier R.P., Moreto C.P.N., Santiago E.S.B., Dufrane, S.A., Aires, B., Santos, A.F.F., 2016, Temporal evolution of the giant Salobo IOCG deposit, Carajas province (Brazil): Constraints from paragenesis of hydrothermal alteration and U-Pb geochronology: *Mineralium Deposita*, v. 52, p. 709–732, doi: 10.1007/s00126-016-0693-5.

Moreto C.P.N., Monteiro L.V.S., Xavier R.P., Amaral W.S., Santos T.J.S., Juliani C., Souza Filho C.R. 2011. Mesoarchean (3.0 and 2.86 Ga) host rocks of the iron oxide–Cu–Au Bacaba deposit, Carajás Mineral Province: U-Pb geochronology and metallogenetic implications. *Mineralium Deposita*, 46: 789–811.

Moyen J.F., Stevens G., Kirsters A., 2006. Record of mid-Archean subduction from metamorphism in the Barberton terrain, South Africa. *Nature* 422, 559–562, doi:10.1038/nature04972.

Nasdala L., Hofmeister W., Norberg N., Valley J.W., 2008. Zircon M257 - a Homogeneous Natural Reference Material for the Ion Microprobe U-Pb Analysis of Zircon. *Geostandards and Geoanalytical Research* 32(3), 247 – 265.

Oliveira D.C., Santos P.J.L., Gabriel E.O., Rodrigues D.S., Faresin A.C., Silva M.L.T., Sousa S.D., Santos R.V., Silva A.C., Souza M.C., Santos R.D., Macambira M.J.B. 2010. Aspectos geológicos e geocronológicos das rochas magmáticas e metamórficas da região entre os municípios de Água Azul do Norte e Canaã dos Carajás – Província Mineral de Carajás. In: SBG, 45º Congresso brasileiro de geologia, Belém. Resumos. 1 CD-ROM.

Oliveira E.C., Lafon J.M., Gioia S.M.C.L., Pimentel M.M. 2008. Datação Sm-Nd em rocha total e granada do metamorfismo granulítico da região de Tartarugal Grande, Amapá Central. *Revista Brasileira de Geociências*, 38: 114–127 (in portuguese).

Oliveira M.A., Dall'Agnol R., Althoff F.J., Leite A.A.S., 2009. Mesoarchean sanukitoid rocks of the Rio Maria Granite-Greenstone Terrane, Amazonian craton, Brazil. *Journal of South American Earth Sciences*, 27: 146–160.

Paiva Jr., A.L.P., Lamarão C.N., Lima P.H.A., 2011. Geologia, Petrografia e Geoquímica do Batólito Seringa, Província Carajás, SSE do Pará. *Braz. J. Genet.* 41 (2), 185–202.

- Passchier C.W., Trouw R.A.J., 2005. Microtectonics, second ed. Springer-Verlag, Berlin–Heidelberg–New York.
- Patchett P.J., Tatsumoto M., 1980. A routine high-precision method for Lu-Hf isotope geochemistry and chronology. Contributions to Mineralogy and Petrology 75, 263–267.
- Pearce J.A., Harris N.B.W., Tindle A.G., 1984. Trace element discrimination diagrams for the tectonic interpretation of granitic rocks. Journal of Petrology 25, 956–983.
- Petford N., Cruden A.R, McCaffrey K.J.W., Vigneresse J.L., 2000. Granite magma formation, transport and emplacement in the Earth's crust. Nature 408:669–73.
- Pidgeon R.T. MacAmbira M.J.B. Lafon J.M. 2000. Th-U-Pb isotopic systems and internal structures of complex zircons from an enderbite from the Pium Complex, Carajás Province, Brazil: Evidence for the ages of granulite facies metamorphism and the protolith of the enderbite. Chemical Geology 166, 159–171. [https://doi.org/10.1016/S0009-2541\(99\)00190-4](https://doi.org/10.1016/S0009-2541(99)00190-4).
- Rodrigues D.S., Oliveira D.C., Macambira M.J.B. 2014. Geologia, geoquímica e geocronologia do Granito Mesoarqueano Boa Sorte, município de Água Azul do Norte, Pará – Província Carajás. Boletim do Museu Paraense Emílio Goeldi. Série Ciências Naturais, 9(3): 597–633.
- Rollinson H., 1993. Using Geochemical Data. Longman, London.
- Ronaib C. & Oliveira D. C., 2013. Geologia, petrografia e geoquímica das associações TTG e leucogranodioritos do extremo norte do Domínio Rio Maria, Província Carajás. Boletim do Museu Paraense Emílio Goeldi. Ciências Naturais 8(3): 383-415.
- Santos J.O.S., 2003. Geotectônica do Escudo das Guianas e Brasil-Central. In: Bizzi, L.A. et al. (Ed.). Geologia, tectônica e recursos minerais do Brasil: texto, mapas e SIG. Brasília, CPRM – Serviço Geológico do Brasil, p. 169–226.
- Santos J.O.S., Gaudette, H.E., Olszewski, W.J., 1996 Geochronology of Precambrian rocks from the northern part of the Guiana Shield, State of Roraima, Brazil. Journal of South American Earth Sciences, Great Britain, v. 9, n.3/4, p. 183-195.
- Santos R.D., Galarza M.A., Oliveira D.C. 2013. Geologia, geoquímica e geocronologia do Diopsídio-Norito Pium, Província Carajás. Boletim do Museu Paraense Emílio Goeldi. Série Ciências da Terra, 8: 355–382.
- Santos P.J.L. & Oliveira D.C., 2012. Geologia, Petrografia e Geoquímica das Associações Granodioríticas-Graníticas de Nova Canadá, Subdomínio de Transição, Província Carajás. In: SBG, Congresso Brasileiro de Geologia, 46, Santos-SP, CDrom.

Sardinha A.S., Barros C.E.M., Krymsky R., 2006. Geology, geochemistry, and U–Pb geochronology of the Archean (2.74 Ga) Serra do Rabo granite stocks, Carajás Metallogenetic Province, northern Brazil. *Journal South American Earth Science* 20, 327–339.

Sardinha A.S., Dall’Agnol R., Gomes A.C.B., Macambira M.J.B., Galarza M.A. 2004. Geocronologia Pb-Pb e U-Pb em zircão de granitoides arqueanos da região de Canaã dos Carajás, Província Mineral de Carajás. In: SBG, 42º Congresso brasileiro de geologia, Araxá. Anais. 1 CD-ROM.

Sato K., Tassinari C.C.G., Basei M.A.S., Siga Júnior, O., Onoe A.T., Souza M.D., 2014. Sensitive High Resolution Ion Microprobe (SHRIMP IIe/MC) of the Institute of Geosciences of the University of São Paulo, Brazil: analytical method and first results. *Geologia USP, Série Científica* 14(3), 3–18.

Silva A.C., Dall’Agnol R., Guimarães F.V., Oliveira D.C. 2014. Geologia, petrografia e geoquímica de Associações Tonalíticas e Trondjemíticas Arqueanas de Vila Jussara, Província Carajás, Pará. *Boletim do Museu Paraense Emílio Goeldi. Ciências Naturais*, 9(1): 13–46.

Silva F.F., Oliveira D.C., Dall’Agnol R., Silva, L.R. Cunha, I.V. 2020 Lithological and structural controls on the emplacement of a Neoarchean plutonic complex in the Carajás province, southeastern Amazonian craton (Brazil). *Journal of South American Earth Sciences* 102, 102696.

Sun S.S. 1980. Lead isotopic study of young volcanic rocks from mid ocean ridges, ocean islands and island arcs. *Phil. Trans. Royal Soc. Lond.*, A297, 409–45.

Stacey J.S., Kramers J.D., 1975. Approximation of terrestrial lead isotope evolution by a two-stage model. *Earth and Planetary Science Letters* 26, 207–221.

Stern R.A., 2001. A new isotopic and trace element standard for the ion microprobe: preliminary TIMS U – Pb and electron microprobe data, current research. *Radiogenic Age and Isotopic Studies: Report 14*. Geological Survey of Canada, Ottawa, Canada.

Tassinari C.C.G. & Macambira M.J.B. 2004. Evolução tectônica do Cráton Amazônico. In: Mantesso-Neto V., Bartorelli A., Carneiro C.D.R., Brito Neves B.B. (Ed.). *Geologia do continente Sul-Americano: evolução da obra de F.F.M. de Almeida*. São Paulo, BECA, p. 471–486.

Teixeira L.R., 2005. GENESIS 4.0 – Software de Modelamento Geoquímico.

Teixeira M.F.B., Dall’Agnol R., Santos J.O.S., Oliveira D.C., Lamarão C.N., McNaughton N.J., 2018. Crystallization ages of Paleoproterozoic A-type granites of Carajás

province, Amazon craton: constraints from U-Pb geochronology of zircon and titanite. *J. S. Am. Earth Sci.* 88, 312–331.

Teixeira M.F.B., Dall’Agnol R., Silva A.C., Santos P.A. 2013. Geologia, petrografia e geoquímica do Leucogranodiorito Pantanal e dos leucogranitos arqueanos da área a norte de Sapucaia, Província Carajás, Pará: implicações petrogenéticas. *Boletim do Museu Paraense Emílio Goeldi. Série Ciências Naturais*, 8(3): 291–323.

Vasquez L.V., Rosa-Costa L.R., Silva C.G., Ricci P.F., Barbosa J.O., Klein E.L., Lopes E.S., Macambira E.B., Chaves C.L., Carvalho J.M., Oliveira J.G., Anjos G.C., Silva H.R. 2008. Escala 1:1.000.000. In: Vasquez M.L. & Rosa-Costa L.T. (Ed.). *Geologia e recursos minerais do Estado do Pará: Sistema de Informações Geográficas e SIG: texto explicativo dos mapas geológico e tectônico e de recursos minerais do Estado do Pará*. Belém, CPRM, 328 p.

Whalen J.W., Currie K.L., Chappel B.W., 1987. A-type granites: geochemical characteristics, discrimination and petrogenesis. *Contribution to Mineralogy and Petrology* 95, 407–419.

Wilson M., 1989. *Igneous Petrogenesis – A Global Tectonic Approach*, Springer, Dordrecht.

4 CONCLUSÕES E CONSIDERAÇÕES FINAIS

A área de Vila Jussara apresenta um extenso magmatismo granitoide neoarqueano que faz parte do contexto geológico do Domínio Carajás (Subdomínio Sapucaia) (Província Carajás. No Mesoarqueano (entre 2,89 a 2,84 Ga), este domínio foi afetado por um regime tectônico colisional (transpressional), coincidente com metamorfismo regional de uma crosta de composição TTG sob fácies granulito de alta temperatura e que seria responsável pela formação dos ortogranulitos félsicos da área de Ouro Verde. No Neoarqueano, (entre 2,76 a 2,74 Ga) essa porção da crosta sofreu processo de delaminação, provocado pelo “descolamento” da base da crosta (mais densa e refratária do que a crsota sobrejacente), que induziu ao *underplating* máfico. Esse processo promoveu a fusão parcial da crosta granulítica (máfica e félsica) mesoarqueana, que gerou líquidos em níveis crustais profundos. As idades U-Pb (2,74 - 2,76 Ga) e os dados isotópicos de Nd e Hf sugerem uma fonte crustal mesoarqueana para os magmas da Vila Jussara [ε Nd (-1,5 a -3,5); ε Hf (-1,2 a -3,5) e TDM > 3,0 Ga].

Com base nos resultados obtidos nos tipos granitoides (ferrosos oxidados e reduzidos e magnesianos) de Via Jussara, foi possível propor um modelo petrogenético para geração dos magmas que construíram os plútons desta suíte. Neste modelo, admite-se que a origem deste magmatismo está relacionada à fusão parcial de granulitos mesoarqueanos da área de Ouro Verde do subdomínio Canaã dos Carajás. O grau de fusão entre 14 a 22% de um granulito máfico são necessários para gerar os granitoides portadores de anfibólios, e que são os tipos mais expressivos nos plút ons estudados. Por sua vez, a fusão (8%) de um granulito félsico foi investigada para gerar a variedade BG. Dessa forma, conclui-se que a fusão sucessiva de fontes crustais refratárias produziu o amplo espectro composicional dos granitoides da Vila Jussara.

A consolidação (e construção) do magmatismo de Vila Jussara se deu por múltiplas injeções de magmas e extensa hibridização sob um regime tectônico transpressional/transtensional dominado por cisalhamento puro, cuja colocação foi condicionada por estruturas E-W pré-existentes, de idade mesoarqueana e reativadas no neoarqueano (Cinturão de Cisalhamento Itacaiúnas). Esse regime tectônico também foi o responsável pela exumação da crosta granulítica mesoarqueana da área de Ouro Verde através de sistemas imbricados. Dado o caráter dinâmico das zonas de cisalhamento que controlaram a colocação dos magmas, o caráter sintectônico desses granítoides pode ter contribuído para os processos de hibridização dentro desses sistemas.

REFERÊNCIAS

- Almeida F.F.M., Hasui Y., Brito Neves B.B., Fuck R.A. 1981. Brazilian Structural Provinces: an introduction. *Earth-Science Reviews*, **17**: 1–29.
- Almeida J.A.C., Dall’Agnol R., Oliveira M.A., Macambira M.J.B., Pimentel M.M., Rämö O.T., Guimarães F.V., Leite A.A.S. 2011. Zircon geochronology and geochemistry of the TTG suites of the Rio Maria granite-greenstone terrane: implications for the growth of the Archean crust of Carajás Province, Brazil. *Precambrian Research*, **187**: 201–221.
- Almeida J.A.C., Dall’Agnol R., Leite A.A.S. 2013. Geochemistry and zircon geochronology of the Archean granite suites of the Rio Maria granite-greenstone terrane, Carajás Province. *Brazil Journal of South American Earth Sciences*, **42**: 103–126.
- Almeida J.A.C., Oliveira M.A., Dall’Agnol R. Althoff F.J. 2008. Relatório de mapeamento geológico na escala 1: 100.000 da Folha Marajoara (SB-22-zc v). *Programa GeoBrasil*, CPRM–Serviço Geológico do Brasil **147**.
- Althoff F.J., Barbey P., Boullier A.M. 2000. 2.8–3.0 Ga plutonism and deformation in the SE Amazonian craton: the Archean granitoids of Marajoara (Carajás Mineral Province, Brazil). *Precambrian Research*, **104**: 187–206.
- Andersen T., Andersson U.B., Graham S., Aberg G., Simonsen S.L. 2009. Granitic magmatism by melting of juvenile continental crust: new constraints on the source of Paleoproterozoic granitoids in Fennoscandia from Hf isotopes in zircon. *Journal of the Geological Society*, **166**: 233–247.
- Araújo O.J.B. & Maia R.G.N. 1991. *Serra dos Carajás, Folha SB-22-Z-A*. Rio de Janeiro, CPRM. Relatório Final. 136 p.
- Araújo O.J. Maia R.G. Jorge João X. Costa, J.B S. 1988. A megaestrutura arqueana da Folha Serra dos Carajás. Anais do Congresso Latino-Americano de Geologia 7, 324–338.
- Avelar V.G. 2002. *Geocronologia Pb-Pb em zircão e Sm-Nd em rocha total da porção centro-norte do estado do Amapá – Brasil: implicações para a evolução geodinâmica do setor oriental dos Escudos das Guianas*. PhD Thesis, Programa de Pós-Graduação em Geologia e Geoquímica, Instituto de Geociências, Universidade Federal do Pará, Belém, 213 p.
- Avelar V.G. 1996. *Geocronologia Pb-Pb por evaporação em monocrystal de zircão do magmatismo da região de Tucumã, SE do estado do Pará, Amazônia Oriental*. MS Dissertation, Programa de Pós-Graduação em Geologia e Geoquímica, Instituto de Geociências, Universidade Federal do Pará, Belém, 149 p.
- Avelar V.G., Lafon J.M., Correia Jr. F.C., Macambira E.M.B. 1999. O magmatismo arqueano da região de Tucumã – Província Mineral de Carajás: novos resultados geocronológicos. *Revista Brasileira de Geociências*, **29**(4): 453–460.

- Barbosa J.P.O. 2004. *Geologia estrutural, geoquímica, petrografia e geocronologia de granitoides da região do Igarapé Gelado, norte da Província Mineral de Carajás*. MS Dissertation, Programa de Pós-Graduação em Geologia e Geoquímica, Instituto de Geociências, Universidade Federal do Pará, Belém, 96 p.
- Barros C.E.M., Barbey P., Boullier A.M. 2001. Role of magma pressure, tectonic stress and crystallization progress in the emplacement of the syntectonic A-type Estrela Granite Complex (Carajás Mineral Province, Brazil). *Tectonophysics*, **343**: 93–109.
- Barros C.E.M., Macambira M.J.B., Barbey P., Scheller, T., 2004. Dados isotópicos Pb–Pb em zircão (evaporação) e Sm–Nd do Complexo Granítico Estrela, Província Mineral de Carajás, Brasil: Implicações petrológicas e tectônicas. *Revista Brasileira de Geociências* **34**, 531–538.
- Barros C.E.M., Sardinha A.S., Barbosa J.P.O., Macambira M.J.B., 2009. Structure, petrology, geochemistry and zircon U-Pb and Pb-Pb geochronology of the synkinematic Archean (2.7 Ga) A-type granites from the Carajas Metallogenic Province, northern Brazil. *Can. Mineral.* **47**, 1423e1440.
- Bedard J.H., Harris L.B., Thrurston P.C., 2013. The hunting of the snArc. *Precambrian Res.* **229**, 20e48.
- Black L.P., Kamo S.L., Williams I.S., Mundil R., Davis D.W., Korsch R.J., Foudoulis C. 2003. The application of SHRIMP to Phanerozoic geochronology: a critical application of four zircon standards. *Chemical Geology*, **200**: 171–188.
- Bodorkos S., Cawood P. A., and Oliver N.H.S., 2000a, Timing and duration of synmagmatic deformation in the Mabel Downs Tonalite, northern Australia: *Journal of Structural Geology*, v. **22**, no. 8, p. 1181-1198.
- Bouvier A., Vervoort J.D., Patchett P.J. 2008. The Lu-Hf and Sm-Nd isotopic composition of CHUR: constraints from unequilibrated chondrites and implications for the bulk composition of terrestrial planets. *Earth and Planetary Science Letters*, **273**: 48–57.
- Chayes F. (ed.). 1956. *Petrographic modal analysis: an elementary statistical appraisal*. New York, John Wiley and Sons, 113 p.
- Chu N.C., Taylor R.N., Chavagnac V., Nesbitt R.W., Boella R.M., Milton J.A., German C.R., Bayon G., Burton K. 2002. Hf isotope ratio analysis using multi-collector inductively coupled plasma mass spectrometry: an evaluation of isobaric interference corrections. *Journal of Analytical Atomic Spectrometry*, **17**: 1567–1574.
- Costa J.B.S, Araújo O.J.B., Jorge João X.S., Maia R., Macambira E.M.B., Vale A.G., Santos A., Pena Filho J.I.C., Neves A.P. 1994. Panorama tectono-estrutural da região sudeste do estado do Pará. In: SBG, 4º Simpósio geologia da Amazônia, Belém. *Resumos*. p. 314–317.
- Cunha I.R.V., Dall'Agnol R., Feio G.R.L. 2016. Mineral chemistry and magnetic petrology of the Archean Planalto Suite, Carajás Province – Amazonian Craton: implications for the evolution of ferroan Archean granites. *Journal of South American Earth Sciences*, **67**: 100–121.

- Dall'Agnol R., 1982. Maciço Jamon: Evolução petrológica de um granito da Amazônia oriental. In: SBG, 1º Simpósio de geologia da Amazônia, Belém, 1982. Anais. Belém, v.2, p 139-161.
- Dall'Agnol R., Cunha I.R.V., Guimarães F.V., Oliveira D.C., Teixeira M.F.B., Feio G.R.L., Lamarão C.N., 2017. Mineralogy, geochemistry, and petrology of Neoarchean ferroan to magnesian granites of Carajás Province, Amazonian Craton: the origin of hydrated granites associated with charnockites. *Lithos* **277**, 3-32.
- Dall'Agnol R., Lafon J.M., Macambira M.J.B. 1994. Proterozoic anorogenic magmatism in the Central Amazonian Province, Amazonian Craton: geochronological, petrological and geochemical aspects. *Mineralogy and Petrology*, **50**: 113–138.
- Dall'Agnol R. & Oliveira D.C. 2007. Oxidized, magnetite-series, rapakivi-type granites of Carajás, Brazil: implications for classification and petrogenesis of A-type granites. *Lithos*, **93**: 215–233.
- Dall'Agnol R., Oliveira D.C., Guimarães F.V., Gabriel E.O., Feio G.R.L., Lamarão C.N., Althoff F.J., Santos P.A., Teixeira M.F.B., Silva A.C., Rodrigues D.S., Santos M.J.P., Silva C.R.P., Santos R.D., Santos P.J.L. 2013. Geologia do Subdomínio de Transição do Domínio Carajás – implicações para a evolução arqueana da Província Carajás – Pará. In: SBG, 13º Simpósio de geologia da Amazônia, Belém. *Anais*. 1 CD-ROM.
- Dall'Agnol R., Oliveira M.A., Almeida J.A.C., Althoff F.J., Leite A.A.S., Oliveira D.C., Barros C.E.M. 2006. Archean and Paleoproterozoic granitoids of the Carajás metallogenetic province, eastern Amazonian craton. In: Dall'Agnol R., Rosa-Costa L.T., Klein E.L. (Ed.), Symposium on magmatism: crustal evolution, and metallogenesis of the Amazonian Craton. Volume and field trips guide, Belém. PRONEX-UFPB/SBG-NO. *Abstracts*. p. 99–150.
- Dall'agnol R. Scaillet B. Pichavant M. 1999. An Experimental Study of a Lower Proterozoic A-type Granite from the Eastern Amazonian Craton, Brazil. *Journal of Petrology* **40**, 1673–1698. <https://doi.org/10.1093/petroj/40.11.1673>
- Dall'Agnol R., Teixeira N.P., Rämö O.T., Moura C.A.V., Macambira M.J. B., Oliveira D.C. 2005. Petrogenesis of the Paleoproterozoic, rapakivi, A-type granites of the Archean Carajás Metallogenetic Province, Brazil. *Lithos*, **80**: 101–129.
- Deer W.A., Howie R.A., Zussman J. 1997. Rock-forming minerals. London, Second Edition Longmans (eds.). 696 p.
- Delinardo M.A.S., Monteiro L.V.S., Moreto C.P.N., Sousa S.D., Melo G.H.C. 2014. Complexo Xingu: Uma secção da crosta inferior exumada durante a evolução do Domínio Carajás, PA. In: SBG, 47º Congresso brasileiro de geologia, Salvador. *Anais*. 1 CD-ROM.
- Delinardo M.A.S., Monteiro L.V.S., Santos T.J.S., Moreto C.P.N., Sousa S.D. 2015. Partial melting and magma generation in the Mesoarchean (ca. 3.0 Ga) TTG gneisses of the Xingu Complex, Carajás Province, Amazon Craton. In: 8th Hutton symposium on granites and related rocks, Florianópolis. *Abstracts*. 1 CD-ROM.

- Delinardo da Silva M.A., Monteiro L.V.S., Santos T. J. S., Moreto C.P.N., Sousa S.D., Faustinoni J. M., Melo G.H.C., Xavier R. P., Toledo B.A.M., 2021, Mesoarchean migmatites of the Carajás Province: From intra-arc melting to collision: *Lithos*, v. **388**: 101–129.
- DePaolo D.J. & Wasserburg G.J. 1976. Nd isotope variations and petrogenetic models. *Geophysical Research Letters*, **3**: 249–252.
- DePaolo D.J. 1981. Neodymium isotope in the Colorado Front Range and crust–mantle evolution in the Proterozoic. *Nature*, **291**: 193–196.
- De Wit M.J., 1998. On Archean granites, greenstones, cratons and tectonics: does the evidence demand a verdict? *Precambrian Research* **91**, 181–226.
- Dias S.B. 2009. *Caracterização geológica, petrográfica e geoquímica de granitos arqueanos da Folha Marajoara, terreno granito-greenstone de Rio Maria, sudeste do Pará*. MS Dissertation, Programa de Pós-Graduação em Geologia e Geoquímica, Instituto de Geociências, Universidade Federal do Pará, Belém, 129 p.
- DOCEGEO, 1988. Revisão litoestratigráfica da Província Mineral de Carajás e Litoestratigrafia e principais depósitos minerais. In: 35th Congresso Brasileiro de Geologia, Belém.
- Feio G.R.L. & Dall'Agnol R. 2012. Geochemistry and petrogenesis of the Mesoarchean granites from the Canaã dos Carajás area, Carajás Province, Brazil: implications for the origin of Archean granites. *Lithos*, **154**: 33–52.
- Feio G.R.L., Dall'Agnol R., Dantas E.L., Macambira M.J.B., Gomes A.C.B., Sardinha A.S., Oliveira D.C., Santos R.D., Santos P.A., 2012. R. Geochemistry, geochronology and origin of the Neoarchean Planalto Granite suite, Carajás, Amazonian craton: atype or hydrated charnockitic granites? *Lithos* **151**, 57–73.
- Feio G.R.L., Dall'Agnol R., Dantas E.L., Macambira M.J.B., Santos J.O.S., Althoff F.J., Soares J.E.B. 2013. Archean granitoid magmatism in the Canaã dos Carajás area: implications for crustal evolution of the Carajás province, Amazonian craton, Brazil. *Precambrian Research*, **227**: 157–185.
- Florisbal L.M., Janasi V.A., Bitencourt M.F., Heaman L.M., 2012. Space–time relation of post-collisional granitic magmatism in Santa Catarina, southern Brazil: U–Pb LA-MC ICP-MS zircon geochronology of coeval mafic-felsic magmatism related to the Major Gercino Shear Zone. *Precambrian Research*, **216**, 132–15.
- Gabriel E.O., Oliveira D.C., Galarza M.A. 2010. Geologia, petrografia e geocronologia de granitoides do Complexo Xingu da região nordeste de Água Azul do Norte – PA, Província Mineral de Carajás. In: SBG, 45º Congresso brasileiro de geologia, Belém. *Anais*. 1 CD-ROM.
- Gabriel E.O. & Oliveira D.C. 2014. Geologia, petrografia e geoquímica dos granitoides arqueanos de alto magnésio da região de Água Azul do Norte, porção sul do Domínio

Carajás, Pará. *Boletim do Museu Paraense Emílio Goeldi. Ciências Naturais*, **9**(3): 533–564.

Galarza M.A. Macambira M.J.B. Villas R.N. 2008. Dating and isotopic characteristics (Pb and S) of the Fe Oxide-Cu-Au-U-REE Igarapé Bahia ore deposit, Carajás mineral province, Pará state, Brazil. *Journal of South American Earth Sciences* **25**, 377–397. <https://doi.org/10.1016/j.jsames.2007.07.006>.

Galarza M.A., Oliveira D.C., Rodrigues E.A., Santos A.C., Marangoanha B., 2017. Granitoides neoarqueanos (2,73 – 2,74 Ga) intrusivos e associados ao Diopsídio Norito Pium, Canaã dos Carajás, Província Carajás (PA). *Contrib. à Geologia da Amaz.* SBG, Belém **10**, 225–246.

Gomes A.C.B. 2003. *Geologia, petrografia e geoquímica dos granitoides de Canaã dos Carajás, SE do estado do Pará*. MS Dissertation, Programa de Pós-Graduação em Geologia e Geoquímica, Instituto de Geociências, Universidade Federal do Pará, Belém, 160 p.

Griffin W.L., Wang X., Jackson S.E., Pearson N.J., O'Reilly S.Y. 2002. Zircon geochemistry and magma mixing, SE China: in-situ analysis of Hf isotopes, Tonglu and Pingtan igneous complexes. *Lithos*, **61**: 237–269.

Guimarães F.V. 2009. *Geologia, petrografia e geoquímica do Trondjemito Mogno e rochas arqueanas associadas, terreno granito-greenstone de Rio Maria – SE do Pará*. MS Dissertation, Programa de Pós-Graduação em Geologia e Geoquímica, Instituto de Geociências, Universidade Federal do Pará, Belém, 102 p.

Hamilton P.J., O’Nions R.K., Evensen N.M. 1977. Sm-Nd dating of Archean basic and ultrabasic volcanics. *Earth and Planetary Science Letters*, **36**: 263–268.

Hamilton W.B., 2011. Plate tectonics began in Neoproterozoic time, and plumes from deep mantle have never operated. *Lithos* **123**, 1–20.

Hibbard M.J. (Ed.). 1995. *Petrography to Petrogenesis*. New Jersey, Prentice-Hall Incorporation, 587 p.

Hirata W.K. Rigon J.C. Kadekaru K. Cordeiro A.A.C. Meireles E. de M. 1982. Geologia regional da província mineral de Carajás. Simpósio de Geologia da Amazônia 1, 100–110.

Hühn S.B., Macambira M.J.B., Dall’Agnol R. 1999. Geologia e Geocronologia Pb-Pb do granito alcalino arqueano Planalto, Região da Serra do Rabo, Carajás – PA. In: SBG, 6º Simpósio de geologia da Amazônia, Manaus. *Anais*. v. 1, p. 463–466.

Hutchison C.S. (Ed.). 1974. *Laboratory handbook of petrography techniques*. London, John Wiley and Sons, 527 p.

Ianhez A.C., Souza A.M.S., Montalvão R.M.G. 1980. Geologia da sequência vulcanosedimentar da Serra do Inajá – Santana do Araguaia. In: SBG, 31º Congresso brasileiro de geologia, Camboriú. *Anais*. v. 5, p. 2918–2928.

- Jorge João X.S. & Araújo J.B. 1992. Magmatismo granítico sin-cisalhamento Itacaiúnas no SW do estado do Pará. In: SBG, 37º Congresso brasileiro de geologia, São Paulo. *Resumos Expandidos*. v. 2, p. 36–38.
- Jorge João X.S., Neves A.P., Leal J.W.L. 1982. Ouro da Serra Pelada: aspectos da geologia e garimpagem. In: SBG, 1º Simpósio de geologia da Amazônia, Belém. *Anais*. v. 2, p. 52–62.
- Karlstrom K.E., and Bowring S.A., 1993, Proterozoic orogenic history in Arizona, in Reed, J.C., Jr., et al., eds., Precambrian: Conterminous U.S.: Boulder, Colorado, Geological Society of America, *Geology of North America*, v. C-2, p. 188–211.
- Kerr P. 1959. Optical Mineralogy. McGraw-Hill Book Co., New York, Third Edition, 492 p.
- Lafon J.M., Macambira M.J.B., Pidgeon R.T. 2000. Zircon U-Pb SHRIMP dating of Neoarchean magmatism in the southwestern part of the Carajás Province (eastern Amazonian Craton, Brazil). In: 31st International geological congress, Rio de Janeiro, *Abstracts*. 1 CD-ROM.
- Lafon J.M., Rodrigues E., Duarte K.D. 1994. Le granite Mata Surrão: um magmatisme monzogranitique contemporain des associations tonalitiques-trondhjemítiques-granodioríticas archéennes de la région de Rio Maria (Amazonie Orientale, Brésil). *Comptes Rendus de la Academie de Sciences de Paris*, **318**(2): 642–649.
- Leite A.A.S. 2001. *Geoquímica, petrogênese e evolução estrutural dos granitoides arqueanos da região de Xinguara, SE do Cráton Amazônico*. PhD Thesis, Programa de Pós-Graduação em Geologia e Geoquímica, Instituto de Geociências, Universidade Federal do Pará, Belém, 330 p.
- Leite A.A.S., Dall'Agnol R., Macambira M.J.B., Althoff F.J. 2004. Geologia e geocronologia dos granitoides arqueanos da região de Xinguara (PA) e suas implicações na evolução do Terreno Granito-Greenstone de Rio Maria. *Revista Brasileira de Geociências*, **34**: 447–458.
- Le Maître R.W., Streckeisen A., Zanettin B., Le Bas M.J., Bonin B., Bateman P., Bellieni G., Dudek A., Efremova J., Keller J., Lameyre J., Sabine P.A., Schmidt R., Sørensen H., Woolley A.R. (Ed.). 2002. *Igneous rocks. A classification and glossary of terms. Recommendations of the International Union of Geological Sciences Subcommission on the Systematics of Igneous Rocks*. Cambridge, Cambridge University Press, 252 p.
- Leite-Santos P.J. & Oliveira D.C. 2014. Trondhjemitos da área de Nova Canadá: novas ocorrências de associações magmáticas tipo TTG no Domínio Carajás. *Boletim do Museu Paraense Emílio Goeldi. Ciências Naturais*, **9**(3): 635–659.
- Leite-Santos P.J.S. & Oliveira D.C. 2016. Geologia, petrografia e geoquímica das associações leucogranítica arqueanas da área de Nova Canadá: Província Carajás. *Geologia USP. Série Científica*, **16**(2): 37–66.
- Ludwig K.R. 2001. SQUID 1.02: A User's Manual. Berkeley, Berkeley Geochronology Center Special Publication

- Ludwig K.R. 2008. *User's manual for Isoplot 3.6: a geochronological toolkit for Microsoft Excel*. Berkeley, Berkeley Geochronology Center (Special Publication).
- Lugmair G.W. 1974. Sm-Nd ages: a new dating method. *Meteoritics*, **9**: 369.
- Lugmair G.W., Scheinin N.B., Marti K. 1975. Sm-Nd age and history of Apollo 17 basalt 75075: evidence of early differentiation of the lunar exterior. Proc. Lunar Sci. Conf. 6th vol. 2. *Geochimica et Cosmochimica Acta Suppl.* **6**: 1419–1429.
- Macambira M.J.B., Barros C.E.M., Silva D.C.C., Santos M.C.C. 2001. Novos dados geológicos e geocronológicos para a região ao norte da Província de Carajás, evidências para o estabelecimento do limite Arqueano-Paleoproterozóico no sudeste do Cráton Amazônico. In: SBG, 7º Simpósio de geologia da Amazônia, Belém. *Resumos Expandidos*. 1 CD-ROM.
- Macambira M.J.B. & Lafon J.M. 1995. Geocronologia da síntese dos dados e novos desafios. *Boletim do Museu Paraense Emílio Goeldi*. Série Ciências da Terra, **7**: 263-288.
- Macambira M.J.B. & Lancelot J. 1991. Em busca do embasamento arqueano da região de Rio Maria, sudeste do estado do Pará. In: SBG, 3º Simpósio de geologia da Amazônia, Belém. *Resumos Expandidos*. p. 49–58.
- Macambira M.J.B. Lancelot J.R. 1996. Time constraints for the formation of the Archean Rio Maria crust, southeastern Amazonian Craton, Brazil. *International Geology Review* **38**, 1134–1142. <https://doi.org/10.1080/00206819709465386>
- Macambira E.M.B. & Vale A.G. 1997. *Programa Levantamentos Geológicos Básicos do Brasil. São Félix do Xingu. Folha SB.22-Y-B, Estado do Pará*. Brasília, DNPM/CPRM, 384 p.
- Machado N., Lindenmayer Z.G., Krogh T.E., Lindenmayer D. 1991. U-Pb geochronology of Archean magmatism and basement reactivation in the Carajás area, Amazon shield, Brazil. *Precambrian Research*, **49**: 329–354.
- Marangoanha B., Oliveira D.C. Galarza M.A. Marques G.T. 2020. Crustal anatexis and mantle-derived magmas forming Neoarchean A-type granitoids in Carajás Province, northern Brazil: Petrological evidence and tectonic control. *Precambrian Research* **338**
- Marangoanha B., Oliveira D.C., Oliveira V.E., Galarza M.A., & Lamarão C.N., 2019a. Neoarchean A-type granitoids from Carajás province (Brazil): New insights. *Precambrian Research*, Volume **324**, pp. 86-108.
- Marangoanha B., Oliveira D.C., Dall'Agnol R. 2019b. The Archean granulite-enderbite complex of the northern Carajás province, Amazonian craton (Brazil): Origin and implications for crustal growth and cratonization. *Lithos* **350–351**, 105275. <https://doi.org/https://doi.org/10.1016/j.lithos.2019.105275>
- Martin H. 1994. The Archean grey gneisses and the genesis of continental crust. Developments in *Precambrian Geology*, **11**:205-259. [https://doi.org/10.1016/S0166-2635\(08\)70224-X](https://doi.org/10.1016/S0166-2635(08)70224-X).

- Martins P.L.G., Toledo C.L.B., Silva A.M., Chemale F., Santos J.O.S., Assis L.M., 2017. Neoarchean magmatism in the southeastern Amazonian Craton, Brazil: Petrography, geochemistry and tectonic significance of basalts from the Carajás Basin. *Precambrian Research* **302**, 340–357. <https://doi.org/10.1016/j.precamres.2017.10.013>
- Medeiros Filho C.A. & Meireles E.M. 1985. Dados preliminares sobre a ocorrência de cromita na área de Luanga. In: SBG, 2º Simpósio de geologia da Amazônia, Belém. *Atas*. v. 3, p. 1488–1499.
- Medeiros H. & Dall'Agnol R. 1988. Petrologia da porção leste do batólito granodiorítico Rio Maria, sudeste do Pará. In: SBG, 35º Congresso brasileiro de geologia, Belém. *Anais*. v. 3, 1488–1499.
- Meireles E.M., Hirata W.K., Amaral A.F., Medeiros Filho C.A., Gato W.C. 1984. Geologia das folhas Carajás e Rio Verde, Província Mineral dos Carajás, estado do Pará. In: SBG, 33º Congresso brasileiro de geologia, Rio de Janeiro. *Anais*. v. 5, p. 2164–2174.
- Melo G.H.C., Monteiro L.V.S., Xavier R.P., Santiago E.B.S. 2014. Geocronologia U-Pb e uma nova perspectiva sobre a evolução do depósito IOCG de classe mundial Salobo, Província Carajás, Brasil. In: SBG, 47º Congresso brasileiro de geologia, Salvador. *Anais*. 1 CD-ROM.
- Melo G.H.C., Monteiro L.V.S., Xavier, R.P., Moreto C.P.N., Santiago E.S.B., Dufrane S.A., Aires B., Santos A.F.F., 2016. Temporal evolution of the giant Salobo IOCG deposit, Carajas province (Brazil): Constraints from paragenesis of hydrothermal alteration and U-Pb geochronology: *Mineralium Deposita*, **v. 52**, p. 709–732, doi: 10.1007/s00126-016-0693-5
- Moreto C.P.N., Monteiro L.V.S., Xavier R.P., Creaser R.A., DuFrane S.A., Tassinari C.C.G., Sato K., Kemp A.I.S., Amaral W.S. 2015. Neoarchean and Paleoproterozoic Iron Oxide-Copper-Gold events at the Sossego Deposit, Carajás Province, Brazil: Re-Os and U-Pb geochronological evidence. *Economic Geology*, **110**: 809–835.
- Moreto C.P.N., Monteiro L.V.S., Xavier R.P., Amaral W.S., Santos T.J.S., Juliani C., Souza Filho C.R. 2011. Mesoarchean (3.0 and 2.86 Ga) host rocks of the iron oxide–Cu–Au Bacaba deposit, Carajás Mineral Province: U-Pb geochronology and metallogenetic implications. *Mineralium Deposita*, **46**: 789–811.
- Moreto C.P.N., Monteiro L.V.S., Xavier R.P., Souza Filho C.R. 2010. Hospedeiras, Geocronologia U-Pb das roc mesoárqueanas (3.0 e 2.86 Ga) do depósito de óxido de ferrocobre-ouro bacaba, Província Mineral de Carajás.
- Moura C.A.V. 1992. *Geochronology and geochemistry of the basement orthogneisses of the Araguaia Belt, Brazil*. PhD Thesis, University of New Hampshire, New Hampshire, 236 p.
- Moyen J.F., Stevens, G., Kirsters, A., 2006. Record of mid-Archean subduction from metamorphism in the Barberton terrain, South Africa. *Nature* **422**, 559–562, doi:10.1038/nature04972.

- Nogueira A.C.R., Truckenbrodt W., Pinheiro R.V.L. 1995. Formação Águas Claras, Pré-Cambriano da Serra dos Carajás: redescrição e redefinição. *Boletim do Museu Paraense Emílio Goeldi. Ciências da Terra*, **7**: 177–197.
- Oliveira D.C., Santos P.J.L., Gabriel E.O., Rodrigues D.S., Faresin A.C., Silva M.L.T., Sousa S.D., Santos R.V., Silva A.C., Souza M.C., Santos R.D., Macambira M.J.B. 2010. Aspectos geológicos e geocronológicos das rochas magmáticas e metamórficas da região entre os municípios de Água Azul do Norte e Canaã dos Carajás – Província Mineral de Carajás. In: SBG, 45º Congresso brasileiro de geologia, Belém. *Resumos*. 1 CD-ROM.
- Oliveira E.C., Lafon J.M., Gioia S.M.C.L., Pimentel M.M. 2008. Datação Sm-Nd em rocha total e granada do metamorfismo granulítico da região de Tartarugal Grande, Amapá Central. *Revista Brasileira de Geociências*, **38**: 114–127.
- Oliveira M.A., Dall’Agnol R., Almeida J.A.C. 2011. Petrology of the Mesoarchean Rio Maria suite and the discrimination of sanukitoid series. *Lithos*, **127**: 192–209.
- Oliveira M.A., Dall’Agnol R., Althoff F.J., Leite A.A.S. 2009. Mesoarchean sanukitoid rocks of the Rio Maria Granite-Greenstone Terrane, Amazonian craton, Brazil. *Journal of South American Earth Sciences*, **27**: 146–160.
- Oliveira V.E.S., Oliveira D.C., Marangoanha B., Lamarão C.N. 2018. Geology, mineralogy and petrological affinities of the Neoarchean granitoids from the central portion of the Canaã dos Carajás domain, Amazonian craton, Brazil. *Journal of South American Earth Sciences*, **85**: 135–159.]
- Passchier C.W. & Trouw R.A.J. (Ed.). 2005. *Microtectonics*. Second ed. Berlin–Heidelberg–New York, Springer-Verlag, 371 p.
- Patchett P.J. & Tatsumoto M. 1980. A routine high-precision method for Lu-Hf isotope geochemistry and chronology. *Contributions to Mineralogy and Petrology*, **75**: 263–267.
- Paterson S.R., Tobisch O.T., 1992 Rates of processes in magmatic arcs: implications for the timing and nature of pluton emplacement and wall rock deformation. *Journal of Structural Geology*. **14**: 291–300.
- Petford N., Cruden A.R., McCaffrey K.J.W., Vigneresse J.L., 2000. Granite magma formation, transport and emplacement in the Earth’s crust. *Nature* **408**: 669–73.
- Pidgeon R.T. Macambira M.J.B. Lafon J.M. 2000. Th-U-Pb isotopic systems and internal structures of complex zircons from an enderbite from the Pium Complex, Carajás Province, Brazil: Evidence for the ages of granulite facies metamorphism and the protolith of the enderbite. *Chemical Geology* **166**, 159–171.
- Pimentel M.M. & Machado N. 1994. Geocronologia U-Pb do Terrenos Granito-Greenstone de Rio Maria, Pará. In: SBG, 38º Congresso brasileiro de geologia, Camboriú. *Resumos Expandidos*. p. 390–391.
- Pinheiro R.V.L. 1997. *Reactivation history of the Carajás and Cinzento Strike-Slip System, Amazon, Brazil*. PhD Thesis, University of Durham, Durham, 408 p.

- Pinheiro R.V.L & Holdsworth R.E. 2000. Evolução tectonoestratigráfica dos Sistemas Transcorrentes Carajás e Cinzento, Cinturão Itacaiúnas, na borda leste do Cráton Amazônico, Pará. *Revista Brasileira de Geociências*, **30**(4): 597–606.
- Ragland P. 1989. Basic analytical petrology, 1st ed. Oxford University Press, New York.
- Ricci P.S.F. & Carvalho M.A. 2006. Rocks of the Pium-Area, Carajás Block, Brazil – A deep seated high-T gabbroic pluton (charnockitoid-like) with xenoliths of enderbitic gneisses dated at 3002 Ma – the basement problem revisited, In: SBG, 8º Simpósio de geologia da Amazônia, Manaus. *Anais*. 1 CD-ROM.
- Rodrigues D.S., Oliveira D.C., Macambira M.J.B. 2014. Geologia, geoquímica e geocronologia do Granito Mesoarqueano Boa Sorte, município de Água Azul do Norte, Pará – Província Carajás. *Boletim do Museu Paraense Emílio Goeldi*. Série Ciências Naturais, **9**(3): 597–633.
- Rolando A.P. & Macambira M.J.B. 2003. Archean crust formation in Inajá range area, SSE of Amazonian Craton, Brazil, based on zircon ages and Nd isotopes. In: 4th South American Symposium on Isotope Geology, Salvador. *Expanded Abstracts*. 1 CD-ROM.
- Rollinson H.R. 1993. Using geochemical data: evaluation, presentation, interpretation. Pearson Education Limited, Harlow, 352 pp.
- Rosenberg C.L., 2004. Shear zones and magma ascent: a model based on a review of the Tertiary magmatism in the Alps. *Tectonics*, **23**, TC3002.
- Santos J.O.S. 2003. Geotectônica do Escudo das Guianas e Brasil-Central. In: Buzzi, L.A. et al. (Ed.). *Geologia, tectônica e recursos minerais do Brasil: texto, mapas e SIG*. Brasília, CPRM – Serviço Geológico do Brasil, p. 169–226.
- Santos P.J.L., Oliveira D.C., Galarza M.A., Macambira M.J.B. 2010. Geologia, petrografia e geocronologia das rochas granitoides do Complexo Xingu da região de Nova Canadá, município de Água Azul do Norte – Província mineral de Carajás. In: SBG, 45º Congresso brasileiro de geologia, Belém. *Anais*. 1 CD-ROM.
- Santos R.D., Galarza M.A., Oliveira D.C. 2013. Geologia, geoquímica e geocronologia do Diopsídio-Norito Pium, Província Carajás. *Boletim do Museu Paraense Emílio Goeldi*. Série Ciências da Terra, **8**: 355–382.
- Sardinha A.S., Barros C.E.M., Krymsky R., 2006. Geology, geochemistry, and U–Pb geochronology of the Archean (2.74 Ga) Serra do Rabo granite stocks, Carajás Metallogenetic Province, northern Brazil. *Journal South American Earth Science* **20**, 327–339.
- Sardinha A.S., Dall’Agnol R., Gomes A.C.B., Macambira M.J.B., Galarza M.A. 2004. Geocronologia Pb-Pb e U-Pb em zircão de granitoides arqueanos da região de Canaã dos Carajás, Província Mineral de Carajás. In: SBG, 42º Congresso brasileiro de geologia, Araxá. *Anais*. 1 CD-ROM.
- Sato K., Basei M.A.S., Siga Jr. O., Sproesser W.M., Passarelli C.R. 2008. Novas técnicas aplicadas ao método U-Pb no CPGeo – IGc/USP: avanços na digestão química,

espectrometria de massa (TIMS) e exemplos de aplicação integrada com SHRIMP. *Geologia USP. Série Científica*, 7: 77–99.

Sato K., Tassinari C.C.G.T., Basei M.A.S., Siga Júnior O., Onoe A.T., Souza M.D. 2014. Sensitive high resolution, ion microprobe (SHRIMP IIe/MC) of the Institute of Geoscience of University of São Paulo, Brazil: analytical method and first results. *Geologia USP. Série Científica*, 14(3): 3–18.

Scherer E.E., Münker C., Mezger K. 2001. Calibration of the lutetium-hafnium clock. *Science*, 293: 683–687.

Silva A.C., Dall’Agnol R., Guimarães F.V., Oliveira D.C. 2014. Geologia, petrografia e geoquímica de Associações Tonalíticas e Trondhjemíticas Arqueanas de Vila Jussara, Província Carajás, Pará. *Boletim do Museu Paraense Emílio Goeldi. Ciências Naturais*, 9(1): 13–46.

Silva A.C. Oliveira D.C. Macambira M.J.B. 2010. Individualização e geocronologia de granitóides do Complexo Xingu, região de Vila Jussara, município de Água Azul do Norte-PA, Província Mineral de Carajás, in: 45º Congresso Brasileiro de Geologia, Belém, Anais.

Silva F.F., Oliveira D.C., Dall’Agnol R., Silva L.R., Cunha I.V., 2020. Lithological and structural controls on the emplacement of a Neoarchean plutonic complex in the Carajás province, southeastern Amazonian craton (Brazil). *Journal of South American Earth Sciences* 102, 102696. <https://doi.org/10.1016/j.jsames.2020.102696>.

Silva G.C., Lima, M.I.C., Andrade A.R.F., Issler R.S., Guimarães G. 1974. *Geologia das folhas SB-22 Araguaia e parte da SC-22 Tocantins*. Belém, DNPM, v. 4, p. 1–143.

Sousa S.D., Oliveira D.C., Gabriel E.O., Macambira M.J.B. 2010. Geologia, petrografia e geocronologia das rochas granitoides do Complexo Xingu da porção a leste da cidade de Água Azul do Norte (PA) – Província Mineral de Carajás. In: SBG, 45º Congresso brasileiro de geologia, Belém. *Anais*. 1 CD-ROM.

Souza Z.S., Potrel H., Lafon J.M., Althoff F.J., Pimentel M.M., Dall’Agnol R., Oliveira C.G. 2001. Nd, Pb and Sr isotopes of the Identidade Belt, an Archaean greenstone belt of the Rio Maria region (Carajás Province, Brazil): implications for the Archaean geodynamic evolution of the Amazonian Craton. *Precambrian Research*, 109: 293–315.

Stern R.A. 1998. High resolution SIMS determination of radiogenic trace isotope ratios in minerals. In: Cabri L.J., Vaughan D.J. (Ed.). *Modern approaches to ore and environmental mineralogy*. Ottawa, p. 241–268. (Mineralogical Association of Canada, v. 27).

Tallarico F.H.B. Figueiredo B.R. Groves D.I. Kositsin N. McNaughton N.J. Fletcher I.R. Rego J.L. 2005. Geology and SHRIMP U-Pb geochronology of the Igarapé Bahia deposit, Carajás copper-gold belt, Brazil: An Archean (2.57 Ga) example of iron-oxide Cu-Au-(U-REE) mineralization. *Economic Geology* 100, 7–28.

Tassinari C.C.G., Macambira, M.J.B., 1999. Geochronological provinces of the Amazonian craton. *Episodes*, 22: 174–182.

Tassinari C.C.G. & Macambira M.J.B. 2004. Evolução tectônica do Cráton Amazônico. In: Mantesso-Neto V., Bartorelli A., Carneiro C.D.R., Brito Neves B.B. (Ed.). *Geologia do continente Sul Americano: evolução da obra de F. F. M. de Almeida*. São Paulo, BECA, p. 471–486.

Tassinari C.C.G. Tachibana J. Tilio M. Livio R. Gaia C. 2005. Geologia isotópica aplicada nas mineralizações de Cu-Au do greenstone belt da Serra dos Gradaús, Província Mineral de Carajás, Cráton Amazônico: exemplo de mineralizações policíclicas. 1st Simpósio Brasileiro de Metalogenia, Gramado.

Teixeira, L.R., 2005. GENESIS 4.0 – Software de Modelamento Geoquímico.

Teixeira M.F.B., Dall'Agnol R., Silva A.C., Santos P.A. 2013. Geologia, petrografia e geoquímica do Leucogranodiorito Pantanal e dos leucogranitos arqueanos da área a norte de Sapucaia, Província Carajás, Pará: implicações petrogenéticas. *Boletim do Museu Paraense Emílio Goeldi. Série Ciências Naturais*, **8**(3): 291–323.

Teixeira M.F.B., Dall'Agnol R., Santos J.O.S., Sousa L.A.M., Lafon J.M., 2017. Geochemistry, geochronology and Nd isotopes of the Gogó da Onça Granite: A new Paleoproterozoic A-type granite of Carajás Province, Brazil. *Journal of South American Earth Sciences*, **80**: 47–65.

Vasquez L.V., Rosa-Costa L.R., Silva C.G., Ricci P.F., Barbosa J.O., Klein E.L., Lopes E.S., Macambira E.B., Chaves C.L., Carvalho J.M., Oliveira J.G., Anjos G.C., Silva H.R. 2008. Escala 1:1.000.000. In: Vasquez M.L. & Rosa-Costa L.T. (Ed.). *Geologia e recursos minerais do Estado do Pará: Sistema de Informações Geográficas e SIG: texto explicativo dos mapas geológico e tectônico e de recursos minerais do Estado do Pará*. Belém, CPRM, 328 p.

Williams I.S. 1998. U-Th-Pb Geochronology by ion microprobe. In: McKibben M.A., Shanks III W.C., Ridley W.I. (Ed.). *Applications of microanalytical techniques to understanding mineralizing processes*. [S.l.], Society of Economic Geologists, p. 1–35. (Reviews in Economic Geology, V.7).

Yardley B.W.D., Mackenzie W.S., Guilford C. 1990. *Atlas of metamorphic rocks and their textures*. New York, John Wiley and Sons, 120 p.



UNIVERSIDADE FEDERAL DO PARÁ
INSTITUTO DE GEOCIÊNCIAS
PROGRAMA DE PÓS-GRADUAÇÃO EM GEOLOGIA E GEOQUÍMICA

PARECER

Sobre a Defesa Pública da Tese de Doutorado de **FERNANDO FERNANDES DA SILVA**

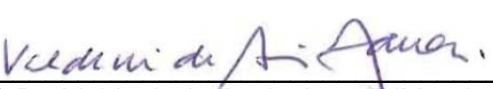
A banca examinadora da Tese de Doutorado de **FERNANDO FERNANDES DA SILVA**, orientando do Prof. Dr. **Davis Carvalho de Oliveira** (UFPA), composta pelos professores doutores **Valdecir de Assis Janasi** (USP), **Moacir José Buenano Macambira** (UFPA), **Bhrenno Marangoanha** (UFPA) e **Claudio Nery Lamarão** (UFPA), após apresentação da sua tese intitulada “**ORIGEM E EVOLUÇÃO DO COMPLEXO GRANITOIDE NEOARQUEANO DE VILA JUSSARA: IMPLICAÇÕES PARA A EVOLUÇÃO CRUSTAL DA PROVÍNCIA CARAJÁS**”, emite o seguinte parecer:

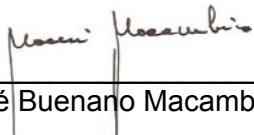
O candidato realizou sua apresentação de forma clara, bem organizada e segura no tempo estipulado. Na arguição mostrou domínio da temática abordada e respondeu adequadamente às perguntas formuladas pela banca. O trabalho escrito foi apresentado na forma de dois artigos submetidos a periódicos de impacto internacional, sendo um já publicado. Dessa forma, o documento atende às exigências básicas para uma tese de doutorado.

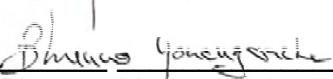
Finalmente, a banca examinadora decidiu por unanimidade aprovar a tese de doutorado.

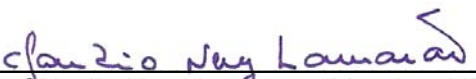
Belém, 15 de julho de 2022.


Prof. Dr. Davis Carvalho de Oliveira (Orientador – UFPA)


Prof. Dr. Valdecir de Assis Janasi (Membro-USP)


Prof. Dr. Moacir José Buenano Macambira (Membro-UFPA)


Prof. Dr. Bhrenno Marangoanha (Membro-UFPA)


Prof. Dr. Cláudio Nery Lamarão (Membro-UFPA)